

RL4CO: an Extensive Reinforcement Learning for Combinatorial Optimization Benchmark

Federico Berto^{*1}, Chuanbo Hua^{*1}, Junyoung Park^{*1}, Laurin Luttmann^{*2},
 Yining Ma³, Fanchen Bu¹, Jiarui Wang⁴, Haoran Ye⁵, Minsu Kim¹,
 Sanghyeok Choi¹, Nayeli Gast Zepeda⁶, André Hottung⁶, Jianan Zhou³, Jieyi Bi³,
 Yu Hu⁷, Fei Liu⁸, Hyeonah Kim¹, Jiwoo Son¹⁵, Haeyeon Kim¹,
 Davide Angioni⁹, Wouter Kool¹⁰, Zhiguang Cao¹¹, Qingfu Zhang⁸, Joungho Kim¹,
 Jie Zhang³, Kijung Shin¹, Cathy Wu¹², Sungsoo Ahn¹³, Guojie Song⁵
 Changhyun Kwon^{1,15}, Kevin Tierney⁶, Lin Xie^{2,14}, Jinkyoo Park^{1,15}

¹KAIST, ²Leuphana University, ³Nanyang Technological University,
⁴Southeast University, ⁵Peking University, ⁶Bielefeld University,
⁷Soochow University, ⁸City University of Hong Kong, ⁹University of Brescia,
¹⁰ORTEC, ¹¹Singapore Management University, ¹²MIT, ¹³POSTECH,
¹⁴Twente University, ¹⁵OMELET, AI4CO[✉]

Abstract

Deep reinforcement learning (RL) has recently shown significant benefits in solving combinatorial optimization (CO) problems, reducing reliance on domain expertise, and improving computational efficiency. However, the field lacks a unified benchmark for easy development and standardized comparison of algorithms across diverse CO problems. To fill this gap, we introduce RL4CO, a unified and extensive benchmark with in-depth library coverage of 23 state-of-the-art methods and more than 20 CO problems. Built on efficient software libraries and best practices in implementation, RL4CO features modularized implementation and flexible configuration of diverse RL algorithms, neural network architectures, inference techniques, and environments. RL4CO allows researchers to seamlessly navigate existing successes and develop their unique designs, facilitating the entire research process by decoupling science from heavy engineering. We also provide extensive benchmark studies to inspire new insights and future work. RL4CO has attracted numerous researchers in the community and is open-sourced at <https://github.com/ai4co/r14co>.

1 Introduction

Combinatorial optimization (CO) focuses on finding optimal solutions for problems with discrete variables and has broad applications, including vehicle routing [106, 74], scheduling [153], and hardware device placement [67]. Given that the combinatorial space expands exponentially and exhibits NP-hard characteristics, the operations research (OR) community has traditionally tackled these challenges through the development of mathematical programming algorithms [44] and handcrafted heuristics [35]. Despite their success, these methods still face significant limitations: mathematical programming struggles with scaling, while handcrafted heuristics require significant domain-specific adjustments for different CO problems.

Recently, to address these limitations, neural combinatorial optimization (NCO) [10] has emerged. It employs deep neural networks to automate the problem-solving process and significantly reduces

^{*}Equal contribution.

[✉]Work made with contributions from the AI4CO open research community.

computation demands and domain expertise requirements. Recent NCO works mainly leverage the reinforcement learning (RL) paradigm, making significant strides in improving exploration efficiency [76, 68], relaxing the needs of obtaining optimal solutions, and extending to various CO tasks [153, 106, 74, 67]. Although supervised learning (SL) methods [37] are shown to be effective in NCO, they require the availability of high-quality solutions, which is unrealistic for large instances or theoretically hard problems. Therefore, we focus on the RL paradigm in this paper.

Despite the growing popularity and advancements in using reinforcement learning for solving combinatorial optimization, there remains a lack of a unified benchmark for analyzing past works under consistent implementations and conditions. The absence of a standardized benchmark hinders NCO researchers' efforts to make impactful advancements and leverage existing successes, as it becomes challenging to determine the superiority of one method over another. Moreover, the significance of NCO lies in its potential for generalizability across multiple problems without extensive problem-specific knowledge. Variations in implementation can make it difficult for new researchers to engage with the NCO community, and inconsistent comparisons obstruct straightforward performance evaluations. These issues pose significant challenges and underscore the need for a comprehensive benchmark to streamline research and foster consistent progress.

Contributions. To bridge this gap, we introduce RL4CO, the first comprehensive benchmark with multiple baselines, environments, and boilerplate from the literature, all implemented in a *modular*, *flexible*, *accelerated*, and *unified* manner. Our aim is to facilitate the entire research process for the NCO community with the following key contributions: 1) **Simplifying development** through modularizing 27 environments and 23 existing baseline models, allowing for flexible and automated combinations for effortless testing, switching, and achieving state-of-the-art performance; 2) **Enhancing the training and testing efficiency** through the customized unified pipeline tailored for the NCO community based on advanced libraries such as TorchRL [20], PyTorch Lightning [39], Hydra [148], and TensorDict [20]; 3) **Standardizing evaluation** to ensure fair and comprehensive comparisons, enabling researchers to automatically test a broader range of problems from diverse distributions and gather valuable insights using our testbed. Overall, RL4CO eliminates the need for repetitive heavy engineering in the NCO community and fosters seamless future development by building on existing successes, enabling advanced innovation and progress in the field.

2 Related Works

Neural Combinatorial Optimization. Neural combinatorial optimization (NCO) utilizes machine learning techniques to automatically develop novel heuristics for solving NP-hard CO problems. We classify the majority of NCO research from the following perspectives: 1) *Learning Paragiams*: researchers have employed supervised learning [139, 127, 37, 93] to approximate optimal solutions to CO instances. Further research leverages reinforcement learning [8, 106, 74, 76], and unsupervised learning [49, 102] to ease the difficulty of obtaining (near-)optimal solutions. 2) *Models*: various deep learning architectures such as recurrent neural networks [139, 30, 83], graph neural networks [61, 102], Transformers [74, 76], diffusion models [127], and GFlowNets [154, 70] have been employed. 3) *Problems*: NCO has demonstrated great success in various problems, including vehicle routing problems (VRPs) (e.g., traveling salesman problem and capacitated VRP), scheduling problems (e.g., job shop scheduling problems [153]), hardware device placement [67], and graph-based CO problems (e.g., maximum independent set [31, 3] and maximum cut [154]). 4) *Heuristic Types*: generally, the learned heuristics can be categorized as *constructive* in an autoregressive [74] or non-autoregressive [61] way, and *improvement* heuristics, which leverage traditional heuristics [145, 98] and meta-heuristics [124]. We refer to Bengio et al. [10] for a comprehensive survey. In this paper, we focus on the reinforcement learning paradigm due to its effectiveness and flexibility. Notably, the proposed RL4CO is versatile to support most combinations of models, problems and heuristic types, making it an apt library and benchmark for future research in NCO.

Related Benchmark Libraries. Despite the variety of general-purpose RL software libraries [23, 85, 114, 143, 32, 42, 99], there is a lack of a unified and extensive benchmark for CO problems. Balaji et al. [5] propose an RL benchmark for Operations Research (OR) with a PPO baseline [119]; Hubbs et al. [53], Biagioni et al. [17] provide a collection of OR environments. Wan et al. [140] propose a general-purpose library for OR, and benchmarks the canonical TSP and CVRP environments. However, a major downside of the above libraries is that they cannot be massively parallelized due to their reliance on the OpenAI Gym API, which can only run on CPU, unlike RL4CO, which is

Table 1: Comparison of libraries in reinforcement learning for combinatorial optimization.

Library	Environments #	Baselines [†] #	Hardware Acceleration	Availability	Modular Baselines	Open Community
ORL [5]	3	1	✗	✗	✗	✗
OR-Gym [53]	9	-	✗	✓	✗	✗
Graph-Env [17]	2	-	✗	✓	✗	✗
RLOR [140]	2	2	✗	✓	✓	✗
RoutingArena [133]	1	8	✓	✗	✗	✗
Jumanji [19]	22	3	✓	✓	✗	✗
RL4CO (ours)	27 [‡]	23	✓	✓	✓	✓

[†] We consider as *baselines* ad-hoc network architectures (i.e., policies) and RL algorithms from the literature.

[‡] We also consider the possible 16 combinations of environments generated by the unified Multi-Task VRP, as they have been historically considered separate environments in the NCO literature.

based on the TorchRL [20], a recent official PyTorch [110] library for RL that enables hardware-accelerated execution of both environments and algorithms. Prouvost et al. [113] introduces a library specialized for CO problems that work in combination with traditional MILP [88] solvers. We also mention Routing Arena [133], whose scope is different from RL4CO, namely, comparing NCO and classical solvers only for the CVRP. The most related work is Jumanji [19], which provides a variety of CO environments written in JAX [21] that can be hardware-accelerated alongside an actor-critic baseline. While Jumanji is an RL environment suite, RL4CO is a full-stack library that integrates environments, policies, and RL algorithms under a unified framework.

3 RL4CO: Taxonomy

We describe the RL4CO taxonomy, categorizing components into *Environments*, *Policies*, and *RL Algorithms*. Then we translate the taxonomy to implementation in § 4.

Environments. Given a CO problem instance \mathbf{x} , we formulate the solution-generating procedure as a Markov Decision Process (MDP) characterized by a tuple $(\mathcal{S}, \mathcal{A}, \mathcal{T}, \mathcal{R}, \gamma)$ as follows. **State** \mathcal{S} is the space of states that represent the given problem \mathbf{x} and the current partial solution being updated in the MDP. **Action** \mathcal{A} is the action space, which includes all feasible actions a_t that can be taken at each step t . **State Transition** \mathcal{T} is the deterministic state transition function $s_{t+1} = \mathcal{T}(s_t, a_t)$ that updates a state s_t to the next state s_{t+1} . **Reward** \mathcal{R} is the reward function $\mathcal{R}(s_t, a_t)$ representing the immediate reward received after taking action a_t in state s_t . Finally, $\gamma \in [0, 1]$ is a discount factor that determines the importance of future rewards. Since the state transition is deterministic, we represent the solution for a problem \mathbf{x} as a sequence of T actions $\mathbf{a} = (a_1, \dots, a_T)$. Then the total return $\sum_{t=1}^T \mathcal{R}(s_t, a_t)$ translates to the negative cost function of the CO problem.

Policies. The policies can be categorized into constructive policies, which generate a solution from scratch, and improvement policies, which refine an existing solution.

Constructive policies. A policy π is used to construct a solution from scratch for a given problem instance \mathbf{x} . It can be further categorized into autoregressive (AR) and non-autoregressive (NAR) policies. An AR policy is composed by an encoder f that maps the instance \mathbf{x} into an embedding space $\mathbf{h} = f(\mathbf{x})$ and by a decoder g that iteratively determines a sequence of actions \mathbf{a} as follows:

$$a_t \sim g(a_t | a_{t-1}, \dots, a_0, s_t, \mathbf{h}), \quad \pi(\mathbf{a} | \mathbf{x}) \triangleq \prod_{t=1}^{T-1} g(a_t | a_{t-1}, \dots, a_0, s_t, \mathbf{h}). \quad (1)$$

A NAR policy encodes a problem \mathbf{x} into a heuristic $\mathcal{H} = f(\mathbf{x}) \in \mathbb{R}_+^N$, where N is the number of possible assignments across all decision variables. Each number in \mathcal{H} represents a (unnormalized) probability of a particular assignment. To obtain a solution \mathbf{a} from \mathcal{H} , one can sample a sequence of assignments from \mathcal{H} while dynamically masking infeasible assignments to meet problem-specific constraints. It can also guide a search process, e.g., Ant Colony Optimization [36, 150, 70], or be incorporated into hybrid frameworks [152]. Here, the heuristic helps identify promising transitions and improve the efficiency of finding an optimal or near-optimal solution.

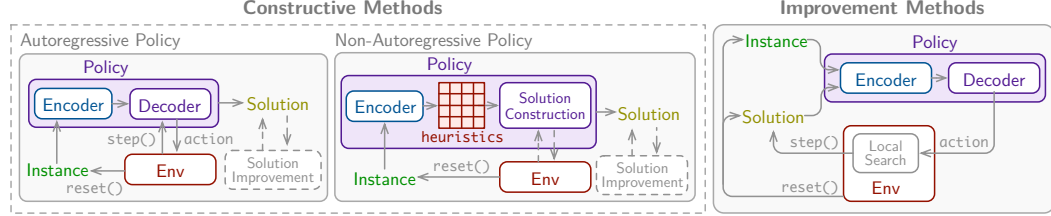


Figure 1: Overview of different types of policies and their modularization in RL4CO.

Improvement policies. A policy can be used for improving an initial solution $\mathbf{a}^0 = (a_0^0, \dots, a_{T-1}^0)$ into another one potentially with higher quality, which can be formulated as follows:

$$\mathbf{a}^k \sim g(\mathbf{a}^0, \mathbf{h}), \quad \pi(\mathbf{a}^K | \mathbf{a}^0, \mathbf{x}) \triangleq \prod_{k=1}^{K-1} g(\mathbf{a}^k | \mathbf{a}^{k-1}, \dots, \mathbf{a}^0, \mathbf{h}), \quad (2)$$

where \mathbf{a}^k is the k -th updated solution and K is the budget for number of improvements. This process allows continuous refinement for a long time to enhance the solution quality.

RL Algorithms. The RL objective is to learn a policy π that maximizes the expected cumulative reward (or equivalently minimizes the cost) over the distribution of problem instances:

$$\theta^* = \underset{\theta}{\operatorname{argmax}} \mathbb{E}_{\mathbf{x} \sim P(\mathbf{x})} \left[\mathbb{E}_{\pi(\mathbf{a}|\mathbf{x})} \left[\sum_{t=0}^{T-1} \gamma^t \mathcal{R}(s_t, a_t) \right] \right], \quad (3)$$

where θ is the set of parameters of π and $P(\mathbf{x})$ is the distribution of problem instances. Eq. (3) can be solved using algorithms such as variations of REINFORCE [128], Advantage Actor-Critic (A2C) methods [73], or Proximal Policy Optimization (PPO) [119]. These algorithms are employed to train the policy network π , by transforming the maximization problem in Eq. (3) into a minimization problem involving a loss function, which is then optimized using gradient descent algorithms. For instance, the REINFORCE loss function gradient is given by:

$$\nabla_{\theta} \mathcal{L}_a(\theta | \mathbf{x}) = \mathbb{E}_{\pi(\mathbf{a}|\mathbf{x})} [(R(\mathbf{a}, \mathbf{x}) - b(\mathbf{x})) \nabla_{\theta} \log \pi(\mathbf{a}|\mathbf{x})], \quad (4)$$

where $b(\cdot)$ is a baseline function used to stabilize training and reduce gradient variance. We also distinguish between two types of RL (pre)training: 1) *inductive* and 2) *transductive* RL. In inductive RL, the focus is on learning patterns from the training dataset to generalize to new instances, thus amortizing the inference procedure. Conversely, transductive RL (or test-time optimization) optimizes parameters during testing on target instances. Typically, a policy π is trained using inductive RL, followed by transductive RL for test-time optimization.

4 RL4CO: Library Structure

RL4CO is a unified reinforcement learning (RL) for Combinatorial Optimization (CO) library that aims to provide a *modular*, *flexible*, and *unified* code base for training and evaluating RL for CO methods with extensive benchmarking capabilities on various settings. As shown in Fig. 2, RL4CO decouples the major components of an RL pipeline, prioritizing their reusability in the implementation. Following also the taxonomy of § 3, the main components are: (§ 4.1) Environments, (§ 4.2) Policies, (§ 4.3) RL algorithms, (§ 4.4) Utilities, and (§ 4.5) Environments & Baselines Zoo.

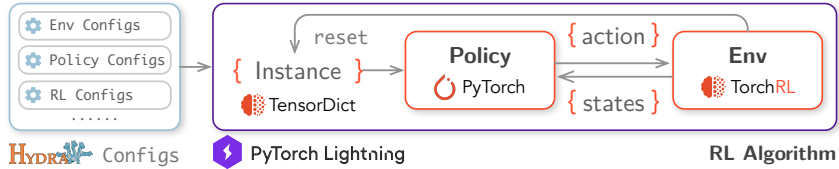


Figure 2: Overview of the RL4CO pipeline: from configurations to training a policy.

4.1 Environments

Environments in RL4CO fully specify the CO problems and their logic. They are based on the RL4COEnvBase class that extends from the EnvBase in TorchRL [20]. A modular generator

can be provided to the environment. The generator provides CO instances to the environment, and different generators can be used to generate different data distributions. Static instance data and dynamic variables, such as the current state s_t , current solution a^k for improvement environments, policy actions a_t , rewards, and additional information are passed in a *stateless* fashion in a `TensorDict` [104], that we call `td`, through the environment `reset` and `step` functions. Additionally, our environment API contains several functions, such as `render`, `check_solution_validity`, `select_start_nodes` (i.e., for POMO-based optimization [76]) and optional API as `local_search` solution improvement.

It is noteworthy that RL4CO enhances the efficiency of environments when compared to vanilla TorchRL, by overriding and optimizing some methods in TorchRL EnvBase. For instance, our new `step` method brings a decrease of up to 50% in latency and halves the memory impact by avoiding saving duplicate components in the stateless `TensorDict`.

4.2 Policies

Policies in RL4CO are subclasses of PyTorch’s `nn.Module` and contain the encoding-decoding logic and neural network parameters θ . Different policies in the RL4CO “zoo” can inherit from metaclasses like `ConstructivePolicy` or `ImprovementPolicy`. We modularize components to process raw features into the embedding space via a parametrized function ϕ_ω , called *feature embeddings*. 1) *Node Embeddings* ϕ_n : transform m_n node features of instances x from the feature space to the embedding space h , i.e., $[B, N, m_n] \rightarrow [B, N, h]$. 2) *Edge Embeddings* ϕ_e : transform m_e edge features of instances x from the feature space to the embedding space h , i.e., $[B, E, m_e] \rightarrow [B, E, h]$, where E is the number of edges. 3) *Context Embeddings* ϕ_c : capture contextual information by transforming m_c context features from the current decoding step s_t from the feature space to the embedding space h , i.e., $[B, m_c] \rightarrow [B, h]$, for nodes or edges. Overall, Fig. 3 illustrates a generic constructive AR policy in RL4CO, where the feature embeddings are applied similarly to other types of policies. Embeddings can be automatically selected by RL4CO at runtime by simply passing the `env_name` to the policy. Additionally, we allow for granular control of any higher-level policy component independently, such as encoders and decoders.

4.3 RL Algorithms

RL algorithms in RL4CO define the process that takes the Environment with its problem instances and the Policy to optimize its parameters θ . The parent class of algorithms is the `RL4COLitModule`, inheriting from PyTorch Lightning’s `pl.LightningModule` [39]. This allows for granular support of various methods including the `[train, val, test]_step`, automatic logging with several logging services such as Wandb via `log_metrics`, automatic optimizer configuration via `configure_optimizers` and several useful callbacks for RL methods such as `on_train_epoch_end`. RL algorithms are additionally attached to an `RL4COTrainer`, a wrapper we made with additional optimizations around `pl.Trainer`. This module seamlessly supports features of modern training pipelines, including logging, checkpoint management, mixed-precision training, various hardware acceleration supports (e.g., CPU, GPU, TPU, and Apple Silicon), and multi-device hardware accelerator in distributed settings [84]. For instance, using mixed-precision training significantly decreases training time without sacrificing much convergence and enables us to leverage recent routines, e.g., FlashAttention [34, 33], which we investigate in Appendix.

4.4 Utilities

Configuration Management. Optionally, but usefully, we adopt Hydra [148], an open-source Python framework that enables hierarchical config management, making it easier to manage complex configurations and experiments with different settings as shown in Appendix. Hydra additionally allows for automatically parsing parameters (un-)defined in configs - i.e., `python run.py experiment=routing/pomo env=cvrp env.generator_params.num_loc=50` launches an experiment defined under `routing/pomo` and changes the environment to CVRP with 50 locations.

Decoding Schemes. Decoding schemes handle the logic of model logits z by applying preprocessing, such as masking of infeasible actions and/or additional techniques to select better actions during training and testing. We implement the model and problem-agnostic decoding schemes under the `DecodingStrategy` class in the RL4CO codebase that can be easily reused: 1) *Greedy*, which

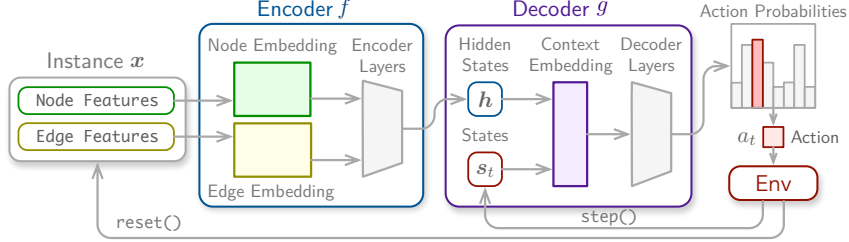


Figure 3: Overview of modularized RL4CO policies. Any component such as the encoder/decoder structure and feature embeddings can be replaced and thus the model is adaptable to various new environments.

selects the action with the highest probability; 2) *Sampling*, which samples `n_samples` solutions from the current masked probability distribution of the policy, incorporating sampling strategies like 2.a) Softmax Temperature τ , 2.b) top-k sampling [75], and 2.c) top-p (or Nucleus) sampling [48] (more details in Appendix); 3) *Multistart*, which enforces diverse starting actions as demonstrated in POMO [76], such as starting from different cities in the Traveling Salesman Problem (TSP) with N nodes; 4) *Augmentation*, which applies transformations to instances, such as random rotations and flipping in Euclidean problems [69], to create an augmented set of problems.

Documentation, Tutorials, and Testing. We release extensive documentation to make it as accessible as possible for both newcomers and experts. RL4CO can be easily installed by running `pip install rl4co` with open-source code available at <https://github.com/ai4co/rl4co>. Several tutorials and examples are also available under the `examples/` folder. We thoroughly test our library via continuous integration on multiple Python versions and operating systems. The following code snippet shows minimalistic code that can train a model in a few lines:

```
from rl4co.envs.routing import TSPEnv, TSPGenerator
from rl4co.models import AttentionModelPolicy, POMO
from rl4co.utils import RL4COTrainer
# Instantiate generator and environment
generator = TSPGenerator(num_loc=50, loc_distribution="uniform")
env = TSPEnv(generator)
# Create policy and RL model
policy = AttentionModelPolicy(env_name=env.name, num_encoder_layers=6)
model = POMO(env, policy, batch_size=64)
# Instantiate Trainer and fit
trainer = RL4COTrainer(max_epochs=10, accelerator="gpu", precision="16-mixed")
trainer.fit(model)
```

4.5 Environments & Baselines Zoo

Environments. We include benchmarking from the following environments, divided into four areas. 1) **Routing**: Traveling Salesman Problem (TSP) [79], Capacitated Vehicle Routing Problem (CVRP) [18], Orienteering Problem (OP) [78, 28], Prize Collecting TSP (PCTSP) [6], Pickup and Delivery Problem (PDP) [63, 118] and Multi-Task VRP (MTVRP) [89, 157, 13] (which modularizes with 16 problem variants including the basic VRPTW, OVRP, VRPB, VRPL and VRPs with their constraint combinations); 2) **Scheduling**: Flexible Job Shop Scheduling Problem (FJSSP) [22], Job Shop Scheduling Problem (JSSP) [115] and Flow Shop Scheduling Problem (FJSP); 3) **Electronic Design Automation**: multiple Decap Placement Problem (mDPP) [67]; 4) **Graph**: Facility Location Problem (FLP) [38] and Max Cover Problem (MCP) [65].

Baseline Zoo. Given that several works contribute to both new policies and new RL algorithm variations, we list the papers we reproduce. For 1) **Constructive AR** methods, we include the Attention Model (AM) [74], Ptr-Net [139], POMO [76], MatNet [77], HAM [82], SymNCO [69], PolyNet [51], MTPOMO [89], MVMoE [157], L2D [153], HGNN [125] and DevFormer [67]. For 2) **Constructive NAR** methods, we benchmark Ant Colony Optimization-based DeepACO [150] and GFACS [70] as well as the hybrid NAR/AR GLOP [152]. 3) **Improvement methods** include DACT [96], N2S [97] and NeuOpt [98]. We also include 4) **General-purpose RL** algorithm from the literature, including REINFORCE [128] with various baselines, Advantage Actor-Critic (A2C)

[73] and Proximal Policy Optimization (PPO) [119] that can be readily be combined with any policy. Finally, we include 5) **Active search** (i.e., Transductive RL) methods AS [8] and EAS [50].

5 Benchmarking Study

We perform several benchmarking studies with our unified RL4CO library. Given the limited space, we invite the reader to check out the [Appendix](#) for supplementary material.

5.1 Flexibility and Modularity

Changing policy components. The integration of many state-of-the-art methods in RL4CO from the NCO field in a modular framework makes it easy to implement and improve upon state-of-the-art neural solvers for complex CO problems with only a few lines of code and improve upon them.² We demonstrate this in [Table 2](#) for the FJSSP by gradually replacing or adding elements to the original SotA policy [125]. First, replacing the HGNN encoder with the more expressive MatNet encoder [77] already improves the average makespan by around 7%. Further improvements can be achieved by replacing the MLP decoder with the Pointer mechanism in the AM decoder [74] with gaps to BKS around 3× lower compared to the original policy in Song et al. [125] even with greedy performance.

5.2 Constructive Policies

Mind Your Baseline. In on-policy RL, which is often employed in RL4CO due to fast reward function evaluations, several different REINFORCE baselines have been proposed to improve the performance. We benchmark several RL algorithms training constructive policies for routing problems of node size 50, whose underlying architecture is based on the encoder-decoder Attention Model [74] and whose main difference lies in how the REINFORCE baseline is calculated (we additionally train the AM with PPO as further reference). For a fair comparison, we run all baselines in controlled settings with the same number of optimization steps and report results in [Table 3](#). We note that A2C generally underperforms other baselines. Such performance can be attributed to the fact that since in routing problems, the rewards are sparse (i.e., can only be calculated upon solving an entire problem), estimating the value of an entire instance x is inherently a challenging task.

Table 3: Optimality Gap obtained via greedy decoding.

Method	TSP	CVRP	OP	PCTSP	PDP
A2C	2.22	7.09	8.64	14.96	10.02
AM-Rollout	1.41	5.30	4.40	2.46	9.88
POMO	0.89	3.99	14.26	11.61	10.64
Sym-NCO	0.47	4.61	3.09	2.12	7.73
AM-PPO	0.92	4.60	3.05	2.45	8.31

of nodes should be selected in an optimal solution, while several states will be discarded. Hence, forcing the policy to select all of them makes up for a poor baseline. We remark that while SymNCO (whose shared baseline involves symmetric rotations and flips) [69] may perform well in Euclidean problems, this is not applicable in non-Euclidean CO, including asymmetric routing problems and scheduling. We found similar trends regarding actor-critic methods as A2C and PPO in the EDA mDPP problem [67], which we report in [Appendix](#). Namely, a greedy rollout baseline [74] can do better than value-based methods due to the challenging task of instance value estimation.

Decoding Schemes. The solution quality of different solvers often shows significant improvements in performance with different decoding schemes. We evaluate the pre-trained solver with different strategies and settings as shown in [Fig. 4](#).

Table 2: Solutions obtained with RL4CO for the FJSSP with different model configurations.

Encoder / Decoder	FJSSP	
	10×5	20×5
HGNN + MLP (g.) [125]	Obj. Gap	111.82 15.8%
MatNet + MLP (g.)	Obj. Gap	103.91 7.6%
MatNet + Pointer (g.)	Obj. Gap	101.17 4.8%
MatNet + Pointer (s. x128)	Obj. Gap	98.31 1.8%
		191.21 12.1%
		197.92 5.0%
		196.3 4.2%
		192.02 1.9%

Interestingly, while POMO [76], which takes as a baseline the shared baseline of all routes forcing each starting node to be different, may work well as baselines for problems in which near-optimal solutions can be constructed from any node (e.g., TSP), this may not be true for other problems such as the Orienteering Problem (OP): the reason is that in OP only a *subset*

²The different model configurations shown here can be obtained by simply changing the Hydra configuration file like the one shown in [Appendix](#).

Generalization. Using RL4CO, we can easily evaluate the generalization performance of existing baselines by employing supported environments that incorporate various VRP variant tasks and instance distributions (termed MTPOMO and MDPMO, respectively). Empirical results on CVRPLib, shown in Table 4, reveal that training on different tasks significantly enhances generalization performance. This finding underscores the necessity of building foundation models across diverse CO domains.

Large-Scale Instances. We evaluate large-scale CVRP instances of thousands of nodes, with more visualizations and scaling in Appendix. The last row of Table 5 illustrates the performance of the hybrid NAR/AR GLOP [152], while others refer to reproduced results from Ye et al. [152]. Our implementation in RL4CO improves the performance in not only speed but also solution quality.

Table 4: Results on CVRPLIB instances with models trained on $N = 50$. Greedy multi-start decoding is used.

	POMO		MTPOMO		MDPMO	
	Obj.	Gap	Obj.	Gap	Obj.	Gap
Set A	1075	3.13%	1076	3.20%	1074	2.97%
Set B	996	3.41%	1003	4.06%	995	3.26%
Set E	761	5.04%	760	4.82%	762	5.07%
Set F	813	13.52%	798	12.09%	825	13.66%
Set M	1259	16.37%	1234	13.58%	1263	16.03%
Set P	620	6.72%	608	3.72%	613	5.04%
Set X	73953	16.80%	73763	16.69%	81848	23.69%

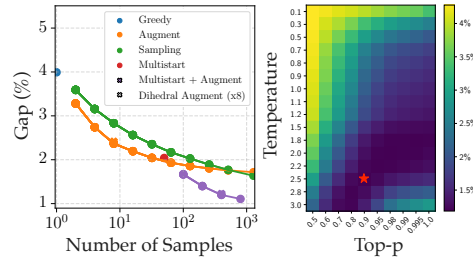


Figure 4: Decoding schemes study of POMO on CVRP50. [Left]: Pareto front of decoding schemes by the number of samples; [Right]: performance of sampling with different temperatures τ and p values for top- p sampling.

Table 5: Performance on large-scale CVRP instances with thousands of nodes.

	CVRP1K		CVRP2K		CVRP7K	
	Obj.	Time	Obj.	Time	Obj.	Time
LKH-3	46.4	6.2	64.9	20	245.0	501
AM	61.4	0.6	114.4	1.9	354.3	26
TAM (AM)	50.1	0.8	74.3	2.2	233.4	26
TAM (LKH-3)	46.3	1.8	64.8	5.6	196.9	33
GLOP-G (AM)*	47.1	0.4	63.5	1.2	191.7	2.4
GLOP-G (LKH-3)*	45.9	1.1	63.0	1.5	191.2	5.8
GLOP-G (AM)	46.9	0.3	64.7	0.7	190.9	2.0
GLOP-G (LKH-3)	45.5	0.5	62.8	0.8	190.1	3.9

5.3 Combining Construction and Improvement: Best of Both Worlds?

While constructive policies can build solutions in seconds, their performance is often limited, even with advanced decoding schemes such as sampling or augmentations. On the other hand, improvement methods are more suitable for larger computing budgets. We benchmark models on TSP with 50 nodes: the AR constructive method POMO [76] and the improvement methods DACT [96] and NeuOpt [98]. In the original implementation, DACT and NeuOpt started from a solution constructed randomly. To further demonstrate the flexibility of RL4CO, we show that bootstrapping improvement methods with constructive ones enhance convergence speed. Fig. 5 shows that bootstrapping with a pre-trained POMO policy significantly enhances the convergence speed. To further investigate the performance, we report the Primal Integral (PI) [12, 138, 133], which evaluates the evolution of solution quality over time. Improvement methods alone, such as DACT and NeuOpt, achieve 2.99 and 2.26 respectively, while sampling from POMO achieves 0.08. This shows that the “area under the curve” can be better even if the final solution is worse for constructive methods. Bootstrapping with POMO then improves DACT and NeuOpt to 0.08 and 0.04 respectively, showing the benefits of modularity and hybridization of different components.

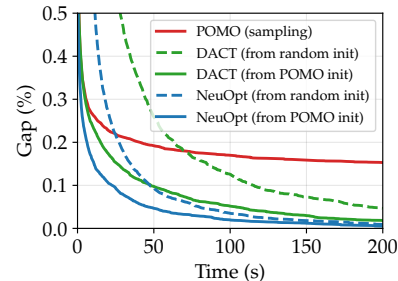


Figure 5: Bootstrapping improvement with constructive methods.

6 Discussion

6.1 Limitations and Future Directions

While RL4CO is an efficient and modular library specialized in CO problems, it might not be suitable for any other task due to a number of area-specific optimizations, and we do not expect

it to seamlessly integrate with, for instance, OpenAI Gym wrappers without some modifications. Another limitation of the library is its scope so far, namely RL. In fact, extending the library to support supervised methods and creating a comprehensive "AI4CO" library could benefit the whole NCO community. We additionally identify in Foundation Models³ for CO and related scalable architectures a promising area of future research to overcome generalization issues across tasks and distributions, for which we provided some early clues.

6.2 Long-term Plans

Our long-term plan is to become the go-to RL for CO benchmark library. While not strictly tied to implementation and benchmarking, we are committed to helping resolve issues and questions from the community. For this purpose, we created a Slack workspace (link available in the online documentation) that by now has attracted more than 130 researchers. It is our hope that our work will ultimately benefit the NCO field with new ideas and collaborations.

7 Conclusion

This paper introduces RL4CO, a modular, flexible, and unified Reinforcement Learning (RL) for Combinatorial Optimization (CO) benchmark. We provide a comprehensive taxonomy from environments to policies and RL algorithms that translate from theory to practice to software level. Our benchmark library aims to fill the gap in unifying implementations in RL for CO by utilizing several best practices with the goal of providing researchers and practitioners with a flexible starting point for NCO research. We provide several experimental results with insights and discussions that can help identify promising research directions. We hope that our open-source library will provide a solid starting point for NCO researchers to explore new avenues and drive advancements. We warmly welcome researchers and practitioners to actively participate and contribute to RL4CO.

Acknowledgements

We want to express our gratitude towards anonymous reviewers of previous submissions who greatly helped us improve our paper. Even though rejections were not easy at first, they helped us refine our benchmark. Importantly, through our journey, we got to know several outstanding researchers in the community, who gave us even more motivation and meaning behind our work. We would also like to thank people in the AI4CO open research community who have contributed, and those who will, to RL4CO. We also thank OMELET for supporting us with additional computing. A special thanks also goes to the TorchRL team for helping us in solving issues and improving the library. We invite practitioners and researchers to join us and contribute with bug reporting, feature requests, or collaboration ideas, for which we are (in advance) thankful for.

Potential Broader Impact

This paper presents work in the field of AI4CO. The main consequence may be that AI methods to solve CO problems may become accessible to the broad public, as our library is open source and readily available on GitHub. As such, we do not see any potential negative societal consequence.

Funding

This work was supported by the Institute of Information & communications Technology Planning & Evaluation (IITP) grant funded by the Korean government(MSIT)[2022-0-01032, Development of Collective Collaboration Intelligence Framework for Internet of Autonomous Things].

³<https://github.com/ai4co/awesome-fm4co>

References

- [1] L. Accorsi, A. Lodi, and D. Vigo. Guidelines for the computational testing of machine learning approaches to vehicle routing problems. *Operations Research Letters*, 50(2):229–234, 2022.
- [2] A. AhmadiTeshnizi, W. Gao, and M. Udell. OptiMUS: Scalable optimization modeling with (MI)LP solvers and large language models. In *International Conference on Machine Learning*, 2024.
- [3] S. Ahn, Y. Seo, and J. Shin. Learning what to defer for maximum independent sets. In *International Conference on Machine Learning*, pages 134–144. PMLR, 2020.
- [4] K. Ali, W. Alsalih, and H. Hassanein. Set-cover approximation algorithms for load-aware readers placement in RFID networks. In *2011 IEEE international conference on communications (ICC)*, pages 1–6. IEEE, 2011.
- [5] B. Balaji, J. Bell-Masterson, E. Bilgin, A. Damianou, P. M. Garcia, A. Jain, R. Luo, A. Maggiar, B. Narayanaswamy, and C. Ye. Orl: Reinforcement learning benchmarks for online stochastic optimization problems. *arXiv preprint arXiv:1911.10641*, 2019.
- [6] E. Balas. The prize collecting traveling salesman problem. *Networks*, 19(6):621–636, 1989.
- [7] A. Bdeir, J. K. Falkner, and L. Schmidt-Thieme. Attention, filling in the gaps for generalization in routing problems. In *Joint European Conference on Machine Learning and Knowledge Discovery in Databases*, pages 505–520. Springer, 2022.
- [8] I. Bello, H. Pham, Q. V. Le, M. Norouzi, and S. Bengio. Neural combinatorial optimization with reinforcement learning, 2017.
- [9] E. Bengio, M. Jain, M. Korablyov, D. Precup, and Y. Bengio. Flow network based generative models for non-iterative diverse candidate generation. *Advances in Neural Information Processing Systems*, 34:27381–27394, 2021.
- [10] Y. Bengio, A. Lodi, and A. Prouvost. Machine learning for combinatorial optimization: a methodological tour d’horizon. *European Journal of Operational Research*, 290(2):405–421, 2021.
- [11] Y. Bengio, S. Lahlou, T. Deleu, E. J. Hu, M. Tiwari, and E. Bengio. Gflownet foundations. *Journal of Machine Learning Research*, 24(210):1–55, 2023.
- [12] T. Berthold. Measuring the impact of primal heuristics. *Operations Research Letters*, 41(6):611–614, 2013.
- [13] F. Berto, C. Hua, N. G. Zepeda, A. Hottung, N. Wouda, L. Lan, K. Tierney, and J. Park. RouteFinder: Towards foundation models for vehicle routing problems. *Arxiv*, 2024. URL <https://github.com/ai4co/routefinder>.
- [14] K. Bestuzheva, M. Besançon, W.-K. Chen, A. Chmiela, T. Donkiewicz, J. van Doornmalen, L. Eifler, O. Gaul, G. Gamrath, A. Gleixner, et al. The SCIP optimization suite 8.0. *arXiv 2112.08872*, 2021.
- [15] M. Bettini, A. Prorok, and V. Moens. Benchmarl: Benchmarking multi-agent reinforcement learning. *arXiv preprint arXiv:2312.01472*, 2023.
- [16] J. Bi, Y. Ma, J. Wang, Z. Cao, J. Chen, Y. Sun, and Y. M. Chee. Learning generalizable models for vehicle routing problems via knowledge distillation. *Advances in Neural Information Processing Systems*, 35:31226–31238, 2022.
- [17] D. Biagioni, C. E. Tripp, S. Clark, D. Duplyakin, J. Law, and P. C. S. John. graphenv: a python library for reinforcement learning on graph search spaces. *Journal of Open Source Software*, 7(77):4621, 2022.
- [18] L. Bodin. Routing and scheduling of vehicles and crews. *Computer & Operations Research*, 10(2):69–211, 1983.

- [19] C. Bonnet, D. Luo, D. Byrne, S. Surana, S. Abramowitz, P. Duckworth, V. Coyette, L. I. Midgley, E. Tegegn, T. Kalloniatis, O. Mahjoub, M. Macfarlane, A. P. Smit, N. Grinsztajn, R. Boige, C. N. Waters, M. A. Mimouni, U. A. M. Sob, R. de Kock, S. Singh, D. Furelos-Blanco, V. Le, A. Pretorius, and A. Laterre. Jumanji: a diverse suite of scalable reinforcement learning environments in jax. In *International Conference on Learning Representations*, 2024.
- [20] A. Bou, M. Bettini, S. Dittert, V. Kumar, S. Sodhani, X. Yang, G. D. Fabritiis, and V. Moens. TorchRL: A data-driven decision-making library for pytorch. In *International conference on learning representations*, 2024.
- [21] J. Bradbury, R. Frostig, P. Hawkins, M. J. Johnson, C. Leary, D. Maclaurin, G. Necula, A. Paszke, J. VanderPlas, S. Wanderman-Milne, and Q. Zhang. JAX: composable transformations of Python+NumPy programs, 2018. URL <http://github.com/google/jax>.
- [22] P. Brandimarte. Routing and scheduling in a flexible job shop by tabu search. *Annals of Operations research*, 41(3):157–183, 1993.
- [23] G. Brockman, V. Cheung, L. Pettersson, J. Schneider, J. Schulman, J. Tang, and W. Zaremba. Openai gym. *arXiv preprint arXiv:1606.01540*, 2016.
- [24] S. Brody, U. Alon, and E. Yahav. How attentive are graph attention networks? In *International Conference on Learning Representations*, 2019.
- [25] F. Bu, H. Jo, S. Y. Lee, S. Ahn, and K. Shin. Tackling prevalent conditions in unsupervised combinatorial optimization: Cardinality, minimum, covering, and more. In *International Conference on Machine Learning*, 2024.
- [26] B. Çatay. Ant colony optimization and its application to the vehicle routing problem with pickups and deliveries. In *Natural intelligence for scheduling, Planning and packing problems*, pages 219–244. Springer, 2009.
- [27] F. Chalumeau, S. Surana, C. Bonnet, N. Grinsztajn, A. Pretorius, A. Laterre, and T. Barrett. Combinatorial optimization with policy adaptation using latent space search. *Advances in Neural Information Processing Systems*, 36, 2024.
- [28] I.-M. Chao, B. L. Golden, and E. A. Wasil. A fast and effective heuristic for the orienteering problem. *European journal of operational research*, 88(3):475–489, 1996.
- [29] J. Chen, Z. Zhang, Z. Cao, Y. Wu, Y. Ma, T. Ye, and J. Wang. Neural multi-objective combinatorial optimization with diversity enhancement. *Advances in Neural Information Processing Systems*, 36, 2024.
- [30] X. Chen and Y. Tian. Learning to perform local rewriting for combinatorial optimization. In *Advances in Neural Information Processing Systems*, 2019.
- [31] H. Dai, E. B. Khalil, Y. Zhang, B. Dilkina, and L. Song. Learning combinatorial optimization algorithms over graphs. In *Advances in Neural Information Processing Systems*, volume 30, 2017.
- [32] S. Dalton et al. Accelerating reinforcement learning through gpu atari emulation. *Advances in Neural Information Processing Systems*, 33:19773–19782, 2020.
- [33] T. Dao. FlashAttention-2: Faster attention with better parallelism and work partitioning. *arXiv preprint arXiv:2307.08691*, 2023.
- [34] T. Dao, D. Fu, S. Ermon, A. Rudra, and C. Ré. Flashattention: Fast and memory-efficient exact attention with io-awareness. *Advances in Neural Information Processing Systems*, 35: 16344–16359, 2022.
- [35] V. C. David Applegate, Robert Bixby and W. Cook. Concorde TSP solver, 2023. URL <https://www.math.uwaterloo.ca/tsp/concorde/index.html>.
- [36] M. Dorigo and T. Stützle. *Ant colony optimization: overview and recent advances*. Springer, 2019.

- [37] D. Drakulic, S. Michel, F. Mai, A. Sors, and J.-M. Andreoli. BQ-NCO: Bisimulation quotienting for generalizable neural combinatorial optimization. *Advances in Neural Information Processing Systems*, 2023.
- [38] Z. Drezner and H. W. Hamacher. *Facility location: applications and theory*. Springer Science & Business Media, 2004.
- [39] W. Falcon and The PyTorch Lightning team. PyTorch Lightning, 3 2019. URL <https://github.com/Lightning-AI/lightning>.
- [40] J. K. Falkner and L. Schmidt-Thieme. Learning to solve vehicle routing problems with time windows through joint attention. *arXiv preprint arXiv:2006.09100*, 2020.
- [41] M. Fischetti, J. J. S. Gonzalez, and P. Toth. Solving the orienteering problem through branch-and-cut. *INFORMS Journal on Computing*, 10(2):133–148, 1998.
- [42] C. D. Freeman, E. Frey, A. Raichuk, S. Girgin, I. Mordatch, and O. Bachem. Brax - a differentiable physics engine for large scale rigid body simulation, 2021. URL <http://github.com/google/brax>.
- [43] N. Grinsztajn, D. Furelos-Blanco, S. Surana, C. Bonnet, and T. Barrett. Winner takes it all: Training performant rl populations for combinatorial optimization. *Advances in Neural Information Processing Systems*, 36:48485–48509, 2023.
- [44] L. Gurobi Optimization. Gurobi optimizer reference manual, 2021. URL <http://www.gurobi.com>.
- [45] W. Hamilton, Z. Ying, and J. Leskovec. Inductive representation learning on large graphs. *Advances in neural information processing systems*, 30, 2017.
- [46] K. Helsgaun. An extension of the Lin-Kernighan-Helsgaun TSP solver for constrained traveling salesman and vehicle routing problems. *Roskilde: Roskilde University*, 12 2017. doi: 10.13140/RG.2.2.25569.40807.
- [47] S. Hochreiter and J. Schmidhuber. Long short-term memory. *Neural computation*, 9(8):1735–1780, 1997.
- [48] A. Holtzman, J. Buys, L. Du, M. Forbes, and Y. Choi. The curious case of neural text degeneration. *arXiv preprint arXiv:1904.09751*, 2019.
- [49] A. Hottung, B. Bhandari, and K. Tierney. Learning a latent search space for routing problems using variational autoencoders. In *International Conference on Learning Representations*, 2020.
- [50] A. Hottung, Y.-D. Kwon, and K. Tierney. Efficient active search for combinatorial optimization problems. *International conference on learning representations*, 2022.
- [51] A. Hottung, M. Mahajan, and K. Tierney. PolyNet: Learning diverse solution strategies for neural combinatorial optimization. *arXiv preprint arXiv:2402.14048*, 2024.
- [52] Y. Hou, H. Ye, Y. Zhang, S. Xu, and G. Song. Routeplacer: An end-to-end routability-aware placer with graph neural network. In *Proceedings of the 30th ACM SIGKDD Conference on Knowledge Discovery and Data Mining*, 2024.
- [53] C. D. Hubbs, H. D. Perez, O. Sarwar, N. V. Sahinidis, I. E. Grossmann, and J. M. Wassick. OR-Gym: A reinforcement learning library for operations research problems. *arXiv preprint arXiv:2008.06319*, 2020.
- [54] J. Hwang, J. S. Pak, D. Yoon, H. Lee, J. Jeong, Y. Heo, and I. Kim. Enhancing on-die pdn for optimal use of package pdn with decoupling capacitor. In *2021 IEEE 71st Electronic Components and Technology Conference (ECTC)*, pages 1825–1830, 2021. doi: 10.1109/ECTC32696.2021.00288.
- [55] Z. Iklassov, Y. Du, F. Akimov, and M. Takac. Self-guiding exploration for combinatorial problems. *arXiv preprint arXiv:2405.17950*, 2024.

- [56] S. Ioffe and C. Szegedy. Batch normalization: Accelerating deep network training by reducing internal covariate shift. In *International conference on machine learning*, pages 448–456. pmlr, 2015.
- [57] R. A. Jacobs, M. I. Jordan, S. J. Nowlan, and G. E. Hinton. Adaptive mixtures of local experts. *Neural computation*, 3(1):79–87, 1991.
- [58] A. D. Jesus, A. Liefoghe, B. Derbel, and L. Paquete. Algorithm selection of anytime algorithms. In *Proceedings of the 2020 genetic and evolutionary computation conference*, pages 850–858, 2020.
- [59] Y. Jiang, Y. Wu, Z. Cao, and J. Zhang. Learning to solve routing problems via distributionally robust optimization. In *36th AAAI Conference on Artificial Intelligence*, 2022.
- [60] M. I. Jordan and R. A. Jacobs. Hierarchical mixtures of experts and the em algorithm. *Neural computation*, 6(2):181–214, 1994.
- [61] C. K. Joshi, T. Laurent, and X. Bresson. An efficient graph convolutional network technique for the travelling salesman problem. *arXiv preprint arXiv:1906.01227*, 2019.
- [62] J. Juang, L. Zhang, Z. Kiguradze, B. Pu, S. Jin, and C. Hwang. A modified genetic algorithm for the selection of decoupling capacitors in pdn design. In *2021 IEEE International Joint EMC/SI/PI and EMC Europe Symposium*, pages 712–717, 2021. doi: 10.1109/EMC/SI/PI/EMCEurope52599.2021.9559292.
- [63] B. Kalantari, A. V. Hill, and S. R. Arora. An algorithm for the traveling salesman problem with pickup and delivery customers. *European Journal of Operational Research*, 22(3):377–386, 1985.
- [64] E. Khalil, H. Dai, Y. Zhang, B. Dilkina, and L. Song. Learning combinatorial optimization algorithms over graphs. *Advances in neural information processing systems*, 30, 2017.
- [65] S. Khuller, A. Moss, and J. S. Naor. The budgeted maximum coverage problem. *Information processing letters*, 70(1):39–45, 1999.
- [66] D. Kikuta, H. Ikeuchi, K. Tajiri, and Y. Nakano. RouteExplainer: An explanation framework for vehicle routing problem. In *Pacific-Asia Conference on Knowledge Discovery and Data Mining*, pages 30–42. Springer, 2024.
- [67] H. Kim, M. Kim, F. Berto, J. Kim, and J. Park. DevFormer: A symmetric transformer for context-aware device placement. *International Conference on Machine Learning*, 2023.
- [68] M. Kim, J. Park, and J. Kim. Learning collaborative policies to solve NP-hard routing problems. In *Advances in Neural Information Processing Systems*, 2021.
- [69] M. Kim, J. Park, and J. Park. Sym-NCO: Leveraging symmetry for neural combinatorial optimization. *Advances in Neural Information Processing Systems*, 2022.
- [70] M. Kim, S. Choi, J. Son, H. Kim, J. Park, and Y. Bengio. Ant colony sampling with GFlowNets for combinatorial optimization. *arXiv preprint arXiv:2403.07041*, 2024.
- [71] D. P. Kingma and J. Ba. Adam: A method for stochastic optimization. *arXiv preprint arXiv:1412.6980*, 2014.
- [72] T. N. Kipf and M. Welling. Semi-supervised classification with graph convolutional networks. In *International Conference on Learning Representations*, 2017.
- [73] V. Konda and J. Tsitsiklis. Actor-critic algorithms. *Advances in neural information processing systems*, 12, 1999.
- [74] W. Kool, H. Van Hoof, and M. Welling. Attention, learn to solve routing problems! *International Conference on Learning Representations*, 2019.

- [75] W. Kool, H. Van Hoof, and M. Welling. Stochastic beams and where to find them: The gumbel-top-k trick for sampling sequences without replacement. In *International Conference on Machine Learning*, pages 3499–3508. PMLR, 2019.
- [76] Y.-D. Kwon, J. Choo, B. Kim, I. Yoon, Y. Gwon, and S. Min. POMO: Policy optimization with multiple optima for reinforcement learning. *Advances in Neural Information Processing Systems*, 33:21188–21198, 2020.
- [77] Y.-D. Kwon, J. Choo, I. Yoon, M. Park, D. Park, and Y. Gwon. Matrix encoding networks for neural combinatorial optimization. *Advances in Neural Information Processing Systems*, 34: 5138–5149, 2021.
- [78] G. Laporte and S. Martello. The selective travelling salesman problem. *Discrete applied mathematics*, 26(2-3):193–207, 1990.
- [79] E. Lawler, J. Lenstra, A. R. Kan, and D. Shmoys. The traveling salesman problem: A guided tour of combinatorial optimization. *The Journal of the Operational Research Society*, 37(5): 535, 1986.
- [80] F. Li, B. Golden, and E. Wasil. The open vehicle routing problem: Algorithms, large-scale test problems, and computational results. *Computers & Operations Research*, 34(10):2918–2930, 2007. ISSN 0305-0548. doi: <https://doi.org/10.1016/j.cor.2005.11.018>.
- [81] G. Li, C. Xiong, A. Thabet, and B. Ghanem. Deepgcn: All you need to train deeper gcns. *arXiv preprint arXiv:2006.07739*, 2020.
- [82] J. Li, L. Xin, Z. Cao, A. Lim, W. Song, and J. Zhang. Heterogeneous attentions for solving pickup and delivery problem via deep reinforcement learning. *IEEE Transactions on Intelligent Transportation Systems*, 23(3):2306–2315, 2021.
- [83] J. Li, Y. Ma, Z. Cao, Y. Wu, W. Song, J. Zhang, and Y. M. Chee. Learning feature embedding refiner for solving vehicle routing problems. *IEEE Transactions on Neural Network and Learning Systems*, 2023.
- [84] S. Li, Y. Zhao, R. Varma, O. Salpekar, P. Noordhuis, T. Li, A. Paszke, J. Smith, B. Vaughan, P. Damania, et al. Pytorch distributed: Experiences on accelerating data parallel training. *arXiv preprint arXiv:2006.15704*, 2020.
- [85] E. Liang, R. Liaw, R. Nishihara, P. Moritz, R. Fox, J. Gonzalez, K. Goldberg, and I. Stoica. Ray rllib: A composable and scalable reinforcement learning library. *arXiv preprint arXiv:1712.09381*, 85, 2017.
- [86] I. Lima, E. Uchoa, D. Pecin, A. Pessoa, M. Poggi, T. Vidal, A. Subramanian, R. W. D. Oliveira, and E. Queiroga. CVRPLIB: Capacitated vehicle routing problem library, 2014. URL <http://vrp.galgos.inf.puc-rio.br/index.php/en/>. Last checked on October 6, 2024.
- [87] X. Lin, Z. Yang, and Q. Zhang. Pareto set learning for neural multi-objective combinatorial optimization. *arXiv preprint arXiv:2203.15386*, 2022.
- [88] J. T. Linderoth, A. Lodi, et al. Milp software. *Wiley encyclopedia of operations research and management science*, 5:3239–3248, 2010.
- [89] F. Liu, X. Lin, Q. Zhang, X. Tong, and M. Yuan. Multi-task learning for routing problem with cross-problem zero-shot generalization. In *Proceedings of the 30th ACM SIGKDD Conference on Knowledge Discovery and Data Mining*, 2024.
- [90] F. Liu, X. Tong, M. Yuan, X. Lin, F. Luo, Z. Wang, Z. Lu, and Q. Zhang. Evolution of heuristics: Towards efficient automatic algorithm design using large language model. In *International Conference on Machine Learning*, 2024.
- [91] S. Liu, C. Chen, X. Qu, K. Tang, and Y.-S. Ong. Large language models as evolutionary optimizers. *arXiv preprint arXiv:2310.19046*, 2023.

- [92] R. Lotfi, A. Mostafaeipour, N. Mardani, and S. Mardani. Investigation of wind farm location planning by considering budget constraints. *International Journal of Sustainable Energy*, 37(8):799–817, 2018.
- [93] F. Luo, X. Lin, F. Liu, Q. Zhang, and Z. Wang. Neural combinatorial optimization with heavy decoder: Toward large scale generalization. *Advances in Neural Information Processing Systems*, 36, 2024.
- [94] F. Luo, X. Lin, Z. Wang, T. Xialiang, M. Yuan, and Q. Zhang. Self-improved learning for scalable neural combinatorial optimization. *arXiv preprint arXiv:2403.19561*, 2024.
- [95] L. Luttmann and L. Xie. Neural combinatorial optimization on heterogeneous graphs: An application to the picker routing problem in mixed-shelves warehouses. In *Proceedings of the International Conference on Automated Planning and Scheduling*, volume 34, pages 351–359, 2024.
- [96] Y. Ma, J. Li, Z. Cao, W. Song, L. Zhang, Z. Chen, and J. Tang. Learning to iteratively solve routing problems with dual-aspect collaborative transformer. *Advances in Neural Information Processing Systems*, 34, 2021.
- [97] Y. Ma, J. Li, Z. Cao, W. Song, H. Guo, Y. Gong, and Y. M. Chee. Efficient neural neighborhood search for pickup and delivery problems. *arXiv preprint arXiv:2204.11399*, 2022.
- [98] Y. Ma, Z. Cao, and Y. M. Chee. Learning to search feasible and infeasible regions of routing problems with flexible neural k-opt. *Advances in Neural Information Processing Systems*, 36, 2024.
- [99] V. Makoviychuk, L. Wawrzyniak, Y. Guo, M. Lu, K. Storey, M. Macklin, D. Hoeller, N. Rudin, A. Allshire, A. Handa, and G. State. I: High performance GPU-based physics simulation for robot learning, 2021.
- [100] S. Manchanda, S. Michel, D. Drakulic, and J.-M. Andreoli. On the generalization of neural combinatorial optimization heuristics. In *Machine Learning and Knowledge Discovery in Databases: European Conference, ECML PKDD 2022, Grenoble, France, September 19–23, 2022, Proceedings, Part V*, pages 426–442. Springer, 2023.
- [101] V. Marianov, D. Serra, et al. Location problems in the public sector. *Facility location: Applications and theory*, 1:119–150, 2002.
- [102] Y. Min, Y. Bai, and C. P. Gomes. Unsupervised learning for solving the travelling salesman problem. In *Neural Information Processing Systems*, 2023.
- [103] V. Mnih, K. Kavukcuoglu, D. Silver, A. A. Rusu, J. Veness, M. G. Bellemare, A. Graves, M. Riedmiller, A. K. Fidjeland, G. Ostrovski, et al. Human-level control through deep reinforcement learning. *nature*, 518(7540):529–533, 2015.
- [104] V. Moens. TensorDict: your PyTorch universal data carrier, 2023. URL <https://github.com/pytorch-labs/tensordict>.
- [105] A. T. Murray, K. Kim, J. W. Davis, R. Machiraju, and R. Parent. Coverage optimization to support security monitoring. *Computers, Environment and Urban Systems*, 31(2):133–147, 2007.
- [106] M. Nazari, A. Oroojlooy, L. Snyder, and M. Takáć. Reinforcement learning for solving the vehicle routing problem. *Advances in neural information processing systems*, 31, 2018.
- [107] M. Pagliardini, D. Paliotta, M. Jaggi, and F. Fleuret. Faster causal attention over large sequences through sparse flash attention. *arXiv preprint arXiv:2306.01160*, 2023.
- [108] H. Park, H. Kim, H. Kim, J. Park, S. Choi, J. Kim, K. Son, H. Suh, T. Kim, J. Ahn, et al. Versatile genetic algorithm-bayesian optimization (ga-bo) bi-level optimization for decoupling capacitor placement. In *2023 IEEE 32nd Conference on Electrical Performance of Electronic Packaging and Systems (EPEPS)*, pages 1–3. IEEE, 2023.

- [109] J. Park, C. Kwon, and J. Park. Learn to solve the min-max multiple traveling salesmen problem with reinforcement learning. In *Proceedings of the 2023 International Conference on Autonomous Agents and Multiagent Systems*, pages 878–886, 2023.
- [110] A. Paszke, S. Gross, F. Massa, A. Lerer, J. Bradbury, G. Chanan, T. Killeen, Z. Lin, N. Gimelshein, L. Antiga, et al. PyTorch: An imperative style, high-performance deep learning library. *Advances in neural information processing systems*, 32, 2019.
- [111] L. Perron and V. Furnon. OR-Tools, 2023. URL <https://developers.google.com/optimization/>.
- [112] J. Pirnay and D. G. Grimm. Self-improvement for neural combinatorial optimization: Sample without replacement, but improvement. *arXiv preprint arXiv:2403.15180*, 2024.
- [113] A. Prouvost, J. Dumouchelle, L. Scavuzzo, M. Gasse, D. Chételat, and A. Lodi. Ecole: A gym-like library for machine learning in combinatorial optimization solvers. In *Learning Meets Combinatorial Algorithms at NeurIPS2020*, 2020. URL <https://openreview.net/forum?id=IVc9hqgibyB>.
- [114] A. Raffin, A. Hill, A. Gleave, A. Kanervisto, M. Ernestus, and N. Dormann. Stable-baselines3: Reliable reinforcement learning implementations. *Journal of Machine Learning Research*, 22(268):1–8, 2021. URL <http://jmlr.org/papers/v22/20-1364.html>.
- [115] G. K. Rand. Sequencing and scheduling: An introduction to the mathematics of the jobshop. *Journal of the Operational Research Society*, 33:862, 1982. URL <https://api.semanticscholar.org/CorpusID:62592932>.
- [116] G. Reinelt. Tsplib—a traveling salesman problem library. *ORSA journal on computing*, 3(4):376–384, 1991.
- [117] B. Romera-Paredes, M. Barekatain, A. Novikov, M. Balog, M. P. Kumar, E. Dupont, F. J. Ruiz, J. S. Ellenberg, P. Wang, O. Fawzi, et al. Mathematical discoveries from program search with large language models. *Nature*, 625(7995):468–475, 2024.
- [118] M. W. Savelsbergh and M. Sol. The general pickup and delivery problem. *Transportation science*, 29(1):17–29, 1995.
- [119] J. Schulman, F. Wolski, P. Dhariwal, A. Radford, and O. Klimov. Proximal policy optimization algorithms. *arXiv preprint arXiv:1707.06347*, 2017.
- [120] W. Shan, Q. Yan, C. Chen, M. Zhang, B. Yao, and X. Fu. Optimization of competitive facility location for chain stores. *Annals of Operations research*, 273:187–205, 2019.
- [121] N. Shazeer, A. Mirhoseini, K. Maziarz, A. Davis, Q. Le, G. Hinton, and J. Dean. Outrageously large neural networks: The sparsely-gated mixture-of-experts layer. In *International Conference on Learning Representations*, 2017.
- [122] J. Son, M. Kim, H. Kim, and J. Park. Meta-SAGE: Scale meta-learning scheduled adaptation with guided exploration for mitigating scale shift on combinatorial optimization. In *Proceedings of the 40th International Conference on Machine Learning*, volume 202, pages 32194–32210. PMLR, 2023.
- [123] J. Son, M. Kim, S. Choi, H. Kim, and J. Park. Equity-Transformer: Solving NP-hard min-max routing problems as sequential generation with equity context. In *Proceedings of the AAAI Conference on Artificial Intelligence*, volume 38, pages 20265–20273, 2024.
- [124] J. Song, Y. Yue, B. Dilkina, et al. A general large neighborhood search framework for solving integer linear programs. *Advances in Neural Information Processing Systems*, 33:20012–20023, 2020.
- [125] W. Song, X. Chen, Q. Li, and Z. Cao. Flexible job-shop scheduling via graph neural network and deep reinforcement learning. *IEEE Transactions on Industrial Informatics*, 19(2):1600–1610, 2022.

- [126] L. Sun, W. Huang, P. S. Yu, and W. Chen. Multi-round influence maximization. In *Proceedings of the 24th ACM SIGKDD international conference on knowledge discovery & data mining*, pages 2249–2258, 2018.
- [127] Z. Sun and Y. Yang. DIFUSCO: Graph-based diffusion solvers for combinatorial optimization. In *Advances in Neural Information Processing Systems*, volume 36, pages 3706–3731, 2023.
- [128] R. S. Sutton, D. McAllester, S. Singh, and Y. Mansour. Policy gradient methods for reinforcement learning with function approximation. *Advances in neural information processing systems*, 12, 1999.
- [129] E. Taillard. Benchmarks for basic scheduling problems. *european journal of operational research*, 64(2):278–285, 1993.
- [130] H. Tang, F. Berto, Z. Ma, C. Hua, K. Ahn, and J. Park. Himap: Learning heuristics-informed policies for large-scale multi-agent pathfinding. *arXiv preprint arXiv:2402.15546*, 2024.
- [131] H. Tang, F. Berto, and J. Park. Ensembling prioritized hybrid policies for multi-agent pathfinding. *arXiv preprint arXiv:2403.07559*, 2024.
- [132] P. Tassel, M. Gebser, and K. Schekotihin. A reinforcement learning environment for job-shop scheduling. *arXiv preprint arXiv:2104.03760*, 2021.
- [133] D. Thyssens, T. Dernedde, J. K. Falkner, and L. Schmidt-Thieme. Routing arena: A benchmark suite for neural routing solvers. *arXiv preprint arXiv:2310.04140*, 2023.
- [134] H. Touvron, T. Lavril, G. Izacard, X. Martinet, M.-A. Lachaux, T. Lacroix, B. Rozière, N. Goyal, E. Hambro, F. Azhar, et al. Llama: Open and efficient foundation language models. *arXiv preprint arXiv:2302.13971*, 2023.
- [135] D. Ulyanov, A. Vedaldi, and V. Lempitsky. Instance normalization: The missing ingredient for fast stylization. *arXiv preprint arXiv:1607.08022*, 2016.
- [136] A. Vaswani, N. Shazeer, N. Parmar, J. Uszkoreit, L. Jones, A. N. Gomez, Ł. Kaiser, and I. Polosukhin. Attention is all you need. *Advances in neural information processing systems*, 30, 2017.
- [137] P. Velickovic, G. Cucurull, A. Casanova, A. Romero, P. Lio, Y. Bengio, et al. Graph attention networks. *stat*, 1050(20):10–48550, 2017.
- [138] T. Vidal. Hybrid genetic search for the CVRP: Open-source implementation and SWAP* neighborhood. *Computers & Operations Research*, 140:105643, 2022.
- [139] O. Vinyals, M. Fortunato, and N. Jaitly. Pointer networks. In *Advances in Neural Information Processing Systems*, volume 28, pages 2692–2700, 2015.
- [140] C. P. Wan, T. Li, and J. M. Wang. RLOR: A flexible framework of deep reinforcement learning for operation research. *arXiv preprint arXiv:2303.13117*, 2023.
- [141] R. Wang, L. Shen, Y. Chen, X. Yang, D. Tao, and J. Yan. Towards one-shot neural combinatorial solvers: Theoretical and empirical notes on the cardinality-constrained case. In *The Eleventh International Conference on Learning Representations*, 2022.
- [142] S. Wasserkrug, L. Boussioux, D. d. Hertog, F. Mirzazadeh, I. Birbil, J. Kurtz, and D. Maragno. From large language models and optimization to decision optimization CoPilot: A research manifesto. *arXiv preprint arXiv:2402.16269*, 2024.
- [143] J. Weng, H. Chen, D. Yan, K. You, A. Duburcq, M. Zhang, Y. Su, H. Su, and J. Zhu. Tianshou: A highly modularized deep reinforcement learning library. *Journal of Machine Learning Research*, 23(267):1–6, 2022.
- [144] N. A. Wouda, L. Lan, and W. Kool. PyVRP: A high-performance vrp solver package. *INFORMS Journal on Computing*, 2024.

- [145] Y. Wu, W. Song, Z. Cao, J. Zhang, and A. Lim. Learning improvement heuristics for solving routing problems. *IEEE transactions on neural networks and learning systems*, 33(9):5057–5069, 2021.
- [146] Z. Xiao, D. Zhang, Y. Wu, L. Xu, Y. J. Wang, X. Han, X. Fu, T. Zhong, J. Zeng, M. Song, and G. Chen. Chain-of-experts: When LLMs meet complex operations research problems. In *International Conference on Learning Representations*, 2024.
- [147] L. Xin, W. Song, Z. Cao, and J. Zhang. Generative adversarial training for neural combinatorial optimization models, 2022. URL <https://openreview.net/forum?id=9vsRT9mc7U>.
- [148] O. Yadan. Hydra - a framework for elegantly configuring complex applications. Github, 2019. URL <https://github.com/facebookresearch/hydra>.
- [149] C. Yang, X. Wang, Y. Lu, H. Liu, Q. V. Le, D. Zhou, and X. Chen. Large language models as optimizers. In *International Conference on Learning Representations*, 2024.
- [150] H. Ye, J. Wang, Z. Cao, H. Liang, and Y. Li. DeepACO: Neural-enhanced ant systems for combinatorial optimization. *arXiv preprint arXiv:2309.14032*, 2023.
- [151] H. Ye, J. Wang, Z. Cao, F. Berto, C. Hua, H. Kim, J. Park, and G. Song. Large language models as hyper-heuristics for combinatorial optimization. *arXiv preprint arXiv:2402.01145*, 2024. <https://github.com/ai4co/LLM-as-HH>.
- [152] H. Ye, J. Wang, H. Liang, Z. Cao, Y. Li, and F. Li. GLOP: Learning global partition and local construction for solving large-scale routing problems in real-time. In *Proceedings of the AAAI Conference on Artificial Intelligence*, volume 38, pages 20284–20292, 2024.
- [153] C. Zhang, W. Song, Z. Cao, J. Zhang, P. S. Tan, and X. Chi. Learning to dispatch for job shop scheduling via deep reinforcement learning. *Advances in Neural Information Processing Systems*, 33:1621–1632, 2020.
- [154] D. Zhang, H. Dai, N. Malkin, A. C. Courville, Y. Bengio, and L. Pan. Let the flows tell: Solving graph combinatorial problems with gflownets. In A. Oh, T. Naumann, A. Globerson, K. Saenko, M. Hardt, and S. Levine, editors, *Advances in Neural Information Processing Systems*, volume 36, pages 11952–11969. Curran Associates, Inc., 2023.
- [155] Z. Zheng, S. Yao, Z. Wang, X. Tong, M. Yuan, and K. Tang. Dpn: Decoupling partition and navigation for neural solvers of min-max vehicle routing problems. *arXiv preprint arXiv:2405.17272*, 2024.
- [156] J. Zhou, Y. Wu, W. Song, Z. Cao, and J. Zhang. Towards omni-generalizable neural methods for vehicle routing problems. In *International Conference on Machine Learning*, 2023.
- [157] J. Zhou, Z. Cao, Y. Wu, W. Song, Y. Ma, J. Zhang, and C. Xu. MVMoE: Multi-task vehicle routing solver with mixture-of-experts. In *International Conference on Machine Learning*, 2024.

RL4CO: an Extensive Reinforcement Learning for Combinatorial Optimization Benchmark

Supplementary Material

Table of Contents

A	RL4CO Library: Additional Material	21
A.1	Why Choosing the RL4CO Library?	21
A.2	On the Choice of the Software	22
A.3	Licenses	22
B	Environments	22
B.1	Routing	23
B.1.1	Traveling Salesman Problem (TSP)	23
B.1.2	Capacitated Vehicle Routing Problem (CVRP)	23
B.1.3	Orienteering Problem (OP)	24
B.1.4	Prize Collecting TSP (PCTSP)	24
B.1.5	Pickup and Delivery Problem (PDP)	24
B.1.6	Multi-Task VRP (MTVRP)	25
B.2	Scheduling	27
B.2.1	Job Shop Scheduling Problem (JSSP)	27
B.2.2	Flexible Job Shop Scheduling Problem (FJSSP)	28
B.2.3	Flexible Flow Shop Problem (FFSP)	28
B.3	Electronic Design Automation	28
B.3.1	Decap Placement Problem (DPP)	29
B.3.2	Multi-Port Decap Placement Problem (mDPP)	29
B.4	Graph	29
B.4.1	Facility Location Problem (FLP)	30
B.4.2	Maximum Coverage Problem (MCP)	30
B.5	Additional Environments and Beyond	31
C	Baselines	31
C.1	General-purpose RL Algorithms	31
C.1.1	REINFORCE	31
C.1.2	Advantage Actor-Critic (A2C)	32
C.1.3	Proximal Policy Optimization (PPO)	32
C.2	Constructive Autoregressive (AR)	32
C.2.1	Attention Model (AM)	32
C.2.2	Ptr-Net	34
C.2.3	POMO	34
C.2.4	SymNCO	34
C.2.5	PolyNet	35
C.2.6	HAM	35
C.2.7	MTPOMO	35
C.2.8	MVMoE	35
C.2.9	L2D	36
C.2.10	HGNN	36
C.2.11	MatNet	36
C.2.12	DevFormer	37
C.3	Constructive Non-Autoregressive (NAR)	37
C.3.1	DeepACO	37
C.3.2	GFACS	38
C.3.3	GLOP	38
C.4	Improvement methods	39
C.4.1	DACT	39

C.4.2	N2S	39
C.4.3	NeuOpt	39
C.5	Active Search Methods	40
C.5.1	Active Search (AS)	40
C.5.2	Efficient Active Search (EAS)	40
D	Benchmarking Setup	40
D.1	Metrics	40
D.1.1	Gap to BKS	40
D.1.2	Primal Integral	40
D.1.3	Runtime Measurement	41
D.2	Hardware & Software	41
D.2.1	Hardware	41
D.2.2	Software	42
D.3	Hyperparameters	42
D.3.1	Common Hyperparameters	42
D.3.2	Changing Policy Components	42
D.3.3	Mind Your Baseline	42
D.3.4	Generalization: Cross-Task and Cross-Distribution	44
D.3.5	Large-Scale Instances	44
D.3.6	Combining Construction and Improvement	44
D.4	Decoding Schemes	45
D.4.1	Augmentations	45
D.4.2	Sampling	45
E	Additional Experiments	47
E.1	Mind your Baseline: Further Insights	47
E.1.1	Main In-distribution Results	47
E.1.2	Decoding Schemes Comparison	47
E.1.3	Sample Efficiency	48
E.1.4	Out-of-distribution	49
E.1.5	Search Methods	51
E.1.6	Additional Large-scale Results	51
E.2	Learning Heuristics for Ant Colony Optimization	53
E.2.1	Experiment Settings	53
E.2.2	Results	53
E.3	Learning to Schedule	53
E.3.1	JSSP	54
E.3.2	FJSSP	55
E.3.3	FFSP	56
E.3.4	Dense and Episodic Rewards	57
E.4	Electronic Design Automation: Learning to Place Decaps	57
E.4.1	Main Results	57
E.4.2	Generalization to Different Number of Components	58
E.5	Learning to Improve	58
E.5.1	Main results	58
E.5.2	Discussion	59
E.6	Graph Problems: Facility Location Problem (FLP) and Maximum Coverage Problem (MCP)	60
E.6.1	Experimental settings	60
E.6.2	Benchmark Results	60
E.6.3	Out-of-distribution	62
E.7	Efficient Software Routines	64
E.7.1	Mixed-Precision Training	64
E.7.2	FlashAttention	65
E.7.3	Efficient Memory Handling in Environments	67
E.8	Towards Foundation Models	68
E.8.1	Experimental Setting	68
E.8.2	Empirical Results	69
E.8.3	Discussion	69
E.9	Generalization of Training on Multiple Distributions and Multiple Tasks	70

A RL4CO Library: Additional Material

A.1 Why Choosing the RL4CO Library?

RL4CO, is a *unified* and *extensive* benchmark the RL-for-CO research area. We intend RL4CO to be used by researchers and practitioners alike of various levels of experience.



Figure 6: RL4CO benchmark logo.

Availability and Future Support RL4CO can be installed through PyPI⁴. We adhere to continuous integration, deployment, and testing to ensure reproducibility and accessibility.⁵



Figure 7: Installing the RL4CO package using pip.

Open License We adopt the open MIT license for all content contained in RL4CO with source code available at <https://github.com/ai4co/r14co>. We ascribe to the principles of *libre software*⁶. Most reimplementations are from original authors and are re-licensed under the MIT license. Data and baseline-specific licenses are reported in Appendix A.3.



Figure 8: Unofficial - but widely used - open MIT license logo.

Open Community Through our journey, we started the AI4CO community⁷, which is a non-profit, cross-institution, inclusive, and open research community. AI4CO originally started out as a Slack channel for discussing the RL4CO but evolved into a broader-visioned and inclusive space to communicate with other researchers about general NCO. The RL4CO library can be discussed in the AI4CO Slack⁸ under the #library-r14co channel. We warmly invite all interested people to join us.



Figure 9: AI4CO community logo.

⁴<https://pypi.org/project/r14co/>

⁵<https://r14co.readthedocs.io/en/latest/>

⁶<https://www.gnu.org/philosophy/free-sw.en.html>

⁷Community Github: <https://github.com/ai4co>

⁸Slack invitation link: <https://bit.ly/ai4co-slack>

A.2 On the Choice of the Software

During the development of RL4CO, we wanted to make it as simple as possible to integrate reproducible and standardized code adhering to the latest guidelines. As a main template for our codebase, we use Lightning-Hydra-Template⁹ which we believe is a solid starting point for reproducible deep learning. We further discuss framework choices below.

PyTorch PyTorch [110] is a popular open-source deep-learning framework that has gained significant traction in the research community. We chose PyTorch as the primary framework for RL4CO due to its intuitive API, dynamic computational graphs, strong community support, and seamless integration with the Python ecosystem. These features make PyTorch well-suited for rapid prototyping and experimentation, which are essential in research settings. Moreover, most of the existing research in NCO has been implemented. It is currently being implemented using PyTorch, making it not only easier to build upon and compare with previous work but also easier for newcomers and experienced researchers.

TorchRL and TensorDict One of the software hindrances in RL is the bottleneck between CPU and GPU communication, majorly due to CPU-based operating environments. For this reason, we did not opt for OpenAI Gym [23] since, although it includes some level of parallelization, this does not happen on GPU and would thus greatly hinder performance. Kool et al. [74] creates *ad-hoc* environments in PyTorch to handle batched data efficiently. However, it could be cumbersome to integrate into standardized routines that include `step` and `reset` functions. As we searched for a better alternative, we found that TorchRL library [20], an official PyTorch project that allows for efficient batched implementations on (multiple) GPUs as well as functions akin to OpenAI Gym. We also employ the TensorDict [20] to handle tensors efficiently on multiple keys (i.e. in CVRP, we can directly operate transforms on multiple keys as locations, capacities, and more). This makes our environments compatible with the models in TorchRL, which we believe could further spread interest in the CO area.

PyTorch Lightning PyTorch Lightning [39] is a useful tool for abstracting away the boilerplate code, allowing researchers and practitioners to focus more on the core ideas and innovations. It features a standardized training loop and an extensive set of pre-built components, including automated checkpointing, distributed training, and logging. PyTorch Lightning accelerates development time and facilitates scalability. We employ PyTorch Lightning in RL4CO to integrate with the PyTorch ecosystem - which includes TorchRL- enabling us to leverage the rich set of tools and libraries available.

Hydra Hydra [148] is a powerful open-source framework for managing complex configurations in machine-learning models and other software. Hydra facilitates creating hierarchical configurations, making it easy to manage even very large and intricate configurations. Moreover, it integrates with command-line interfaces, allowing the execution of different configurations directly from the command line, thereby enhancing reproducibility. We found Hydra to be effective when dealing with multiple experiments since configurations are saved both locally, as `yaml` files, and can be uploaded to monitoring software as Wandb¹⁰ (or to any of the monitoring software supported by PyTorch Lightning).

A.3 Licenses

We summarize the license of software that we employ in RL4CO in a non-exhaustive list in [Table 6](#). Original environments and models from the authors are acknowledged through their respective citations, with several links available in the library. RL4CO is licensed under the MIT license.

B Environments

This section provides an overview of the list of environments we experimented with at the time of writing. We organize environments by categories, which, at the time of writing, are:

⁹<https://github.com/ashleve/lightning-hydra-template>

¹⁰<https://wandb.ai/>

Table 6: Reference code licenses and links.

Type	Asset	License	Link
Library	PyTorch [110]	BSD-3 License	link
	PyTorch Lightning [39]	Apache-2.0 License	link
	TorchRL+TensorDict [20]	MIT License	link
	Hydra [148]	MIT License	link
Dataset	TSPLIB [116]	Available for any non-commercial use	link
	CVRPLib [86]	Available for any non-commercial use	link
	DPP PDNs [108]	Apache-2.0	link
Solver	PyVRP [144]	MIT	link
	LKH3 [46]	Available for any non-commercial use	link
	OR-Tools [111]	Apache 2.0 License	link

1. [Routing \(B.1\)](#)
2. [Scheduling \(B.2\)](#)
3. [Electronic Design Automation \(B.3\)](#)
4. [Graph \(B.4\)](#)

B.1 Routing

Routing problems are perhaps the most known class of CO problems. They are problems of great practical importance, not only for logistics, where they are more commonly framed, but also for industry, engineering, science, and medicine. The typical objective of routing problems is to minimize the total length of the paths needed to visit some (or all) the nodes in a graph. In the following section, we present each of these variants with details of their implementations.

Common instance generation details Following the standard protocol of NCO for routing, we randomly sample node coordinates from the 2D unit square (i.e., $[0, 1]^2$). To ensure reproducibility in our experiments, we use specific random seeds for generating validation and testing instances. For the 10,000 validation instances, we use a random seed of 4321. For the 10,000 testing instances, we use a random seed of 1234. All protocols, including seed selection, align with the practices outlined by Kool et al. [74].

B.1.1 Traveling Salesman Problem (TSP)

The Traveling Salesman Problem (TSP) is a fundamental routing problem that aims to find the Hamiltonian cycle of minimum length. While the original TSP formulation employs mixed-integer linear programming (MILP), in the NCO community, the solution-finding process of TSP is differently formulated for constructive and improvement methods. For constructive methods, the TSP solution is generated by autoregressive solution decoding (i.e., the construction process) in line with Kool et al. [74]. In each step of node selection, we preclude the selection of nodes already picked in previous rounds. This procedure ensures the feasibility of constructed solutions and also allows for the potential construction of an optimal solution for any TSP instance. For improvement methods, it starts with an initial solution and iteratively searches for an optimal one using local search. In each step, the solution is locally adjusted based on a specified local search operator. We support two representative operators for TSP variants, including the 2-opt in line with Ma et al. [96] and the flexible k-opt in line with Ma et al. [98]. The former selects two nodes in the current solution and reverses the solution segment between them to perform a 2-opt exchange. The latter selects k nodes so that a k-opt is performed. Both methods ensure the feasibility of the solutions by masking invalid actions. The best solution after a set number of iterations is the final output.

B.1.2 Capacitated Vehicle Routing Problem (CVRP)

The Capacitated Vehicle Routing Problem (CVRP) is a popular extension of TSP, applicable to a variety of real-world logistics/routing problems (e.g., delivery services). In CVRP, each node has its own demand, and the vehicle visiting them has a specific capacity and always leaves from a special node called “depot”. The vehicle can visit new nodes while their demand fits in its residual capacity

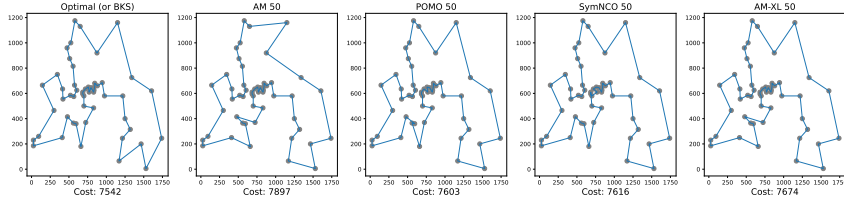


Figure 10: Sample TSP tours on TSPLib’s Berlin 52 with different autoregressive models.

(i.e. the total capacity decreased by the sum of the demands visited in the current path). When no nodes can be added to the path, the vehicle returns to the depot, and its full capacity is restored. Then, it embarks on another tour. The process is repeated until all nodes have been visited. By applying a similar logic to that of the TSP environment, we can reformulate CVRP as a sequential node selection problem, taking into account demands and capacity.

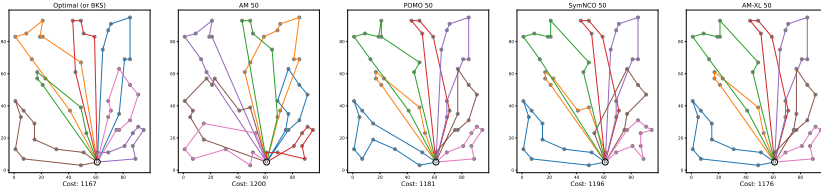


Figure 11: Sample CVRP tours on CVRPLib’s A-n54-k7 instance with different autoregressive models.

Additional generation details To generate the demand, we randomly sample integers between 1 and 10. Without loss of generality, we fix the capacity of the vehicle at 1.0. Then, we normalize the demands by multiplying them by a constant that varies according to the size of the CVRP. The specific constant can be found in our implementation.

B.1.3 Orienteering Problem (OP)

The Orienteering Problem (OP) is a variant of the TSP. In the OP, each node is assigned a prize. The objective of the OP is to find a tour, starting and ending at the depot, that maximizes the total prize collected from visited nodes, while abiding by a maximum tour length constraint. The OP can be framed as a sequential decision-making problem by enforcing the “return to depot” action when no nodes are visitable due to the maximal tour length constraint.

Additional generation details To generate the prize, we use the prize distribution proposed in Fischetti et al. [41], particularly the distribution that allocates larger prizes to nodes further from the depot.

B.1.4 Prize Collecting TSP (PCTSP)

In the Prize Collecting TSP (PCTSP), each node is assigned both a prize and a penalty. The objective is to accumulate a minimum total prize while minimizing the combined length of the tour and the penalties for unvisited nodes. By making a minor adjustment to the PCTSP, it can model different subproblems that arise when using the Branch-Price-and-Cut algorithms for solving routing problems.

B.1.5 Pickup and Delivery Problem (PDP)

The Pickup and Delivery Problem (PDP) is an extension of TSP in the literature Helsgaun [46], Ma et al. [97].¹¹ In PDP, a pickup node has its own designated delivery node. The delivery node can be visited only when its paired pickup node has already been visited. We call this constraint *precedence constraint*. The objective of the PDP is to find a complete tour with a minimal tour length while

¹¹PDP is also called PDTSP (pickup and delivery TSP).

starting from the depot node and satisfying the precedence constraints. We assume that *stacking* is allowed, meaning that the traveling agent can visit multiple pickups prior to visiting the paired deliveries. For constructive methods, the PDP solution construction is similar to that of TSP but must obey precedence constraints. For improvement methods, we consider the ruin and repair local search operator presented by Ma et al. [96]. In each step, a pair of pickup and delivery nodes are removed from the current solution and then reinserted back into the solution with potentially better positions. Invalid actions that violate precedence constraints are masked out to ensure the feasibility of PDP solutions.

Additional generation details To generate the positions of the depot, pickups, and deliveries, we sample the node coordinates from the 2D unit square. The first $N/2$ generated nodes are pickups, and the remaining $N/2$ are their respective deliveries. The pickups and deliveries are paired. For a pickup node i , its respective delivery is $i + N/2$ (excluding the depot index).

B.1.6 Multi-Task VRP (MTVRP)

This environment introduces the 16 VRP variants in Liu et al. [89], Zhou et al. [157] with additional enhancements, such as support for any number of variants in the same batch, as done in Berto et al. [13]. The base logic is the same as CVRP: each node has a demand, and the vehicle has a specific capacity by which it can deliver to nodes and return to the depot to replenish its capacity, with the goal of minimizing the total tour distance. We report each modular constraint definition in the following paragraphs according to Berto et al. [13], Wouda et al. [144]. Table 7 reports the list of all variants and Fig. 12 illustrates the meaning of each MTVRP component.

VRP Variant	Capacity (C)	Open Route (O)	Backhaul (B)	Duration Limit (L)	Time Windows (TW)
CVRP	✓				
OVRP	✓	✓			
VRPB	✓		✓		
VRPL	✓			✓	
VRPTW	✓				✓
OVRPTW	✓	✓			✓
OVRPB	✓	✓	✓		
OVRPL	✓	✓		✓	
VRPBL	✓		✓	✓	
VRPBTLW	✓		✓		✓
VRPLTW	✓			✓	✓
OVRPBL	✓	✓	✓	✓	
OVRPBTLW	✓	✓	✓		✓
OVRPLTW	✓	✓		✓	✓
VRPBTLW	✓		✓	✓	✓
OVRPBTLW	✓	✓	✓	✓	✓

Table 7: The 16 VRP variants that are modeled by the MTVRP environment. All variants include the base Capacity (C). The $k = 4$ features O, B, L, and TW can be combined into any subset, including the empty set and itself (i.e., a power set) with $2^k = 16$ possible combinations.

(C) *Demand and Vehicle Capacity* [$q \in [0, Q]$]: Every node i , except the depot, has a demand q_i that must be satisfied by the vehicle with a uniform capacity of $Q > 0$. The sum of the demands served by a vehicle in the same path must not exceed its capacity Q at any point along its route.

(O) *Open Routes* [$o \in \{0, 1\}$]: With open routes, the distance between the last node and the depot is not counted in the total path length. This represents the scenarios where vehicles are not required to return to the depot after serving all assigned customers. Open routes are commonly found in scenarios involving third-party drivers, who are typically compensated only for the deliveries they complete, without the need to return to the depot [80].

(B) *Backhauls* [$p \in [0, Q]$]: Backhauls extend the concept of demand to include both delivery and pickup requests, thus increasing vehicle utilization and leading to savings. Nodes are categorized as

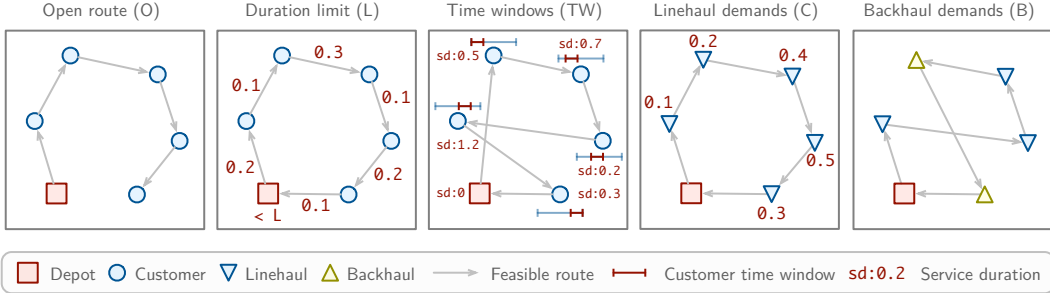


Figure 12: Different VRP attributes. Open routes (O) and duration limits (L) are *global attributes*, whereas time windows (TW), capacitated vehicles for linehaul demands (C) and backhaul demands (B) are *node attributes*. Attributes may be combined in different ways to define VRP variants.

either linehaul or backhaul nodes.¹² Linehaul nodes require delivery of demand q_i from the depot to the node i (similar to CVRP), while backhaul nodes require a pickup of an amount p_i to be transported from the node back to the depot. A vehicle can serve both linehaul and backhaul customers in a single route, but all linehaul customers must be served before any backhaul customers. A typical example of a backhaul problem is a laundry service for hotels that has to deliver clean towels and pick up dirty ones, in which the precedence constraint of linehaul nodes is important due to possible contamination [26].

(L) *Duration Limits* [$l \in [0, L]$]: Imposes a limit L on the total travel duration (or distance) of each vehicle route, ensuring a fair distribution of workload among different paths. This limit is consistently applied to all routes in the problem.

(TW) *Time Windows* [$e, s, l \in [0, T]^3$]: Each node i , except for the depot, has an associated time window $[e_i, l_i]$, which specifies the earliest and latest times at which it can be visited. When visiting node i , the vehicle must wait for a time s_i before leaving. The vehicle must arrive at customer i before the end of its time window l_i , but if they arrive before the start of the time window e_i , they must wait at the customer's location until the time window begins before starting the service. When the vehicle returns to the depot, the time is reset to 0.

Additional generation details We introduce the data generation details as follows:

Locations: We generate $n + 1$ locations randomly with x_i and $y_i \sim U(0, 1)$, $\forall i \in \{0, \dots, n\}$, where $[x_0, y_0]$ represents the depot and $[x_i, y_i]$, $i \in \{1, \dots, n\}$ are the other n nodes.

Capacity: The capacity C of the vehicle is determined based on the following calculation:

$$C = \begin{cases} 30 + \left\lfloor \frac{1000}{5} + \frac{n-1000}{33.3} \right\rfloor & \text{if } 1000 < n \\ 30 + \left\lfloor \frac{n}{5} \right\rfloor & \text{if } 20 < n \leq 1000 \\ 30 & \text{otherwise} \end{cases}$$

Open route: the open route is an instance-wise flag: when set to 1, the route is open, when 0 is closed. We sample the flag from a uniform distribution with the same probability of the route being open or closed.

Linehaul and Backhaul demands: We generate demands according to the following schema:

1. Generate linehaul demands $q_i \in \{0, \dots, Q\}$ for all nodes $i \in \{i, \dots, n\}$. These are needed for both backhaul and linehaul scenarios.
2. Generate backhaul demands $p_i \in \{0, \dots, Q\}$ for all nodes $i \in \{i, \dots, n\}$.
3. For each node $i \in \{i, \dots, n\}$, there is a probability of 0.2 that it is assigned a backhaul demand, otherwise, its backhaul demand is set to be 0.

¹²Note that another name of this problem, as adopted in LKH3 [46], is VRP with Pickup and Deliveries (VRPPD). However, we align with PyVRP [144] and do not use this name to prevent confusion with the *one-to-one PDP*, as we described before, where there is strict precedence between each pair of pickup and delivery.

Note that even in a backhaul setting, usually not all nodes are backhaul nodes, i.e., we need to consider both linehaul and backhaul demands in backhaul problem settings. All demands, both linehauls and backhauls, are scaled to $[0, 1]$ through division by the vehicle capacity.

Duration limits: Each route is assigned a fixed duration limit L with a default value of 3. We check that $2 * d_{0i} < L$ to make sure there is a feasible route for any customer.

Time Windows: We generate the time windows for each node $i \in \{1, \dots, n\}$ according to the following steps:

1. Generate service time $s_i \in [0.15, 0.18]$.
2. Generate time window length $t_i \in [0.18, 0.2]$.
3. Calculate distance d_{0i} from node to depot.
4. Calculate the upper bound for the start time $h_i = \frac{t_{max} - s_i - t_i}{d_{0i}} - 1$, where t_{max} is the maximum time with a default value of 4.6.
5. Calculate the start time as $e_i = (1 + (h_i - 1) \cdot u_i) \cdot d_{0i}$ with $u_i \sim U(0, 1)$.
6. Calculate the end time as $l_i = e_i + t_i$.

Classical solvers We employ the SotA HGS implementation in PyVRP [144] and OR-Tools [111]. We make these solvers conveniently available through the `solve` API of the environment.

B.2 Scheduling

Scheduling problems are a fundamental class of problems in operations research and industrial engineering, where the objective is to optimize the allocation of resources over time. These problems are critical in various industries, such as manufacturing, computer science, and project management. Currently, RL4CO implements three central scheduling problems, namely the flexible flow shop (FFSP), the job shop (JSSP), and the flexible job shop problem (FJSSP). Each of these problems has unique characteristics and complexities that need to be translated into the environment classes that we will describe hereafter.

B.2.1 Job Shop Scheduling Problem (JSSP)

The job shop scheduling problem is a well-known combinatorial optimization problem. It is widely used in the operations research community as well as many industries, such as manufacturing and transportation. In the JSSP, a set of jobs J must be processed by a set of machines M . Each job $J_i \in J$ consists of a set of n_i operations $O_i = \{o_{ij}\}_{j=1}^{n_i}$ which must be processed one after another in a given order. The goal of the JSSP is to construct a valid schedule that adheres to the precedence order of the operations and minimizes the makespan, i.e., the time until the last job is finished. One example of such a schedule is shown in Fig. 13.

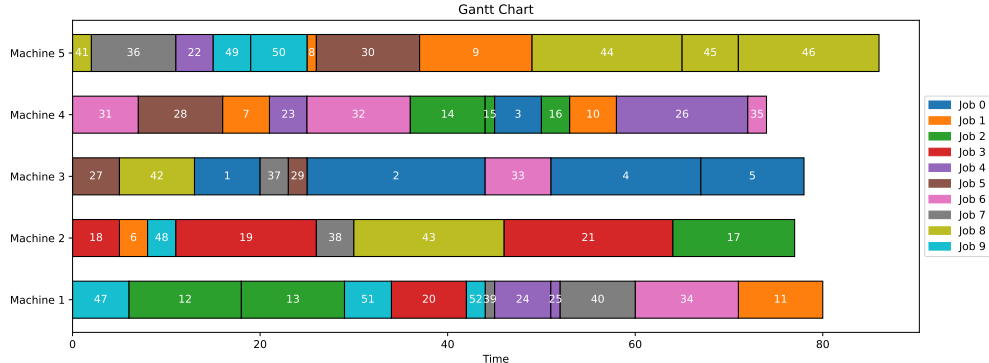


Figure 13: Example Schedule for the JSSP

We formulate the JSSP as a sequential decision problem following the implementation of Tassel et al. [132]. Here, the environment iterates through distinct time steps $t = 1, \dots, T$. At each time

step, the agent decides for each machine whether and which job to process next until all machines are busy or all jobs are being processed. In this case, the environment transitions to the next time step at which a machine becomes idle.

Instance Generation We follow the instance generation method described by Zhang et al. [153], which assumes that each job has exactly one operation per machine, i.e. $n_i = |M|$. Further, processing times for all operations are sampled iid. from a uniform distribution, with parameters specified in Table 8.

B.2.2 Flexible Job Shop Scheduling Problem (FJSSP)

The flexible job shop scheduling problem is very similar to the JSSP. However, while in the classical JSSP, each operation $o_{ij} \in O$ has a specified machine and processing time p_{ij} , the flexible job shop scheduling problem (FJSSP) relaxes this assumption by allowing each operation to be processed by multiple eligible machines $M_k \subseteq M$, potentially with different processing times p_{ijk} associated with the respective operation-machine pair. As a consequence, the agent does not only need to decide which job to process next, but also on which machine it should be processed.

Instance Generation We follow the instance generation method described by Song et al. [125], who sample n_i operations for each job J_i from a uniform distribution. Further, an average processing time \bar{p}_{ij} is drawn for each operation $o_{ij} \in O$, and the actual processing time per eligible operation-machine pair is subsequently sampled from $U(0.8 \cdot \bar{p}_{ij}, 1.2 \cdot \bar{p}_{ij})$. The parameters used for instance generation can be found in Table 8.

Table 8: Instance generation parameters

	JSSP				FJSSP			
	6 × 6	10 × 10	15 × 15	20 × 20	10 × 5	20 × 5	15 × 10	20 × 10
J	6	10	15	20	10	20	15	20
M	6	10	15	20	5	5	10	10
n_i	6	10	15	20	$U(4, 6)$	$U(4, 6)$	$U(8, 12)$	$U(8, 12)$
\bar{p}_{ij}	$U(1, 99)$	$U(1, 99)$	$U(1, 99)$	$U(1, 99)$	$U(1, 20)$	$U(1, 20)$	$U(1, 20)$	$U(1, 20)$
$ M_i $	1	1	1	1	$U(1, 5)$	$U(1, 5)$	$U(1, 10)$	$U(1, 10)$

B.2.3 Flexible Flow Shop Problem (FFSP)

The flexible flow shop problem (FFSP) is a complex and widely studied optimization problem in production scheduling. It involves N jobs to be processed in S stages, each containing multiple machines ($M > 1$). Each job must pass through the stages in a specified order, but within each stage, it can be processed by any available machine. A critical constraint is that no machine can process more than one job at a time. The objective is to find an optimal schedule that minimizes the total time required to complete all jobs. We formulate the FFSP as a sequential decision process, where at each time step $t = 0, 1, \dots$ and for each idle machine, the agent must decide whether and which job to schedule. If all machines are busy or all jobs are currently being processed, the environment moves to the next time step $t + 1$, and the process repeats until all jobs for each stage have been scheduled.

Instance Generation We follow the data generation process described by Kwon et al. [77], who sample processing times for each job-machine pair and for every stage independently from a discrete uniform distribution.

B.3 Electronic Design Automation

Electronic Design Automation (EDA) is a sophisticated process that involves the use of software tools to design, simulate, and analyze electronic systems, particularly integrated circuits (ICs) and printed circuit boards (PCBs). EDA encompasses a wide range of tasks, from schematic capture and layout design to verification and testing. Optimization is a critical aspect of EDA, where the goal is to achieve the best possible performance, power efficiency, and cost within the constraints of the design. This involves solving complex problems that can be either continuous, such as cell

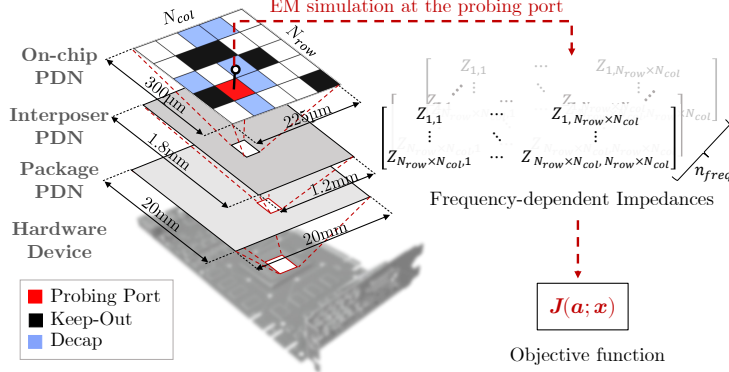


Figure 14: Grid representation of the target on-chip PDN for the DPP problem with a single probing port from Kim et al. [67].

placement [52], or combinatorial, like decap placement [67]. RL4CO integrates CO problems in EDA as benchmarking environments.

B.3.1 Decap Placement Problem (DPP)

The decap placement problem (DPP) is an electronic design automation problem (EDA) in which the goal is to maximize the performance with a limited number of the decoupling capacitor (decap) placements on a hardware board characterized by asymmetric properties, measured via a probing port. The decaps cannot be placed on the location of the probing port or in keep-out regions (which represent other hardware components) as shown in Fig. 14. The optimal placement of a given number of decaps can significantly impact electrical performance, specifically in terms of power integrity (PI) optimization. PI optimization is crucial in modern chip design, including AI processors, especially with the preference for 3D stacking memory systems like high bandwidth memory (HBM) [54]. For comprehensive details, we follow the configuration guidelines provided in [67].

Baseline solvers We employ two meta-heuristic baselines commonly used in hardware design as outlined in [67]: random search (RS) and genetic algorithm (GA) [62]. GA has shown promise as a method for addressing the decap placement problem (DPP).

Instance generation details We use the same data for simulating the hardware board as Kim et al. [67], with power distribution network (PDN) datasets from Park et al. [108]. We randomly select one probing port and a number between 1 and 50 keep-out regions sampled from a uniform distribution for generating instances. As in the routing benchmarks, we select seed 1234 for testing the 100 instances.

B.3.2 Multi-Port Decap Placement Problem (mDPP)

We further consider a more complex and realistic version compared to Kim et al. [67]. The multi-port decap placement problem (mDPP) is a generalization of DPP from Appendix B.3.1 in which measurements from multiple probing ports are performed. The objective function can be either the mean of the reward from the probing ports: 1) (*Maxsum*): the objective is to maximize the average PI among multiple probing ports and 2) (*Maxmin*): maximize the minimum PI between them.

Instance generation details The generation details are the same as DPP, except for the probing port. A number of probing ports between 2 and 5 is sampled from a uniform distribution, and probing ports are randomly placed on the board, just like the other components.

B.4 Graph

Many CO problems can be (re-)formulated on graphs [64]. In typical CO problems on graphs, actions are defined on nodes/edges, while problem variables and constraints are incorporated in graph topology and node/edge attributes (e.g., weights). The graph-based formulation gives us concise and

systematic representations of CO problems. Moreover, existing traditional and machine-learning algorithms for graphs are off-the-shelf tools.

B.4.1 Facility Location Problem (FLP)

The optimal usage of limited resources is an important problem to consider in many different fields and has various forms. One specific form of such a problem can be formulated as the facility location problem (FLP), where one aims to choose a given number of locations among given candidates, and the objective is to minimize the overall cost of service (e.g., the sum of the distance from the users to the nearest facility) [38].

Many real-world problems can be abstracted as instances of FLP. For example, franchise brands may need to determine where to open new retail stores to maximize accessibility and profitability [120]; governments may need to consider the placement of public facilities (e.g., hospitals and schools) to maximize the convenience for citizens to use them [101]; energy companies may need to determine the best locations for power centers (e.g., power plants and wind farms) to minimize transmission losses [92].

Formal definition We consider the following specific form of the facility location problem (FLP) used in existing NCO literature [141, 25]: (1) given a group of n locations $x_1, x_2, \dots, x_n \in \mathbb{R}^d$ in a d -dimensional space (usually $d = 2$ or 3) and $k < n$, (2) we aim to choose k locations $x_{i1}, x_{i2}, \dots, x_{ik}$ among the given n locations as the locations of facilities, (3) to minimize the sum of the distance from all the n locations to the nearest facility, i.e., $\sum_{j=1}^n \min_{t=1}^k \text{dist}(x_j, x_{it})$. We specially consider the Euclidean distance, i.e., $\text{dist}(x_i, x_j) = \|x_i - x_j\|_2$.

Instance generation details The locations are $(d = 2)$ -dimensional generated i.i.d. at random. For each location, each coordinate is sampled i.i.d. uniformly at random between 0 and 1. Each instance contains $n = 100$ locations, and $k = 10$ locations are to be chosen.

Classical solvers We apply two MIP solvers, Gurobi [44] and SCIP [14], to obtain the optimal solutions.

B.4.2 Maximum Coverage Problem (MCP)

In many real-world scenarios, one needs to allocate limited resources to achieve maximum coverage, which is a fundamental concern across various domains. One specific formulation is called the maximum coverage problem (MCP), where the goal is to select a subset of sets from a given family of sets to maximize the coverage, i.e., the (weighted) size of the union of the selected sets [65].

As a mathematical abstraction, the MCP can be used to represent many real-world problems. For example, radio frequency identification (RFID) system engineers may need to set RFID readers in an optimal way to ensure the maximum coverage of RFID tags [4]; marketers may need to choose proper forms of advertisement to reach the maximum number of customers [126]; in security applications (e.g., deploying security cameras), one may need to select the optimal deployment to maximize the coverage of the protected area [105].

Formal definition We consider the following specific form of the maximum coverage problem (MCP) used in existing NCO literature [141, 25]: (1) given m items (WLOG, $[m] := \{1, 2, 3, \dots, m\}$), where each item t has weight w_t , and a family of n sets $S_1, S_2, \dots, S_n \subseteq [m]$ for some positive integer m and $k < n$, (2) we aim to choose k sets $S_{i1}, S_{i2}, \dots, S_{ik}$ among the given n sets, (3) to maximize the total weighted coverage of the k chosen sets, which is the sum of the weights of items contained in any chosen set, i.e., $\sum_{t \in \bigcup_{j=1}^k S_{ij}} w_t$.

Instance generation details First, $m = 200$ items are generated, and the item weights are generated i.i.d., where each weight is a random integer sampled between 1 and 10 (inclusive) uniformly at random. Then, $n = 100$ sets are generated i.i.d., where for each set, we first sample its size between 5 and 15 uniformly at random and then choose that number of items uniformly at random. After generation, $k = 10$ locations are to be chosen.

Classical solvers We apply two MIP solvers, Gurobi [44] and SCIP [14], to obtain the optimal solutions.

B.5 Additional Environments and Beyond

We also include in the library additional environments that have been implemented but not fully benchmarked in this paper yet, such as the ATSP, mTSP, Skill-VRP, SMTWTP, and SPCTSP, to name a few. We did not count these in the total environment count (hence the “conservative” estimate). Moreover, several projects, among which co-authors of this paper, have adapted several new environments to their own tasks, which may be included in the future.

Although RL4CO already contains several environments, we acknowledge that the library can be further extended within new directions, which we briefly describe. One such direction is multi-objective combinatorial optimization [87, 29], which is a recently trending research topic of practical importance. Moreover, providing modular reward evaluators to optimize different objectives (for instance, min-max, tardiness) is another avenue of research that we recommend exploring [109]. Of practical importance is also non-euclidean routing, which so far has received comparatively less attention in this field but is practically important (i.e., DIMACS challenge¹³). Finally, multi-agent CO [40, 130, 131, 15] is another interesting area of research, which recent approaches model as a sequential decision-making process [123, 155].

Implementing new environments is relatively easy: we created a notebook under the `examples/` folder demonstrating how one can implement a custom environment from the base logic to a fully functioning model. We expect to host an even wider variety of environments in the future, thanks to the community, and invite contributors to help us in our journey.

C Baselines

This section provides an overview of the key components and methods implemented in RL4CO that can be used as baselines for comparative evaluation. The term “baselines” broadly refers to both the RL algorithms that define the learning objectives and update rules, as well as the policy architectures that parameterize the agent’s behavior in the environment, given that several papers introduce a mix of RL training schemes and policy improvements. We categorize baselines into:

1. **General-purpose RL algorithms (C.1)**
2. **Constructive autoregressive (AR) methods (C.2)**
3. **Constructive non-autoregressive (NAR) methods (C.3)**
4. **Improvement methods (C.4)**
5. **Active search methods (C.5)**

C.1 General-purpose RL Algorithms

In the following descriptions of RL algorithms, we use the notations of a full problem instance \mathbf{x} and a complete solution \mathbf{a} for simplicity. However, note that these algorithms are also applicable to the usual notion of the sum of rewards over partial states s_t and actions a_t .

C.1.1 REINFORCE [128]

REINFORCE (also known as policy gradients in the literature) is an online RL algorithm whose loss function gradient is given by:

$$\nabla_{\theta} \mathcal{L}_a(\theta | \mathbf{x}) = \mathbb{E}_{\pi(\mathbf{a}|\mathbf{x})} [(R(\mathbf{a}, \mathbf{x}) - b(\mathbf{x})) \nabla_{\theta} \log \pi(\mathbf{a}|\mathbf{x})], \quad (5)$$

where $b(\cdot)$ is a baseline function used to stabilize training and reduce gradient variance. The choice of $b(\cdot)$ can greatly influence the final performance.

¹³<http://dimacs.rutgers.edu/programs/challenge/vrp/>

C.1.2 Advantage Actor-Critic (A2C) [73]

A2C is an algorithm that can be used to solve the RL objective in Eq. (3). It consists of an actor (policy network) and a critic (value function estimator). The actor is trained to maximize the expected cumulative reward by following the policy gradient, while the critic is trained to estimate the value function. The advantage function, computed as the difference between the reward $R(\mathbf{a}, \mathbf{x})$ and the value function $V(\mathbf{x})$, is used to weight the policy gradient update for the actor. This can be seen as a modification of the REINFORCE gradient, where the baseline $b(\mathbf{x})$ is replaced by the value function $V(\mathbf{x})$:

$$\nabla_{\theta} \mathcal{L}_a(\theta | \mathbf{x}) = \mathbb{E}_{\pi(\mathbf{a} | \mathbf{x})} [(R(\mathbf{a}, \mathbf{x}) - V(\mathbf{x})) \nabla_{\theta} \log \pi(\mathbf{a} | \mathbf{x})]. \quad (6)$$

The critic is updated by minimizing the mean-squared error between the estimated value function and the target value, which is the reward for the given problem instance \mathbf{x} :

$$\mathcal{L}_c = \mathbb{E}_{\mathbf{x} \sim P(\mathbf{x})} (R(\mathbf{a}, \mathbf{x}) - V(\mathbf{x}))^2. \quad (7)$$

By using the advantage function, A2C reduces the variance of the policy gradient and stabilizes training compared to the standard REINFORCE algorithm.

C.1.3 Proximal Policy Optimization (PPO) [119]

PPO is another algorithm that can be used to solve the RL objective in Eq. (3). It is an on-policy algorithm that aims to improve the stability of policy gradient methods by limiting the magnitude of policy updates. To this end, PPO introduces a surrogate objective function that constrains the probability ratio between the target policy π_{θ} that is optimized and a reference policy $\pi_{\theta_{\text{old}}}$, which is periodically updated. This clipping mechanism prevents drastic changes to the target policy, ensuring more reliable and stable learning. Formally, the PPO objective function is given by:

$$\begin{aligned} \mathcal{L}_{\text{CLIP}}(\theta) = \mathbb{E}_{\mathbf{x} \sim P(\mathbf{x})} & \left[\mathbb{E}_{\mathbf{a} \sim \pi_{\theta_{\text{old}}}(\mathbf{a} | \mathbf{x})} \left[\min \left(\frac{\pi_{\theta}(\mathbf{a} | \mathbf{x})}{\pi_{\theta_{\text{old}}}(\mathbf{a} | \mathbf{x})} A^{\pi_{\theta_{\text{old}}}(\mathbf{x}, \mathbf{a})}, \right. \right. \right. \\ & \left. \left. \left. \text{clip} \left(\frac{\pi_{\theta}(\mathbf{a} | \mathbf{x})}{\pi_{\theta_{\text{old}}}(\mathbf{a} | \mathbf{x})}, 1 - \epsilon, 1 + \epsilon \right) A^{\pi_{\theta_{\text{old}}}(\mathbf{x}, \mathbf{a})} \right) \right] \right], \end{aligned} \quad (8)$$

where θ_{old} represents the parameters of the reference policy, typically a periodically created copy of the parameters θ of the target policy. Further, $A^{\pi_{\theta_{\text{old}}}(\mathbf{x}, \mathbf{a})}$ is the advantage function estimated using the reference policy, and ϵ is a hyperparameter that controls the clipping range, typically set to a small value like 0.2.

The advantage function in PPO is estimated using a learned value function $V_{\phi}(\mathbf{x})$, where ϕ represents the parameters of the value function. The advantage is computed as:

$$A^{\pi_{\theta_{\text{old}}}(\mathbf{x}, \mathbf{a})} = R(\mathbf{a}, \mathbf{x}) - V_{\phi}(\mathbf{x}). \quad (9)$$

The value function is learned by minimizing the mean-squared error between the estimated value and the actual return:

$$\mathcal{L}_V(\phi) = \mathbb{E}_{\mathbf{x} \sim P(\mathbf{x})} [(R(\mathbf{a}, \mathbf{x}) - V_{\phi}(\mathbf{x}))^2]. \quad (10)$$

An optimization step in PPO updates both, the parameters θ of the target policy and the parameters ϕ of the value function by combining $\mathcal{L}_{\text{CLIP}}$ and $\mathcal{L}_V(\phi)$ in a single loss $\mathcal{L}_{\text{PPO}} = \mathcal{L}_{\text{CLIP}} + \beta \mathcal{L}_V(\phi)$, where β is a hyperparameter [119].

C.2 Constructive Autoregressive (AR)

C.2.1 Attention Model (AM) [74]

The Attention Model (AM) from Kool et al. [74] is an encoder-decoder architecture based on the self-attention mechanism [136] that is at the heart of several state-of-the-art NCO methods, including RL-based ones [76, 69, 51] as well as (self-)supervised ones [37, 93, 94]. In the original AM, only node features are considered: with abuse of notation from Fig. 3, we consider the `InitEmbedding` as the *node embedding*, and split the *context embedding* into a `ContextEmbedding` which updates the current query and `DynamicEmbedding` that updates the current cached keys and values.

Multi-Head Attention Before delving into the encoder and decoder structures, we briefly introduce the notion of Multi-Head Attention (MHA) from Vaswani et al. [136], since it is used across several NCO methods. MHA allows the model to jointly attend to information from different representation subspaces at different positions, enabling it to capture various relationships between the input elements. Importantly, it is flexible in handling a variable number of elements.

In the MHA operation, the input sequences Q (queries), K (keys), and V (values) are linearly projected to H different subspaces using learned matrices W_i^Q , W_i^K , and W_i^V , respectively, where H is the number of attention heads:

$$Q_i = QW_i^Q \quad (11)$$

$$K_i = KW_i^K \quad (12)$$

$$V_i = VW_i^V \quad (13)$$

for $i = 1, \dots, H$.

The attention weights are computed as the scaled dot-product between the queries and keys, followed by a softmax operation:

$$A_i = \text{Softmax} \left(\frac{Q_i K_i^T}{\sqrt{d_k}} + M \right) \quad (14)$$

where d_k is the dimension of the keys, used as a scaling factor to prevent the dot-products from getting too large, and M is an optional mask matrix that can be used to prevent attention to certain positions (e.g. infeasible actions in a CO problem).

The output of each attention head is computed as the weighted sum of the values, using the attention weights:

$$Z_i = A_i V_i \quad (15)$$

Finally, the outputs of all attention heads are concatenated and linearly projected using a learned matrix W^O to obtain the final output of the MHA operation:

$$\text{MHA}(Q, K, V) = \text{Concat}(Z_1, \dots, Z_H) W^O \quad (16)$$

This multi-head attention mechanism allows the model to learn different attention patterns and capture various dependencies between the input elements, enhancing the representational power of the model. The queries, keys, and values can come from the same input sequence (self-attention, i.e. $Q = K = V$) or from different sequences (cross-attention), depending on the application. While the attention operation is at the core of much of the current SotA deep learning [134], this scales as $O(L)^2$ where L is the sequence length, such as the number of nodes in a TSP. Thus, an efficient implementation such as FlashAttention [34, 33] is important, as shown in Appendix E.7.2.

Encoder The encoder's primary task is to encode input \mathbf{x} into a hidden embedding \mathbf{h} . The structure of f_θ comprises two trainable modules: the `InitEmbedding` and encoder blocks. The `InitEmbedding` module typically transforms problem features into the latent space and problem-specific compared to the encoder blocks, which often involve plain multi-head attention (MHA):

$$\mathbf{h} = f_\theta(\mathbf{x}) \triangleq \text{EncoderBlocks}(\text{InitEmbedding}(\mathbf{x})) \quad (17)$$

Each encoder block in the AM is composed of an Attention Layer, similar to Vaswani et al. [136]. Each layer ℓ is composed of multi-head attention (MHA) for message passing and a Multi-Layer Perceptron (MLP, also known as *feed-forward network (FFN)*), with skip-connections and normalization (Norm):

$$\hat{\mathbf{h}} = \text{Norm} \left(\mathbf{h}^{(\ell-1)} + \text{MHA}(\mathbf{h}^{(\ell-1)}, \mathbf{h}^{(\ell-1)}, \mathbf{h}^{(\ell-1)}) \right) \quad (18)$$

$$\mathbf{h}^{(\ell)} = \text{Norm} \left(\hat{\mathbf{h}} + \text{MLP}(\hat{\mathbf{h}}) \right) \quad (19)$$

with $\ell = [1, \dots, N]$ where N is the number of encoding layers and $\mathbf{h}^0 = \text{InitEmbedding}(\mathbf{x})$. In the encoder side, we have $Q = K = V = \mathbf{h}^{(\ell-1)}$, hence self-attention.

The original implementation of the AM uses $N = 3$ layers $H = 8$ heads of dimension $d_k = \frac{d_h}{M} = 16$, an MLP with one hidden layer of dimension 512 with a ReLU activation function, and a Batch Normalization [56] as normalization.

Decoder The decoder g_θ autoregressively constructs the solution based on the encoder output \mathbf{h} and the state at current step t , s_t . The solution decoding involves iterative steps until a complete solution is constructed: at each step, starting from the current node's i query q_t^i

$$q_t^i = \text{ContextEmbedding}(\mathbf{h}, s_t), \quad (20)$$

$$h_t^c = \text{MHA}(q_t^i, K_t^g, V_t^g, M_t), \quad (21)$$

$$\mathbf{z} = \frac{V_t^p h_t^c}{\sqrt{d_k}} \quad (22)$$

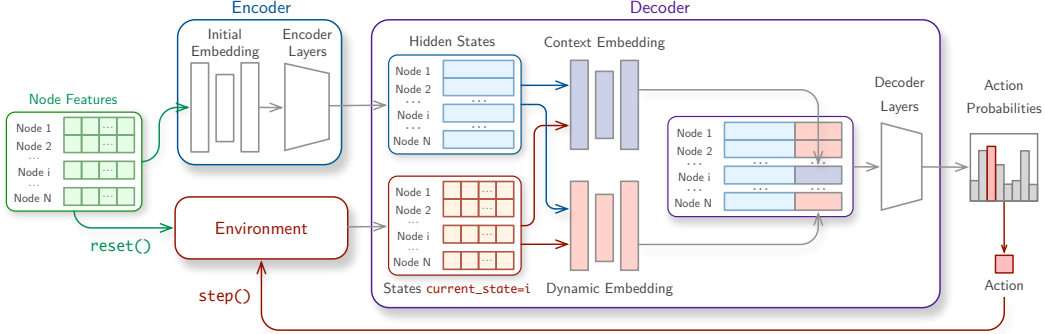


Figure 15: An overview of the modularized Attention Model policy in RL4CO.

where M_t is the set of feasible actions (i.e. the `action_mask`), projections $K_t^g, V_t^g, V_t^p = W_k^g h, W_v^g h, W_v^p h$ can either be precomputed once as cache or updated via a dynamic embedding $K_t^g, V_t^g, V_t^p = \text{DynamicEmbedding}(W_k^g h, W_v^g h, W_v^p h, s_t, h, x)$, depending on the problem. We note that Eq. (22) is usually referred to as the pointer mechanism (in the codebase, we refer to Eq. (21) and Eq. (22) as the `PointerAttention`). Finally, logits z (unnormalized output of policy π) are transformed into a probability distribution over the action space:

$$p = \text{Softmax}(C \cdot \tanh(z)) \quad (23)$$

where logits z for infeasible actions can be set to $-\infty$ to avoid choosing them; and the C value (called *tanh clipping*, usually set to 10) serves in improving the exploration [8]. We note that Eq. (23) can also include additional operations such as temperature scaling, top-k, and top-p filtering.

Baseline Kool et al. [74] additionally introduces the *rollout* baseline b for Eq. (5). At the end of each epoch, a greedy rollout of a baseline policy π_{BL} is executed for each of the sampled instances x , whose values become baselines for REINFORCE. The algorithm compares the current training policy with a saved baseline policy (similar to the DQN target network [103]) at the end of every epoch, and replace the parameters of π_{BL} with the current trained π if the improvement is significant with a paired t-test of (i.e., 5% in the original paper).

C.2.2 Ptr-Net [139]

The original Pointer Network (Ptr-Net) is introduced in Vinyals et al. [139] and further refined to be trained with RL in [8]. The base architecture predates the AM [74]: an attention mechanism is employed to select outputs of variable length, thus “pointing” at them. The baseline architecture additionally uses an LSTM [47], which in practice has less expressivity than full-fledged attention.

C.2.3 POMO [76]

POMO introduces the *shared* baseline to lower the REINFORCE variance. The key idea is that one can sample rollouts when decoding by forcing diverse starting nodes, which is a powerful inductive bias for certain problems, such as the TSP, in which multiple optimal initial starting points exist. The baseline b_{shared} is the average of all rollouts:

$$b_{\text{shared}}(s) = \frac{1}{N} \sum_{j=1}^N R(a_j, x) \quad (24)$$

where N is the number of sampled trajectories (typically set as the number of nodes).

C.2.4 SymNCO [69]

SymNCO considers the symmetric nature of combinatorial problems and solutions. There are two major symmetries in combinatorial optimization: 1) *Problem symmetries*: The representation of the input 2D coordinates should have equivalent optimal solution sets and 2) *Solution symmetries*: Multiple permutations can represent an identical cyclic line graph. To reflect this symmetric nature, SymNCO augments the AM architecture by incorporating an auxiliary invariant representation loss function to ensure input 2D symmetries. Additionally, SymNCO employs a shared baseline as

Eq. (24) similar to POMO but samples rollouts from both different symmetric problem inputs and solutions together. The implementation is not vastly different from AM and POMO; the primary addition is the symmetric-aware augmentation functions.

C.2.5 PolyNet [51]

The PolyNet method proposed by Hottung et al. [51] enables the learning of a set of complementary solution strategies within a single model. This facilitates the easy sampling of diverse solutions at test time, resulting in improved exploration of the search space and, consequently, enhanced overall performance. Unlike many other approaches, PolyNet does not artificially increase exploration by forcing diverse starting actions, as initially proposed by Kwon et al. [76]. Instead, PolyNet utilizes its inherent diversity mechanism, based on its novel architecture and the Poppy loss [43, 27]:

$$\nabla_{\theta} \mathcal{L} = \mathbb{E}_{\pi(\mathbf{a}^*|\mathbf{x})} [(R(\mathbf{a}^*, \mathbf{x}) - b_o(\mathbf{x})) \nabla_{\theta} \log \pi_{\theta}(\mathbf{a}^*|\mathbf{x})], \quad (25)$$

to facilitate exploration during the search process, where \mathbf{a}^* is the *best* solution of K PolyNet samples and $b_o(\mathbf{x})$) is the average reward of the K samples. This can improve performance for problems in which the first action greatly influences the performance.

C.2.6 HAM [82]

The Heterogeneous Attention Model (HAM) [82] is a model specialized for Pickup and Delivery problems (PDP, Appendix B.1.5), characterized by hard one-to-one precedence constraints. To differentiate between pickup and delivery pairs, it introduces *ad hoc* encoder blocks with a specialized attention mechanism that can differentiate between pickup and delivery pairs.

C.2.7 MTPOMO [89]

The MTPOMO developed by Liu et al. [89] proposes to adopt a unified model to learn across various VRP variants. It is motivated by the fact that the diverse VRPs are different combinations of several shared underlying attributes. By training on a limited number of VRPs with basic attributes, the model is capable of generalizing to a vast array of VRP variants, each representing different combinations of these attributes. This approach extends POMO [76] by incorporating an attribute composition block, facilitating learning across different problems. The cross-problem learning demonstrates promising zero-shot generation performance on unseen VRPs and benefits out-of-distribution performance.

C.2.8 MVMoE [157]

The MVMoE architecture proposed by Zhou et al. [157] incorporates mixture-of-experts (MoEs) [57, 60, 121] into attention-based model (e.g., POMO [76]), such that the model capacity can be greatly enhanced without a proportional increase in computation. For the *encoder* part, MVMoE replaces a feed-forward network (FFN) with an MoE layer, which typically consists of 1) m experts $\{E_1, E_2, \dots, E_m\}$, each of which is also an FFN with independent trainable parameters, and 2) a gating network G parameterized by W_G , which decides how the inputs are distributed to experts. Given a single input x , $G(x)$ and $E_j(x)$ denote the output of the gating network (i.e., an m -dimensional vector), and the output of the j th expert, respectively. The output of an MoE layer is calculated as:

$$\text{MoE}(x) = \sum_{j=1}^m G(x)_j E_j(x). \quad (26)$$

The gating algorithm follows the node-level input-choice gating proposed by Shazeer et al. [121], which leverages a sparse gating network: $G(x) = \text{Softmax}(\text{TopK}(x \cdot W_G))$. In this way, only k experts with partial model parameters are activated, hence saving the computation. For the *decoder* part, MVMoE replaces the final linear layer of MHA with an MoE layer, including m linear layers and a gating network G . To balance the empirical performance and computational complexity, a hierarchical gating mechanism is further proposed to utilize MoEs during decoding efficiently. In this case, the MoE layer in the decoder includes two gating networks $\{G, G'\}$, m experts $\{E_1, E_2, \dots, E_m\}$, and a dense layer D . Given a batch of inputs X , the hierarchical gating routes them in two stages. In the first stage, G' decides to distribute inputs X to either the sparse or dense layer. In the second stage, if X is routed to the sparse layer, the gating network G is activated to route nodes to experts on the node level by using the default gating algorithms, i.e., the input-choice

gating. Otherwise, X is routed to the dense layer D and transformed into $D(X)$. In summary, the hierarchical gating learns to output $G'(X)_0 \sum_{j=1}^m G(X)_j E_j(X)$ or $G'(X)_1 D(X)$. Empirically, hierarchical gating has been found to be more efficient, albeit with a slight sacrifice in in-distribution performance, while demonstrating superiority with out-of-distribution data.

C.2.9 L2D [153]

Learning to Dispatch (L2D) proposed by Zhang et al. [153] is a DRL method to solve the JSSP. It comprises of the usual encoder-decoder structure, where a graph convolution network (GCN) is employed to extract hidden representations from the JSSP instance. To this end, L2D formulates the JSSP as a disjunctive graph, with nodes reflecting the operations of the problem instance. Nodes of operations that belong to the same job are connected via directed arcs, specifying their precedence relation. Moreover, operations to be processed on the same machine are connected using undirected arcs. Using the resulting neighborhood \mathcal{N} of the nodes, the GCN performs message passing between adjacent operations to construct their hidden representations. Formally, let \mathbf{h}^0 be the initial embeddings of operations O and $\tilde{\mathbf{A}}$ the adjacency matrix with added self-loops of operations, then a graph convolutional layer can be described as follows:

$$\mathbf{h}^{(l+1)} = \sigma \left(\tilde{\mathbf{D}}^{-\frac{1}{2}} \tilde{\mathbf{A}} \tilde{\mathbf{D}}^{-\frac{1}{2}} \mathbf{h}^{(l)} \mathbf{W}^{(l)} \right)$$

Here, $\mathbf{h}^{(l)}$ are the operation embeddings at layer l , $\mathbf{W}^{(l)}$ is a trainable weight matrix at layer l , and $\sigma(\cdot)$ is an activation function such as ReLU. Further, $\tilde{\mathbf{D}}$ is the diagonal degree matrix of $\tilde{\mathbf{A}}$, ensuring appropriate scaling of the features.

Given the operation embeddings, the decoder of L2D first extracts for each job the embedding of the operation that needs to be scheduled next and then feeds them to an MLP $f : \mathbb{R}^{J \times d} \rightarrow \mathbb{R}^{J \times 1}$ to obtain logits for each job $j \in (1, \dots, J)$. In contrast to Kool et al. [74] for example, who encode the CO problem once and then generate actions autoregressively using only the decoder, Zhang et al. [153] use the GCN encoder after each step to generate new hidden representations that reflect the current state of the problem.

C.2.10 HGNN [125]

The heterogeneous graph neural network (HGNN) is a neural network architecture proposed by [125] to solve the FJSSP. Similar to L2D, HGNN considers an FJSSP instance as a graph. However, instead of treating an FJSSP instance as a disjunctive graph, Song et al. [125] formulate it as heterogeneous graph with operations and machines posing different node types. Again, operations are connected to each other via directed arcs that specify the precedence relation. Machines are only connected to operations that they are able to process, and the edge weights indicate the respective processing times. To encode the graph, HGNN first projects operations $O \in x$ and machines $M \in x$ into a mutual embedding space \mathbb{R}^d using type-specific transformations \mathbf{W}^O and \mathbf{W}^M , respectively. Given the initial hidden representations \mathbf{h}_i^0 and \mathbf{h}_k^0 for operations $o_i \in O$ and machines $m_k \in M$, respectively, as well as edge embeddings \mathbf{h}_{ik} , an HGNN layer conducts weighted message passing between operations and machines using the processing times of operation-machine pairs:

$$\mathbf{h}_i^{l+1} = \sum_{j \in \mathcal{N}_i} \epsilon_i \mathbf{h}_j^l, \quad \text{where} \tag{27}$$

$$\epsilon_{ij} = \text{Softmax}(\mathbf{a}^\top [\mathbf{h}_j^l || \mathbf{h}_{ij}]). \tag{28}$$

Since operations in the FJSSP can be processed by multiple machines, the decoder must specify not only which job to process next but also on which machine the operation of the selected job should be executed. To this end, Song et al. [125] concatenates the hidden representations of every operation with the embeddings of every machine. The resulting embeddings are fed to an MLP $f : \mathbb{R}^{J \times M \times 2d} \rightarrow \mathbb{R}^{J \times M \times 1}$, which generates the sampling probabilities for the respective action.

C.2.11 MatNet [77]

The MatNet architecture proposed by Kwon et al. [77] adjusts the attention model [74] so that it is applicable to bipartite graphs with node types \mathcal{I} and \mathcal{J} as well as a weight matrix $E \in \mathbb{R}^{|\mathcal{I}| \times |\mathcal{J}|}$

corresponding to the edges connecting nodes from the two sets. The novelty of this architecture is that instead of using self-attention as in the attention model, MatNet uses cross-attention to perform message passing between both node sets and augments the resulting attention scores with the weight matrix E . Formally, let \mathcal{Z} be the set of all nodes $i \in \mathcal{I} \cup \mathcal{J}$, \mathcal{Z}_{ϕ_i} the subset of nodes of the same type as i and $\mathcal{Z}_{\phi_i}^C$ the set of nodes of the respective type. Then, cross-attention is defined as:¹⁴

$$\alpha'_{ij} = \frac{\mathbf{q}_i^\top \mathbf{k}_j}{\sqrt{d_k}}, \quad \forall i \in \mathcal{Z}, j \in \mathcal{Z}_{\phi_i}^C \quad (29)$$

where

$$\mathbf{q}_i = W_{\phi_i}^Q \mathbf{h}_i^{l-1} \quad \mathbf{k}_j = W_{\phi_i}^K \mathbf{h}_j^{l-1} \quad (30)$$

and weight matrices $W_{\phi_i}^Q$ and $W_{\phi_i}^K \in \mathbb{R}^{d_k \times d_h}$ being learned by the update function corresponding to nodes of type ϕ_i . After that, MatNet augments α'_{ij} with the corresponding edge weight e_{ij} and maps it through a feed-forward neural network $\text{FF} : \mathbb{R}^2 \rightarrow \mathbb{R}$ to a scalar score, which is then normalized using the softmax function:

$$\alpha_{ij} = \frac{\exp(\epsilon_{ij})}{\sum_{q \in \mathcal{Z}_{\phi_i}^C} \exp(\epsilon_{iq})}, \quad \epsilon_{ij} = \text{FF}([\alpha'_{ij} || e_{ij}]) \quad (31)$$

The resulting weights are used to compute a weighted average of the embeddings $\mathbf{v}_j = W_{\phi_i}^V \mathbf{h}_j^{l-1}$ of the nodes in $\mathcal{Z}_{\phi_i}^C$. In the end, skip connections, layer normalization (LN), and feed-forward layers are used as in Vaswani et al. [136]. Besides the original MatNet implementation, RL4CO also implements a version that applies both self- and cross-attention, successively as proposed by Luttmann and Xie [95]. This makes MatNet not only applicable to bipartite graph problems but to the more general class of heterogeneous graphs [95].

C.2.12 DevFormer [67]

We employ online RL variants of DevFormer [67] (DF), an Attention-Model [74] variant specifically designed for autoregressive construction of DPP solutions from Appendix B.3.1. We note that the DF training scheme was initially designed for offline training; however, in this study, we benchmark DF as a sample-efficient online reinforcement learning approach. We benchmark the DF version for RL with the same node and context embedding structure as the original in Kim et al. [67]. We modify the embeddings in the mDPP environment (Appendix B.3.2) version to include the location of multiple probing ports. Min-max and min-sum mDPP versions utilize the same embeddings and are trained separately.

C.3 Constructive Non-Autoregressive (NAR)

C.3.1 DeepACO [150]

Ant Colony Optimization (ACO) is an evolutionary algorithm that has been successfully applied to various COPs. Traditionally, customizing ACO for a specific problem requires the expert design of knowledge-driven heuristics. However, this routine of algorithm customization exhibits certain deficiencies: 1) it requires extra effort and makes ACO less flexible; 2) the effectiveness of the heuristic measure heavily relies on expert knowledge and manual tuning; and 3) designing a heuristic measure for less-studied problems can be particularly challenging, given the paucity of available expert knowledge.

DeepACO is designed to automatically strengthen the heuristic measures of existing ACO algorithms and dispense with laborious manual design in future ACO applications. DeepACO consists of two stages: 1) training a neural model to map a COP instance to its heuristic measures, and 2) incorporating the learned heuristic measures into ACO to bias solution constructions and local search. During the training phase, DeepACO parameterizes the heuristic space with a graph neural network (GNN) [61]. It trains the GNN across COP instances with REINFORCE, towards minimizing the expected objective value of both constructed solutions and solutions refined by local search. Dur-

¹⁴For succinctness, note that we omit head and layer enumeration.

ing the inference phase, DeepACO utilizes the well-trained GNN to generate heuristic measures for ACO. Optionally, DeepACO interleaves local search with neural-guided perturbation to refine the constructed solutions. For more details, please refer to [150].

DeepACO is the first NAR model implemented in RL4CO, laying the foundation for other NAR models later integrated into RL4CO. DeepACO offers a versatile methodological framework that allows for further algorithmic enhancements in neural architecture, training paradigms, decoding strategies, and problem-specific adaptations. Notable improvements over DeepACO are introduced by GFACS [70].

C.3.2 GFACS [70]

While DeepACO [150] provides promising results and opens new doors for pretraining heuristic measures for the ACO algorithm using deep learning, their method is sub-optimal for two major reasons. Firstly, they utilized policy gradient reinforcement learning (RL), which is an on-policy method that cannot leverage powerful off-policy techniques such as local search. Secondly, their method cannot effectively capture the multi-modality of heuristic distribution because the RL method cannot accurately model multi-modal probabilistic distributions considering the symmetric nature of combinatorial space, where multiple trajectories can lead to identical solutions.

The methodology of GFACS shares a very similar structure with DeepACO. The key difference lies in the learning procedure; GFACS employs generative flow networks (GFlowNets) [9, 11] for learning the heuristic matrix. Additionally, they leverage effective off-policy exploration methods using local search. The inference procedure with the learned heuristic matrix remains exactly the same. With the RL4CO modular implementation, both DeepACO and GFACS can run similarly and be comparable at the modular level, allowing future researchers to improve certain modules of training or inference.

C.3.3 GLOP [152]

Most NCO methods struggle with real-time scaling-up performance; they are unable to solve routing problems involving thousands or tens of thousands of nodes in seconds, falling short of the needs of modern industries. GLOP (Global and Local Optimization Policies) is proposed to address this challenge. It partitions a large routing problem into sub-TSPs and further partitions potentially large (sub-)TSPs into small Shortest Hamiltonian Path Problems (SHPPs). It is the first hybrid method to integrate NAR policies for coarse-grained problem partitions and AR policies for fine-grained route constructions, leveraging the scalability of the former and the meticulousness of the latter.

1) AR (Sub-)TSP Solver. The (Sub-)TSP Solver in GLOP initializes TSP tours using a Random Insertion heuristic, which greedily inserts nodes to minimize cost. These tours are then improved through a process of decomposition and reconstruction. Specifically, the solver decomposes a complete tour into several subtours, which are treated as instances of the Shortest Hamiltonian Path Problem (SHPP). Each subtour is solved using an AR local policy referred to as a “reviser”. These revisers are applied in rounds called “revisions” to enhance the initial tour iteratively. The subtours are normalized and optionally rotated to improve the model’s performance. After solving the SHPP instances, the subtours are reassembled into an improved complete tour. This method allows for efficient and parallelizable improvements on large-scale TSPs.

2) NAR General Routing Solver. The general routing solver in GLOP additionally implements an NAR global policy that either partitions all nodes into multiple sub-TSPs (e.g., for CVRP) or subsets all nodes to form a sub-TSP (e.g., for PCTSP). The NAR global policy is parameterized by a graph neural network (GNN) that processes sparsified input graphs and outputs a partition heatmap. GLOP clusters or subsets nodes by sequentially sampling nodes based on the partition heatmap while adhering to problem-specific constraints. The sub-TSPs are then solved by the (Sub-)TSP solver. The global policy is trained using REINFORCE to output partitions that could lead to the best-performing final solutions after solving sub-TSPs.

GLOP is integrated into RL4CO as the first hybrid method that combines NAR and AR policies, indicating the versatility of RL4CO in accommodating various methodological paradigms. It is promising to further investigate the emerging possibilities that arise when viewing AR and NAR

methods from a unified perspective and combining them synergistically. RL4CO provides a flexible and extensible platform for exploring such hybridization in future research.

C.4 Improvement methods

Improvement methods leverage RL to train a policy that iteratively performs rewriting exchanges on the current solution, aiming to generate a new solution with potentially lower costs. As in constructive methods, the policy of improvement methods is also based on the encoder-decoder structure.

C.4.1 DACT [96]

Improvement methods typically take node features and solution features (positional information of nodes in the current solution) as key inputs. Encoding VRP solutions involves processing complex relationships between Node Feature Embeddings (NFEs) and Positional Feature Embeddings (PFEs). However, directly adopting the original Transformer to add the two types of embeddings, as done by Wu et al. [145], can cause mixed attention score correlations and impairing performance. To address this, the Dual-Aspect Collaborative Transformer (DACT) proposes DAC-Att, which processes NFEs and PFEs separately and employs cross-aspect referential attention to understand the consistencies and differences between the two embedding aspects. This approach avoids mixed correlations and allows detailed modeling of hidden patterns. Another key issue is the Positional Encoding (PE) method. While the original Transformer’s PE works well for linear sequences, it may not suit the cyclic nature of VRP solutions. To address this, DACT proposes Cyclic Positional Encoding (CPE), inspired by cyclic Gray codes, which generates cyclic real-valued coding vectors to capture the topological structure of VRP solutions and improve generalization. Additionally, DACT redesigns the RL algorithm for improvement methods, introducing a Proximal Policy Optimization with Curriculum Learning (PPO-CL) algorithm to improve training stability and efficiency.

In RL4CO, DACT is implemented and modularized so that other methods can easily reuse components like CPE encoding and the PPO-CL algorithm. It also reuses common parts (such as node embedding initialization, decoding functions, etc) from the implementation of constructive methods, indicating the flexibility of the RL4CO framework.

C.4.2 N2S [97]

The Neural Neighborhood Search (N2S) method extends the capabilities of improvement methods to pickup and delivery problems (PDP). Expanding on the DACT approach, N2S leverages a tailored MDP formulation for a ruin-repair neighborhood search process. It uses a Node-Pair Removal decoder in the ruin stage and a Node-Pair Reinsertion decoder in the repair stage, allowing efficient operation on pickup-delivery node pairs. However, more complex decoders increase computational costs in the policy network, requiring a balance between encoders and decoders. To address this, N2S introduces Synthesis Attention (Synth-Att), which learns a single set of embeddings and synthesizes attention scores from various node feature embeddings using a Multilayer Perceptron (MLP) module. This promotes lightweight policy networks and enhances model expressiveness. The N2S encoder with the efficient Synth-Att represents a state-of-the-art design of improvement encoder, which is adopted in the latest works [97, 98].

In RL4CO, N2S reuses the CPE encoding and the PPO-CL algorithm implemented in DACT. The efficient N2S encoder is also modularized and designed to be shared among other improvement methods to process the complex relationships between different feature embeddings.

C.4.3 NeuOpt [98]

A key bottleneck of improvement methods like DACT is their simplistic action space design, which typically uses smaller, fixed k values (2-opt or 3-opt) due to decoders struggling with larger, varying k . To address this, the latest improvement method introduces Neural k-Opt (NeuOpt), a flexible solver capable of handling any given $k \geq 2$. NeuOpt employs an action factorization method to break down complex k-opt exchanges into a sequence of basis moves (S-move, I-move, E-move), with the number of I-moves determining the k value. This step-by-step construction allows the model to automatically determine a suitable k . Similar to variable neighborhood search, NeuOpt combines varying k values across search steps, balancing coarse-grained and fine-grained searches, which is crucial for optimal performance. NeuOpt also features a Recurrent Dual-Stream (RDS)

decoder with recurrent networks and two decoding streams for contextual modeling and attention computation, effectively capturing the complex dependencies between removed and added edges.

In RL4CO, NeuOpt is implemented by reusing the successful CPE and PPO-CL training modules from DACT, as well as the efficient encoder from N2S. This demonstrates the strength and versatility of the RL4CO coding library, which allows for the easy integration of proven methodologies.

C.5 Active Search Methods

Active search methods are examples of *transductive* RL, in which an RL algorithm is run to finetune a pre-trained policy on specific test-time instances.

C.5.1 Active Search (AS) [8]

In active search proposed by Bello et al. [8], a model is fine-tuned to a single test instance. To this end, active search uses the same loss formulation as during the original training of the model. Over the course of the search process, the model’s performance on the single test instance improves, leading to the discovery of high-quality solutions. While active search is easy to implement, as the search process closely follows the training process, it is often very slow since all model weights are adjusted for each test instance individually.

C.5.2 Efficient Active Search (EAS) [50]

Efficient active search (EAS), proposed by Hottung et al. [50], builds upon the idea of active search and trains a model on a single instance at test time to enable a guided search. However, EAS only updates a subset of parameters during the search and allows most operations to be performed in parallel across a batch of different instances. This approach not only reduces computational costs but also results in a more stable fine-tuning process, leading to an overall improvement in solution quality.

D Benchmarking Setup

D.1 Metrics

D.1.1 Gap to BKS

The Gap to Best Known Solution (BKS) is a commonly used metric to evaluate the performance of optimization algorithms on benchmark instances. It measures the relative difference between the best solution found by the algorithm and the BKS for a given problem instance. Given a problem instance i , let a_i be the objective value of the best solution found by the algorithm, and let a_i^* be the objective value of the BKS for that instance. The Gap to BKS for the i -th instance is defined as:

$$\text{Gap to BKS}_i = 100 \times \left(\frac{a_i - a_i^*}{a_i^*} \right) \quad (32)$$

The Gap to BKS is expressed as a percentage, with a value of 0% indicating that the algorithm has found a solution that matches the BKS. A positive Gap to BKS indicates that the algorithm’s solution is worse than the BKS, while a negative Gap to BKS (though less common) indicates that the algorithm has found a new best solution for the instance¹⁵.

D.1.2 Primal Integral

The Primal Integral (PI) is a metric that evaluates the anytime performance of optimization algorithms by capturing the trade-off between solution quality and computational time [12, 133]. It is defined as the area under the curve of the incumbent solution value plotted against time, normalized by the BKS value and the total time budget:

¹⁵Note that when calculating the gap for a set of instances, one should do an average of gaps, i.e. $\frac{1}{n} \sum_{i=1}^n \text{Gap to BKS}_i$, instead of calculating the gap of the average $100 \times \sum a_i / \sum a_i^*$, which might yield similar results in some settings but prone to error especially for certain distributions.

$$PI = 100 \times \left(\frac{\sum_{i=1}^n \mathbf{a}_{i-1} \cdot (t_i - t_{i-1}) + \mathbf{a}_n \cdot (T_{\max} - t_n)}{T_{\max} \cdot \mathbf{a}^*} - 1 \right) \quad (33)$$

where T_{\max} is the total time budget, \mathbf{a}_i is the incumbent solution value at time t_i , and \mathbf{a}^* is the best known solution value. A lower PI percentage indicates better anytime performance. The PI complements other metrics, such as the Gap to BKS, by providing insights into the temporal aspect of an algorithm’s performance, making it particularly useful for assessing anytime algorithms [58].

D.1.3 Runtime Measurement

Runtime normalization Comparing the run-time efficiency of different methods across various hardware configurations can be challenging. In the RL4CO benchmark, we generally run the inference on a single machine; when this is not possible due to resource limitations, we employ the run-time normalization approach based on the *PassMark* hardware rating¹⁶. This approach normalizes time budgets and run times during the evaluation process, allowing for a more equitable comparison of methods. We use the definition of Accorsi et al. [1], Thyssens et al. [133] in normalizing: the reference machine combines a single CPU thread and a single GPU, the *PassMark* score s for GPU-based methods is calculated as:

$$s = \frac{1}{2} (\#CPU \cdot CPU_Mark + \#GPU \cdot GPU_Mark) \quad (34)$$

To normalize the solution time from machine 1 to machine 2, we calculate $\tilde{t}_2 = t_1 \frac{s_1}{s_2}$, where t_1 is the solution time on machine 1, s_1 is the *PassMark* score of machine 1, and s_2 is the *PassMark* score of machine 2. Note that in the case of most classical solvers, the GPU_Mark is simply set to 0 due to them running on CPU.

Cross-solver comparisons Another aspect of NCO evaluation that has to be addressed is the fact that evaluation between classical and learned solvers is often done on different devices, namely on (single-threaded) CPUs and GPUs, respectively. Moreover, while multiple instances in NCO can usually be solved in a batch, this is not usually the case for classical solvers. A more correct way is to measure the *per-instance* solution time (which we do on large-scale NAR routing), which is more realistic for real-world applications. For other studies, we employ the standard procedure of NCO of evaluating times on batches as done in the original methods, making sure to compare “apples with apples” (i.e., different NCO approaches are compared with the same settings). We note that while RL4CO focuses on comparisons between NCO solvers and creating an open-source ecosystem for this specific area, future studies (and possibly works in the RL4CO community) may also include comparisons with classical solvers under different conditions, which we recognize as an important research direction.

D.2 Hardware & Software

D.2.1 Hardware

Most experiments (during testing) were carried out on a machine equipped with two AMD EPYC 7542 32-CORE PROCESSOR CPUs with 64 threads each and four NVIDIA RTX A6000 graphic cards with 48 GB of VRAM, of which only one is used during inference. We note that, due to the amount of experiments and contributions, training was performed on a variety of hardware combinations, particularly University clusters. We found RL4CO to be robust and efficient across different combinations of CPU, GPU, and software. Throughout the text, we may report the hardware setting on which testing took place if it differs from the default one. In case different configurations were used or results were reported from previous works, we refer to Appendix D.1.3 for result standardization.

¹⁶*PassMark*: <https://www.passmark.com/> is also used in the 2022 DIMACS challenge: <http://dimacs.rutgers.edu/programs/challenge/vrp/>.

D.2.2 Software

Software-wise, we used Python 3.11 and PyTorch 2.3 [110]¹⁷, most notably due to the native implementation of `scaled_dot_product_attention`. Given that most models in RL constructive methods for CO generally use attention for encoding states, FlashAttention has some boost on the performance (between 5% and 20% saved time depending on the problem size) when training is subject to mixed-precision training, which we do for all experiments. During decoding, the FlashAttention routine is not called since, at the time of writing, it does not support maskings other than causal; this could further boost performance compared to older implementations. Refer to Appendix A.2 for additional details regarding notable software choices of our library, namely TorchRL, PyTorch Lightning, and Hydra.

D.3 Hyperparameters

D.3.1 Common Hyperparameters

Common hyperparameters can be found in the `config/` folder from the RL4CO library, which can be conveniently loaded by Hydra. We provide yaml-like configuration files below, divided by experiments in Listing 1.

D.3.2 Changing Policy Components

We train the models evaluated in Table 2 using the same number of training instances as well as identical hyperparameters. Specifically, models are trained for 10 epochs on 2.000 training instances using the PPO algorithm with clip range $\epsilon = 0.2$. The training dataset is split into batches of size 100 to construct the replay buffer. For the PPO optimization we sample mini-batches of size 512 from the replay buffer until it is empty and repeat this for $\mathcal{R} = 3$ inner epochs. All models use an embedding dimension d_h of 256. The number of encoder layers is set to $L = 3$ in each case. Further, MatNet and the AM Pointer use $H = 8$ attention heads. The parameters of the models are updated using the Adam optimizer with learning rate 10^{-4} . Afterwards, the trained policies are evaluated on 1.000 randomly generated test instances. The Hydra config files corresponding to this experiment, which also implement the different model architectures, can be found in the `config/experiment/scheduling` folder from the RL4CO library

D.3.3 Mind Your Baseline

We run all models to match the original implementation details under *controlled* settings. In particular, we run all models for 250,000 gradient steps with the same Adam [71] optimizer with a learning rate of 10^{-4} and 0 weight decay. For POMO, we match the original implementation details of weight decay as 10^{-6} . For POMO, the number of multistarts is the same as the number of possible initial locations in the environment (for instance, for TSP50, 50 starts are considered). In the case of Sym-NCO, we use 10 as augmentation for the shared baseline; we match the number of effective samples of AM-XL to the ones of Sym-NCO to demonstrate the differences between models.

¹⁷During development, we also used beta wheels as well as manually installed version of FlashAttention [34, 33]. Note that software version varied in terms of training runs depending on the author who ran experiments (e.g. any range of Python and PyTorch as $[3.9, 3.10, 3.11] \times [2.0, 2.1, 2.2, 2.3]$, which RL4CO can support out of the box on multiple devices and operating systems.

Example Hydra Configuration

```

1  defaults: # override default configurations under configs/
2    - override /env: tsp.yaml
3    - override /model: am.yaml
4    - override /callbacks: default.yaml
5    - override /trainer: default.yaml
6    - override /logger: wandb.yaml
7
8  # Environment
9  env:
10   generator_params:
11     num_loc: 50
12
13 # RL Algorithm and policy (env passed automatically)
14 model:
15   policy: # override policy parameters to pass to the RL algo
16     _target_: rl4co.models.zoo.am.policy.AttentionModelPolicy
17     embed_dim: 128
18     num_heads: 8
19     num_encoder_layers: 3
20     feedforward_hidden: 128
21     env_name: "${env.name}" # automatically construct env embeddings
22     baseline: "rollout" # REINFORCE baseline
23     batch_size: 512
24     train_data_size: 1_280_000
25     optimizer_kwargs:
26       lr: 1e-4
27
28 # Optional override of checkpoint parameters
29 model_checkpoint:
30   dirpath: ${paths.output_dir}/checkpoints
31   filename: "epoch_{epoch:03d}"
32
33 # Trainer
34 trainer:
35   max_epochs: 100
36   gradient_clip_val: 1.0
37   max_epochs: 100
38   precision: "16-mixed" # allows for FlashAttention
39   strategy: DDPStrategy # efficient for multiple GPUs
40   matmul_precision: "medium" # speeds up calculation
41
42 # Logging
43 logger:
44   wandb:
45     project: "rl4co"
46     name: "am-tsp${env.generator_params.num_loc}"

```

Listing 1: Example `example.yaml` configuration for the AM from the AR routing experiments. Additional parameters are modularized in the actual configs and moved to the other config folders (such as `env/tsp.yaml` so that a single experiment config is not too cluttered. Running this configuration is simple: placed under `configs/experiments/`, it can be called with `python run.py experiment=example`.

The number of epochs for all models is 100, except for AM-XL (500). We also employ learning rate scheduling, in particular, MultiStepLR¹⁸ with $\gamma = 0.1$ on epoch 80 and 95; for AM-XL, this applies on epoch 480 and 495.

PPO for the AM We follow other hyperparameters for REINFORCE baselines. We set the number of mini-epochs to 2, mini-batch size to 512, clip range to 0.2, and entropy coefficient $c_2 = 0.01$. Interestingly, we found that normalizing the advantage as done in the Stable Baselines PPO2 imple-

¹⁸https://pytorch.org/docs/stable/generated/torch.optim.lr_scheduler.MultiStepLR.html

mentation¹⁹ slightly hurt performance, so we set the normalize advantage parameter to `False`. We suspect this is because the NCO solvers are trained on *multiple* problem instances, unlike the other RL applications that aim to learn a policy for a single MDP.

Sample Efficiency Experiments We keep the same hyperparameters as the *mind your baseline*, experiments except for the number of epochs and scheduling. We consider 5 independent runs that match the number of samples *per step* (i.e., the batch size is exactly the same for all models after considering techniques such as the multistart and symmetric baselines). For AM Rollout, we employ half the batch size of other models since it requires double the number of evaluations due to its baseline.

Search Methods Experiments For these experiments, we employ the same models trained in the in-distribution benchmark on 50 nodes. For Active Search (AS), we run 200 iterations for each instance and an augmentation size of 8. The Adam optimizer is used with a learning rate of 2.6×10^{-4} and weight decay of 10^{-6} . For Efficient Active Search, we benchmark EAS-Lay (with an added layer during the single-head computation, `PointerAttention` in our code) with the original hyperparameters proposed by Hottung et al. [50]. The learning rate is set to 0.0041 and weight decay to 10^{-6} . The search is restricted to 200 iterations with dihedral augmentation of 8 as well as imitation learning weight $\lambda = 0.013$.

Testing is performed on 100 instances on both TSP and CVRP for $N \in [200, 500, 1000]$, generated with the usual random seed for testing 1234.

D.3.4 Generalization: Cross-Task and Cross-Distribution

In addition to training on uniformly distributed instances, as is standard for POMO [76], we further train POMO [76] on a mixture of multiple distributions (i.e., the exemplar distributions defined in [16]) and multiple VRP tasks (i.e., CVRP, OVRP, VRPL, VRPB, VRPTW, and OVRPTW, as defined in [89, 157, 13]) with fixed problem size $N = 50$, termed as MDPOMO and MTPOMO, respectively. Note that all the models in Table 4 undergo training across 10,000 epochs, each with a batch size of 512 and 10,000 training instances. The other training setups are consistent with the previous work [76]. The whole training time is within one day. During inference, we evaluate their generalization performance on the benchmark datasets in CVRPLib [86] using greedy rollout with 8× instance augmentation and multiple start nodes following Kwon et al. [76].

D.3.5 Large-Scale Instances

The GLOP [152] models’ global policy are trained on random instances of CVRP1K and CVRP2K, respectively. Both models are trained for 100 epochs, with each epoch comprising 1000 instances. To accelerate the training process, random insertion is utilized as the sub-TSP solver.

For the experiment results presented in Table 5, we evaluate our implementation using the identical instances and setup as those utilized in Ye et al. [152]. The AM revisers involved are directly adopted from Ye et al. [152]. Table 13 reports the generalization performance of the CVRP2K model on 100 CVRP10K instances and 24 CVRP20K instances. These test instances are generated following the procedure in Nazari et al. [106], with the capacities fixed to 1000.

D.3.6 Combining Construction and Improvement

To test the potential collaboration between constructive and improvement methods (in Appendix E.5 and Section 5.3), we recorded the performance of improvement methods during inference with initial solutions generated either randomly or by leveraging solutions generated greedily by constructive methods. This was done for both TSP and PDP with a fixed problem size of $N = 50$. We used a test set with 1,000 instances for both TSP and PDP and recorded the runtime for all constructive and improvement solvers based on an INTEL XEON GOLD 5317 CPU @ 3.00GHz and one RTX 3090 GPU.

For the constructive models to bootstrap improvement, we used the POMO and HAM (i.e. AM with rollout baseline, with HAM [82] encoder for construction PDP) directly from Appendix D.3.3. Note

¹⁹<https://stable-baselines.readthedocs.io/en/master/modules/ppo2.html>

that these models were trained under controlled settings and could see a further boost in performance with further training. Moreover, while we used simple greedy evaluation, more complex evaluation schemes may be used, such as combining symmetric augmentation, multistart, or advanced sampling techniques as nucleus sampling.

For the improvement models, we used both DACT and NeuOpt (with $K = 4$) for TSP, and the N2S model for PDP. Training for all models was conducted with 200 epochs and 20 batches per epoch, with a batch size of 512 for TSP and 600 for PDP. The n-step and maximum improvement steps for training were set to 4 and 200, respectively. Other hyperparameters such as learning rate, curriculum learning scaler, and gradient norm clip were set as per their original papers.

D.4 Decoding Schemes

Due to the limited space in the main paper, we further elaborate on the setup of the decoding schemes (or *strategies* in this section, shown in Fig. 16).

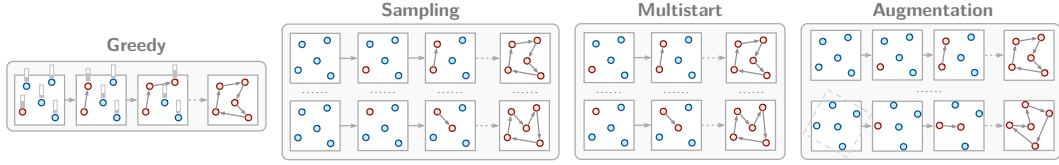


Figure 16: Inference methods we consider in RL4CO. These can also be combined together, such as greedy multistart with augmentation.

D.4.1 Augmentations

In RL4CO, we consider as augmentations any transformation ψ that maps an instance x into an instance x' whose (optimal) solution should be the same or close to the original. Augmentations have been used in various domains, such as computer vision, where, for example, labels are invariant to rotations. Similarly, in Euclidean CO, one can apply the *dihedral transformation* of Table 9 to generate a new instance whose solution is the same as the original one, composed of 4 rotations and 2 flips for a total of $\times 8$ transformation (which is the default used in POMO-based models as Kwon et al. [76], Liu et al. [89], Zhou et al. [157]. As introduced in Kim et al. [69], one may additionally use any angle θ to perform a symmetric transformation as follows:

$\psi(x, y)$	
(x, y)	(y, x)
$(x, 1-y)$	$(y, 1-x)$
$(1-x, y)$	$(1-y, x)$
$(1-x, 1-y)$	$(1-y, 1-x)$

$$\begin{pmatrix} x' \\ y' \end{pmatrix} = \psi(x, y) = \begin{pmatrix} x \cos \theta & -y \sin \theta \\ x \sin \theta & +y \cos \theta \end{pmatrix}$$

where $\theta \in [0, 2\pi]$. Interestingly, we found that, generally, the dihedral augmentation is worse in terms of sample efficiency compared to randomly augmenting by sampling a θ value. We note that other augmentations are possible, including dilation [7] (i.e., rescaling) and possibly new ones such as *jittering*, which may have a broader application than Euclidean CO.

D.4.2 Sampling

In most NCO approaches, sampling is performed by simply increasing the evaluation budget but without additional modifications that can be important for better performance. We include the following techniques in RL4CO: 1) *Sampling with Softmax Temperature*, 2) *Top-k Sampling* and 3) *Top-p Sampling*, visualized in Fig. 17.

Sampling with Softmax Temperature Sampling with softmax temperature is a technique used to control the randomness of the sampling process. The temperature parameter τ is introduced to the softmax function, which converts the logits z into a probability distribution:

$$p_i = \frac{\exp(z_i/\tau)}{\sum_{j=1}^N \exp(z_j/\tau)} \quad (35)$$

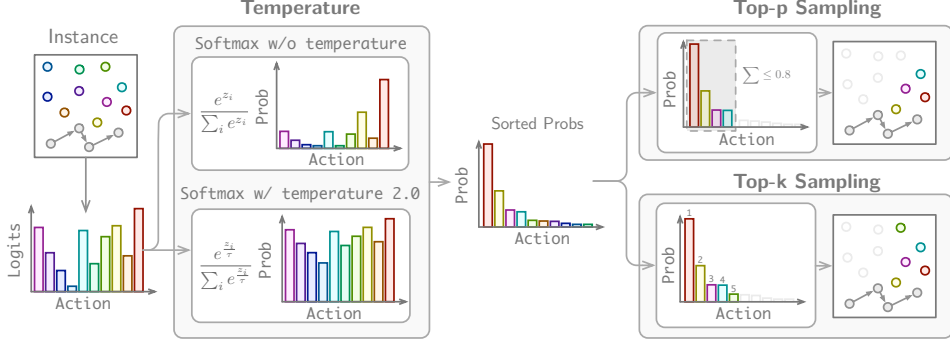


Figure 17: Sampling techniques implemented in RL4CO.

where p_i is the probability of selecting the i -th action, z_i is the corresponding logit, and N is the total number of actions. A higher temperature $\tau > 1$ makes the distribution more uniform, increasing the chances of selecting less likely actions. Conversely, a lower temperature $0 < \tau < 1$ makes the distribution sharper, favoring the most likely actions.

Top-k Sampling Top-k sampling is a method that restricts the sampling space to the k most likely actions. Given the logits \mathbf{z} , the top-k actions with the highest probabilities are selected, and the probabilities of the remaining actions are set to zero. The probability distribution is then renormalized over the selected actions:

$$p_i = \begin{cases} \frac{\exp(z_i/\tau)}{\sum_{j \in \mathcal{T}_k} \exp(z_j/\tau)} & \text{if } i \in \mathcal{T}_k \\ 0 & \text{otherwise} \end{cases} \quad (36)$$

where \mathcal{T}_k is the set of indices corresponding to the top-k actions. Top-k sampling helps to eliminate the possibility of generating low-probability actions, improving the quality and coherence of the generated output. We note that, however, in CO problems, it may not be as straightforward as in large language models to select the k parameter since neighborhoods and distributions are not homogeneous.

Top-p Sampling Top-p sampling, also known as nucleus sampling, is an alternative to top-k sampling that dynamically adjusts the number of actions considered for sampling based on a probability threshold p [48]. The actions are sorted by their probabilities in descending order, and the cumulative probability is calculated. The sampling space is then restricted to the smallest set of actions whose cumulative probability exceeds the threshold p :

$$\mathcal{T}_p = \left\{ i : \sum_{j=1}^i p_j \leq p \right\} \quad (37)$$

where \mathcal{T}_p is the set of indices corresponding to the actions included in the top-p sampling. The probabilities of the actions in \mathcal{T}_p are renormalized, while the probabilities of the remaining actions are set to zero:

$$p_i = \begin{cases} \frac{\exp(z_i/\tau)}{\sum_{j \in \mathcal{T}_p} \exp(z_j/\tau)} & \text{if } i \in \mathcal{T}_p \\ 0 & \text{otherwise} \end{cases} \quad (38)$$

Top-p sampling provides a more dynamic way to control the diversity and quality of the generated output compared to top-k sampling. In CO, this is also a more structured way of performing training or evaluation since top-p sampling is agnostic of the number of nodes, unlike top-k sampling.

E Additional Experiments

E.1 Mind your Baseline: Further Insights

Benchmark Setup We focus on benchmarking the AR routing NCO solvers under controlled settings, aiming to compare all benchmarked methods as closely as possible in terms of network architectures and the number of training samples consumed.

Models We evaluate the following NCO solvers: 1) *AM* [74] with rollout baseline, 2) *POMO* [76] with the shared baseline to train AM instead of the rollout baseline; we also use six MHA layers and InstanceNorm instead of BatchNorm according to the original implementation, 3) *Sym-NCO* [69] utilizes the symmetric baseline to train AM instead of the rollout baseline and the same encoder as POMO, 4) *AM-XL* is an AM model that adopts *POMO*-style MHA encoder, and trained on the same number of samples as POMO, with the goal of seeing whether training for longer, as done in POMO, can significantly improve the results 5) *A2C*, i.e. AM trained with Advantage Actor-Critic (A2C), 6) *AM-PPO* trained via the Proximal Policy Optimization (PPO, Schulman et al. [119]) algorithm and finally 7) PolyNet [51] with shared baseline and setting $K = n$.

For fairness of comparison, we try to match the number of training steps to be the same and adjust the batch size accordingly. Specifically, we train models for 100 epochs as in Kool et al. [74] using the Adam optimizer [71] with an initial learning rate (LR) of 0.001 with a decay factor of 0.1 after the 80th and 95th epochs²⁰. We evaluate the trained solvers using the schemes shown in Fig. 16.

E.1.1 Main In-distribution Results

We first measure the performances of NCO solvers on the same dataset distribution on which they are trained. We first observe that, counter to the commonly known trends that *AM* < *POMO* < *Sym-NCO*, the trends can change to decoding schemes and targeting CO problems. Especially when the solver decodes the solutions with *Augmentation* or *Greedy Multistart + Augmentation*, the performance differences among the benchmarked solvers on TSP and CVRP become less significant. Surprisingly, PolyNet performs well even in the greedy one-shot setting, despite its primary focus on generating diverse solutions. For decoding schemes that generate multiple solutions, PolyNet demonstrates strong performance across various problems. Particularly for decoding schemes without multistarts, PolyNet benefits significantly from its inherent diversity mechanism

We note that the original implementation of POMO²¹ is not directly applicable to OP, PCTSP, and PDP. Adapting it to solve new problems is not straightforward due to the coupling between environment and policy implementations. However, owing to the flexibility of RL4CO, we successfully implemented POMO for OP and PCTSP. Our results indicate that POMO underperforms in OP and PCTSP; unlike TSP, CVRP, and PDP, where all nodes need to be visited, OP and PCTSP are not constrained to visit all nodes. Due to such differences, POMO’s visiting all nodes strategy may not work as an effective inductive bias. Further, we benchmark the NCO solvers for PDP, which was not originally supported natively by each of the benchmarked solvers. We apply the environment embeddings and the Heterogeneous Attention Encoder from HAM [82] to the NCO models for encoding pickup and delivery pairs, further emphasizing RL4CO’s flexibility. We observe that AM-XL, which employs the same RL algorithm as AM but features the encoder architecture of POMO and is trained with an equivalent number of samples, yields performance comparable to NCO solvers using more sophisticated baselines. This suggests that careful controls on architecture and the number of training samples are required when evaluating NCO solvers. We also re-implemented PointerNetworks [139, 8], but we excluded them from the main table due to their poor performance, i.e., more than 4% optimality gap in TSP50.

Table 10 and Table 11 show detailed results for 50 and 20 nodes, respectively.

E.1.2 Decoding Schemes Comparison

During inference, investing more computational resources (i.e., sampling more), the trained NCO solver can discover improved solutions. We examine the performance gains achieved with varying

²⁰We find that simple learning rate scheduling with *MultiStepLinear* can improve performance i.e., compared to the original AM implementation.

²¹<https://github.com/yd-kwon/POMO>

Table 10: In-distribution benchmark results for routing problems with 50 nodes. We report the gaps to the best-known solutions of classical heuristics solvers.

Method	TSP			CVRP			OP			PCTSP			PDP		
	Cost ↓	Gap	Time	Cost ↓	Gap	Time	Prize ↑	Gap	Time	Cost ↓	Gap	Time	Cost ↓	Gap	Time
<i>Classical Solvers</i>															
<i>Gurobi</i>	5.70	0.00%	2m	—	—	—	—	—	—	—	—	—	—	—	—
<i>Concorde</i>	5.70	0.00%	2m	—	—	—	—	—	—	—	—	—	—	—	—
<i>HGS</i>	—	—	—	10.37	0.00%	10h	—	—	—	—	—	—	—	—	—
<i>Compass</i>	—	—	—	—	—	—	16.17	0.00%	5m	—	—	—	—	—	—
<i>LKH3</i>	5.70	0.00%	5m	10.38	0.10%	12h	—	—	—	—	—	—	6.86	0.00%	1h30m
<i>OR Tools</i>	5.80	1.83%	5m	—	—	—	—	—	4.48	0.00%	5h	7.36	7.29%	2h	—
<i>Greedy One Shot Evaluation</i>															
A2C	5.83	2.22%	<1s	11.16	7.09%	<1s	14.77	8.64%	<1s	5.15	14.96%	<1s	7.52	9.90%	<1s
AM	5.78	1.41%	<1s	10.95	5.30%	<1s	15.46	4.40%	<1s	4.59	2.46%	<1s	7.51	9.88%	<1s
POMO	5.75	0.89%	<1s	10.80	3.99%	<1s	13.86	14.26%	<1s	5.00	11.61%	<1s	7.59	10.64%	<1s
Sym-NCO	5.72	0.47%	<1s	10.87	4.61%	<1s	15.67	3.09%	<1s	4.52	2.12%	<1s	7.39	7.73%	<1s
AM-XL	5.73	0.54%	<1s	10.84	4.31%	<1s	15.69	2.98%	<1s	4.53	2.44%	<1s	7.31	6.56%	<1s
AM-PPO	5.76	0.92%	<1s	10.87	4.60%	<1s	15.67	3.05%	<1s	4.55	2.45%	<1s	7.43	8.31%	<1s
PolyNet	5.72	0.68%	2s	10.81	4.24%	2s	15.70	2.93%	2s	4.54	2.45%	2s	8.26	3.46%	2s
<i>Sampling with width M = 1280</i>															
A2C	5.74	0.72%	40s	10.70	3.07%	1m24s	15.14	6.37%	48s	4.96	10.71%	57s	7.32	6.70%	1m15s
AM	5.72	0.40%	40s	10.60	2.22%	1m24s	15.90	1.68%	48s	4.52	0.99%	57s	7.25	5.69%	1m15s
POMO	5.71	0.18%	1m	10.54	1.64%	2m30s	14.62	9.56%	1m10s	4.82	7.59%	1m23s	7.31	6.56%	1m50s
Sym-NCO	5.70	0.14%	1m	10.58	2.03%	2m30s	16.02	0.93%	1m10s	4.52	0.82%	1m23s	7.17	4.52%	1m50s
AM-XL	5.71	0.17%	1m	10.57	1.91%	2m30s	15.97	1.25%	1m10s	4.52	0.88%	1m23s	7.15	4.23%	1m50s
AM-PPO	5.70	0.15%	40s	10.52	1.52%	1m24s	16.04	0.78%	48s	4.48	0.18%	57s	7.17	4.52%	1m15s
PolyNet	5.70	0.15%	1m20s	10.42	0.53%	2m40s	16.08	0.52%	1m15s	4.47	0.13%	2m15s	6.93	0.81%	2m10s
<i>Greedy Multistart (N)</i>															
A2C	5.80	1.81%	2s	10.90	4.86%	6s	14.61	9.65%	4s	5.12	14.29%	5s	7.54	9.85%	4s
AM	5.77	1.21%	2s	10.73	3.39%	6s	15.71	2.84%	4s	4.56	1.89%	5s	7.46	8.75%	4s
POMO	5.71	0.29%	3s	10.58	2.04%	8s	13.95	13.71%	7s	4.98	11.16%	7s	7.46	8.75%	6s
Sym-NCO	5.72	0.36%	3s	10.71	3.17%	8s	15.88	1.79%	7s	4.55	1.59%	7s	7.38	7.58%	6s
AM-XL	5.72	0.42%	3s	10.68	2.88%	8s	15.85	1.95%	7s	4.56	1.79%	7s	7.25	5.69%	6s
AM-PPO	5.74	0.61%	2s	10.67	2.72%	6s	15.98	1.21%	4s	4.53	1.18%	5s	7.23	5.39%	4s
PolyNet	5.70	0.25%	3s	10.52	1.42%	18s	16.05	0.71%	3s	4.54	1.31%	10s	7.18	4.65%	5s
<i>Greedy with Augmentation (1280)</i>															
A2C	5.71	0.18%	40s	10.63	2.49%	1m24s	14.89	7.91%	48s	5.15	14.96%	1m	7.03	2.46%	1m15s
AM	5.70	0.07%	40s	10.53	1.56%	1m24s	15.88	1.79%	48s	4.59	2.46%	1m	7.14	4.08%	1m15s
POMO	5.70	0.06%	1m	10.55	1.72%	2m30s	14.23	11.97%	1m15m	5.09	13.61%	1m42s	7.15	4.23%	1m45s
Sym-NCO	5.70	0.01%	1m	10.53	1.54%	2m30s	15.94	1.41%	1m15m	4.58	2.17%	1m42s	7.03	2.48%	1m45s
AM-XL	5.70	0.01%	1m	10.52	1.47%	2m30s	15.90	1.66%	1m15m	4.59	2.54%	1m42s	6.98	1.75%	1m45s
AM-PPO	5.70	0.15%	40s	10.52	1.52%	1m24s	16.01	0.84%	48s	4.48	0.18%	1m	7.00	2.04%	1m15s
PolyNet	5.70	0.17%	1m30s	10.47	0.92%	3m	16.05	0.72%	2m	4.47	0.10%	2m10s	6.94	1.20%	2m15s
<i>Greedy Multistart with Augmentation (N × 16)</i>															
A2C	5.72	0.41%	32s	10.67	2.81%	1m	15.22	5.88%	30s	5.06	12.94%	35s	7.10	3.51%	50s
AM	5.71	0.21%	32s	10.55	1.73%	2m	16.05	0.76%	30s	4.54	1.28%	35s	7.10	3.50%	50s
POMO	5.70	0.05%	48s	10.48	1.11%	2m	15.05	6.94%	1m	4.92	9.81%	1m10s	7.12	3.79%	1m25s
Sym-NCO	5.70	0.03%	48s	10.54	1.63%	2m	16.09	0.51%	1m	4.53	1.17%	1m10s	7.01	2.19%	1m25s
AM-XL	5.70	0.04%	48s	10.53	1.50%	2m	16.08	0.57%	1m	4.54	1.25%	1m10s	7.00	2.04%	1m25s
AM-PPO	5.70	0.03%	32s	10.51	1.45%	1m	16.09	0.49%	30s	4.49	0.89%	35s	6.98	1.75%	50s
PolyNet	5.70	0.15%	1m	10.41	0.36%	2m16s	16.11	0.37%	1m24s	4.49	0.24%	1m35s	7.02	2.33%	1m50s

numbers of samples. As shown in Fig. 18, the *Augmentation* decoding scheme achieves the Pareto front with limited samples and, notably, generally outperforms other decoding schemes. We note that while sampling with a light decoder can be more efficient in terms of speed than sampling, this may not be true for heavy-decoder [93] or decoder-only models [37, 94, 112], where decoding via greedy augmentations may help improve performance.

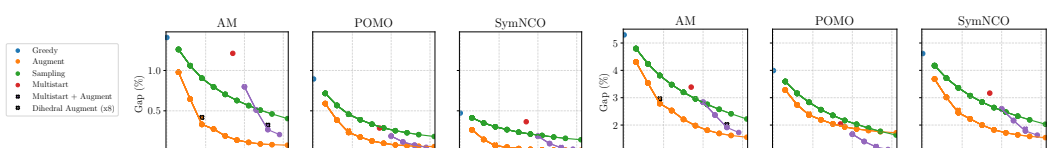


Figure 18: Pareto front of decoding schemes by the number of samples. Left: TSP50; right: CVRP50.

E.1.3 Sample Efficiency

We additionally evaluate the NCO solvers based on the number of training samples (i.e., the number of reward evaluations). As shown in Fig. 19, we found that actor-critic methods (e.g., A2C) and PPO) can exhibit efficacy in scenarios with limited training samples, as demonstrated by the TSP50/100 results in Fig. 19. This observation suggests that NCO solvers with control over the number of

Table 11: In-distribution results for models trained on 20 nodes.

Method	TSP			CVRP			OP			PCTSP			PDP		
	Cost ↓	Gap	Time	Cost ↓	Gap	Time	Prize ↑	Gap	Time	Cost ↓	Gap	Time	Cost ↓	Gap	Time
<i>Classical Solvers</i>															
<i>Gurobi[†]</i>	3.84	0.00%	7s	—	—	—	—	—	—	—	—	—	—	—	—
<i>Concorde</i>	3.84	0.00%	1m	—	—	—	5.39	0.00%	16m	3.13	0.00%	2m	—	—	—
<i>HGS</i>	—	—	—	6.13	0.00%	4h	—	—	—	—	—	—	—	—	—
<i>Compass</i>	—	—	—	—	—	—	—	—	—	—	—	—	—	—	—
<i>LKH3</i>	3.84	0.00%	15s	6.14	0.16%	5h	—	—	—	—	—	—	—	—	—
<i>OR Tools</i>	3.85	0.37%	1m	—	—	—	—	—	—	3.13	0.00%	5h	4.70	3.16%	1h
<i>CPLEX</i>	—	—	—	—	—	—	—	—	—	—	—	—	4.56	0.00%	7m23s
<i>Greedy One Shot Evaluation</i>															
A2C	3.86	0.64%	<1s	6.46	5.00%	<1s	5.01	6.70%	<1s	3.36	7.35%	<1s	4.71	3.31%	<1s
AM	3.84	0.19%	<1s	6.39	3.92%	<1s	5.20	3.17%	<1s	3.17	1.28%	<1s	4.82	5.70%	<1s
POMO	3.84	0.18%	<1s	6.33	3.00%	<1s	4.69	12.69%	<1s	3.41	8.95%	<1s	4.85	6.36%	<1s
Sym-NCO	3.84	0.05%	<1s	6.30	2.58%	<1s	5.30	1.37%	<1s	3.15	0.64%	<1s	4.70	3.07%	<1s
AM-XL	3.84	0.07%	<1s	6.31	2.81%	<1s	5.25	2.23%	<1s	3.17	1.26%	<1s	4.71	3.29%	<1s
PolyNet	3.84	0.10%	<1s	6.40	4.44%	<1s	5.26	2.28%	<1s	3.18	1.98%	<1s	4.69	2.92%	<1s
<i>Sampling with width M = 1280</i>															
A2C	3.84	0.15%	20s	6.26	2.08%	24s	5.12	4.66%	22s	3.28	4.79%	23s	4.64	1.76%	23s
AM	3.84	0.04%	20s	6.24	1.78%	24s	5.30	1.30%	22s	3.15	0.78%	23s	4.66	2.19%	23s
POMO	3.84	0.02%	36s	6.20	1.06%	40s	4.90	8.83%	37s	3.33	6.39%	39s	4.68	2.63%	39s
Sym-NCO	3.84	0.01%	36s	6.22	1.44%	40s	5.34	0.59%	37s	3.14	0.35%	39s	4.64	1.75%	39s
AM-XL	3.84	0.02%	36s	6.22	1.46%	40s	5.32	0.93%	37s	3.15	0.56%	39s	4.64	1.75%	39s
PolyNet	3.84	0.00%	47s	6.14	0.23%	1m15s	5.35	0.52%	37s	3.13	0.15%	1m15s	4.59	0.57%	1m36s
<i>Greedy Multistart (N)</i>															
A2C	3.85	0.36%	<1s	6.33	3.04%	3s	5.06	5.77%	2s	3.30	5.18%	2s	4.85	6.42%	2s
AM	3.84	0.12%	<1s	6.28	2.27%	3s	5.24	2.42%	2s	3.16	0.95%	2s	4.67	2.41%	2s
POMO	3.84	0.05%	<1s	6.21	1.27%	4s	4.76	11.32%	3s	3.35	7.03%	4s	4.66	2.19%	4s
Sym-NCO	3.84	0.03%	<1s	6.22	1.48%	4s	5.32	0.87%	3s	3.15	0.62%	4s	4.69	2.85%	4s
AM-XL	3.84	0.05%	<1s	6.22	1.38%	4s	5.29	1.49%	3s	3.15	0.64%	4s	4.65	1.97%	4s
PolyNet	3.84	0.01%	1s	6.17	0.71%	5s	5.34	0.58%	1s	3.15	0.76%	5s	4.81	5.43%	5s
<i>Greedy with Augmentation (1280)</i>															
A2C	3.84	0.01%	20s	6.22	1.35%	24s	5.04	6.10%	22s	3.33	6.39%	23s	4.61	1.11%	23s
AM	3.84	0.00%	20s	6.20	1.07%	24s	5.25	2.25%	22s	3.16	0.96%	23s	4.63	1.54%	23s
POMO	3.84	0.00%	36s	6.18	0.84%	45s	4.85	9.76%	38s	3.37	7.55%	42s	4.62	1.32%	42s
Sym-NCO	3.84	0.00%	36s	6.17	0.71%	45s	5.33	0.77%	38s	3.15	0.63%	42s	4.61	0.95%	42s
AM-XL	3.84	0.00%	36s	6.17	0.68%	45s	5.30	1.30%	38s	3.15	0.68%	42s	4.61	0.96%	42s
PolyNet	3.84	0.00%	55s	6.16	0.48%	1m10s	5.35	0.50%	57s	3.13	0.16%	1m2s	4.59	0.58%	1m10s
<i>Greedy Multistart with Augmentation (N × 16)</i>															
A2C	3.84	0.01%	9s	6.20	1.12%	48s	5.20	3.17%	32s	3.28	4.95%	25s	4.75	4.06%	23s
AM	3.84	0.00%	9s	6.18	0.78%	48s	5.34	0.56%	32s	3.14	0.32%	25s	4.63	1.52%	23s
POMO	3.84	0.00%	13s	6.16	0.50%	1m	5.09	5.29%	45s	3.35	6.95%	38s	4.61	1.10%	42s
Sym-NCO	3.84	0.00%	13s	6.17	0.61%	1m	5.35	0.39%	45s	3.14	0.24%	38s	4.60	0.89%	42s
AM-XL	3.84	0.00%	13s	6.16	0.44%	1m	5.35	0.46%	45s	3.14	0.28%	38s	4.60	0.87%	42s
PolyNet	3.84	0.00%	18s	6.14	0.16%	1m20s	5.37	0.31%	1m	3.13	0.12%	58s	4.61	1.03%	55s

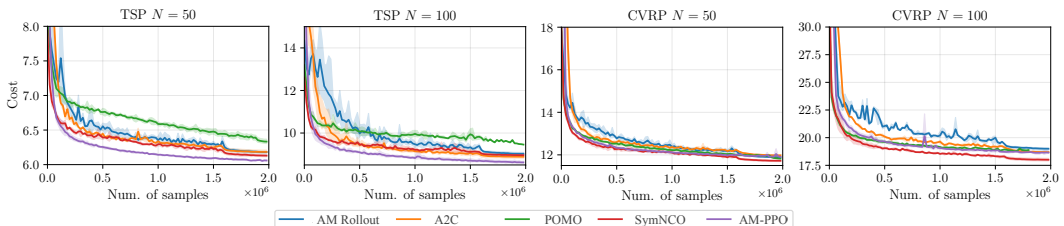


Figure 19: Validation cost curves and number of training samples consumed. Models with greater performance after full training may show worse convergence properties when the number of training samples is limited.

samples may exhibit a different trend in sample efficiency: if reward function evaluation is expensive, REINFORCE baselines that include additional reward function evaluations such as Greedy Rollout, POMO, and SymNCO may be sample-inefficient. While this is not the case for most CO problems (for instance: in routing, it is inexpensive to calculate routes), in other areas as Electronic Design Automation, where reward evaluation is resource-intensive due to the necessity of electrical simulations, in which sample efficiency can become even more crucial.

E.1.4 Out-of-distribution

In this section, we evaluate the out-of-distribution performance of the NCO solvers by measuring the gap compared to the best-known solutions (BKS). The evaluation results are visualized in Fig. 20. Contrary to the in-distribution results, we find that NCO solvers with sophisticated baselines (i.e.,

POMO and Sym-NCO) tend to exhibit worse generalization when the problem size changes, either for solving smaller or larger instances. This can be seen as an indication of “overfitting” to the training sizes. On the other hand, variants of AM show relatively better generalization results overall.

Besides, we also evaluate the model by sampling decoding strategy with different temperatures as shown in Fig. 21, k values for Top- k as shown in Fig. 22, and p values for Top- p as shown in Fig. 23. A higher temperature or a lower p value with Top- p sampling can improve the generalization ability on large-scale problems, while Top- k sampling has limited contribution to generalization cross problem sizes.

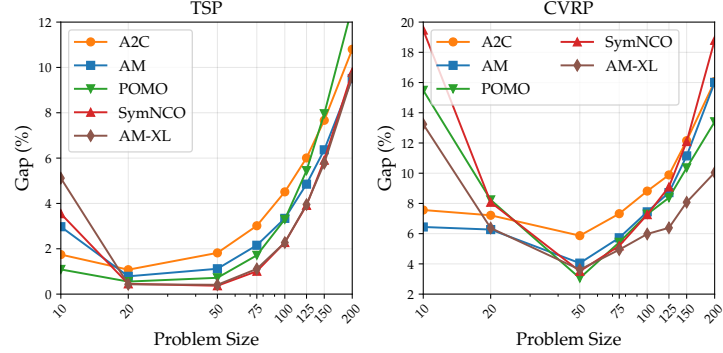


Figure 20: Out-of-distribution generalization by greedy decoding for models with different reinforce baselines trained on 50 nodes. Stronger performance in distribution does not always translate to out-of-distribution.

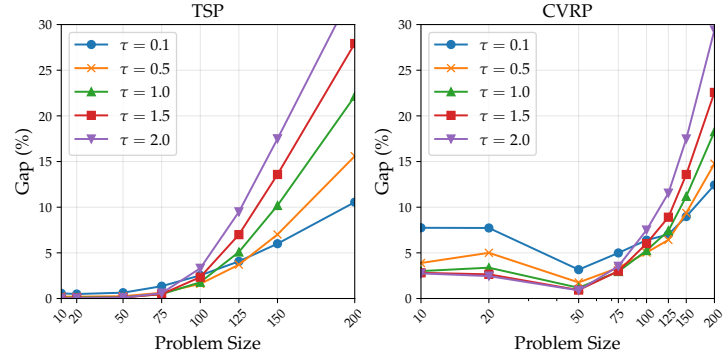


Figure 21: Out-of-distribution generalization by sampling with different temperatures τ for POMO trained on 50 nodes.

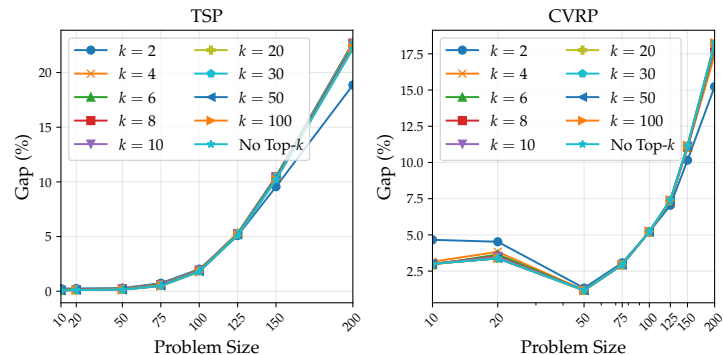


Figure 22: Out-of-distribution generalization by sampling with different Top- k for POMO trained on 50 nodes.

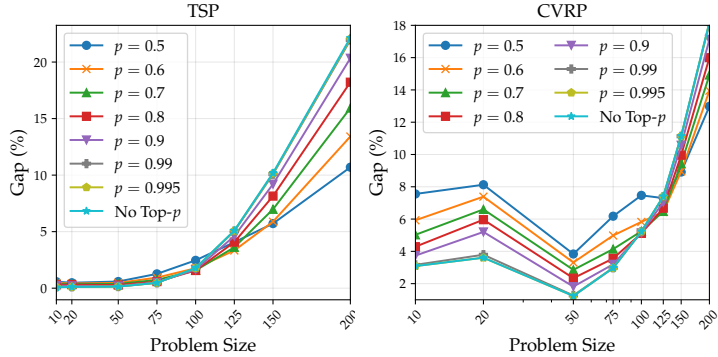


Figure 23: Out-of-distribution generalization by sampling with different Top- p for POMO trained on 50 nodes.

Table 12: Search Methods results of models pre-trained on 50 nodes. *Classic* refers to Concorde [35] for TSP and HGS [138, 144] for CVRP. OOM is "Out of Memory".

Type	Metric	TSP						CVRP					
		POMO			Sym-NCO			POMO			Sym-NCO		
		200	500	1000	200	500	1000	200	500	1000	200	500	1000
<i>Classic</i>	Cost	10.17	16.54	23.13	10.72	16.54	23.13	27.95	63.45	120.47	27.95	63.45	120.47
<i>Zero-shot</i>	Cost	13.15	29.96	58.01	13.30	29.42	56.47	29.16	92.30	141.76	32.75	86.82	190.69
	Gap[%]	29.30	81.14	150.80	24.07	77.87	144.14	4.33	45.47	17.67	17.17	36.83	58.29
	Time[s]	2.52	11.87	96.30	2.70	13.19	104.91	1.94	15.03	250.71	2.93	15.86	150.69
AS	Cost	11.16	20.03	OOM	11.92	22.41	OOM	28.12	63.98	OOM	28.51	66.49	OOM
	Gap[%]	4.13	21.12	OOM	11.21	35.48	OOM	0.60	0.83	OOM	2.00	4.79	OOM
	Time[s]	7504	10070	OOM	7917	10020	OOM	8860	21305	OOM	9679	24087	OOM
EAS	Cost	11.10	20.94	35.36	11.65	22.80	38.77	28.10	64.74	125.54	29.25	70.15	140.97
	Gap[%]	3.55	26.64	52.89	8.68	37.86	67.63	0.52	2.04	4.21	4.66	10.57	17.02
	Time[s]	348	1562	13661	376	1589	14532	432	1972	20650	460	2051	17640

E.1.5 Search Methods

A way to adapt to distribution changes is using *transductive RL*, commonly known as (active) search methods, which involve training (a part of) a pre-trained NCO solver to adapt to CO instances of interest. We evaluate 1) *Active Search* (AS) [8] which finetunes a pre-trained model on the searched instances by adapting all the policy parameters and 2) *Efficient Active Search* (EAS): from [50] which finetunes a subset of parameters (i.e., embeddings or new layers) and adds an imitation learning loss to improve convergence.

We apply AS and EAS to POMO and Sym-NCO pre-trained on TSP and CVRP with 50 nodes to solve larger instances having $N \in [200, 500, 1000]$ nodes. As shown in Table 12, solvers with search methods improve the solution quality. However, POMO generally shows better improvements over Sym-NCO. This suggests once more that the “overfitting” of sophisticated baselines can perform better in training distributions but eventually worse in different downstream tasks.

E.1.6 Additional Large-scale Results

We also show in Table 13 additional large-scale results with $10k+$ nodes obtained with the hybrid AR/NAR GLOP model [152]. Fig. 24 demonstrates a solution obtained through our implementation of GLOP for CVRP35K. It represents the maximum scale of CVRP that RL4CO is capable of solving within 24GB of graphics memory while preserving the performance.

Table 13: Performance on large-scale CVRP instances with ten thousands of nodes.

	CVRP10K		CVRP20K	
	Obj.	Time	Obj.	Time
HGS [138]	108.1	4.01h	182.7	6.03h
Random Insertion	187.9	0.16s	330.4	0.61s
GLOP-G (Insertion)	127.0	2.42s	208.3	10.9s
GLOP-G (AM)	119.6	4.68s	199.6	14.8s
GLOP-G (LKH)	111.4	5.06s	191.4	17.9s

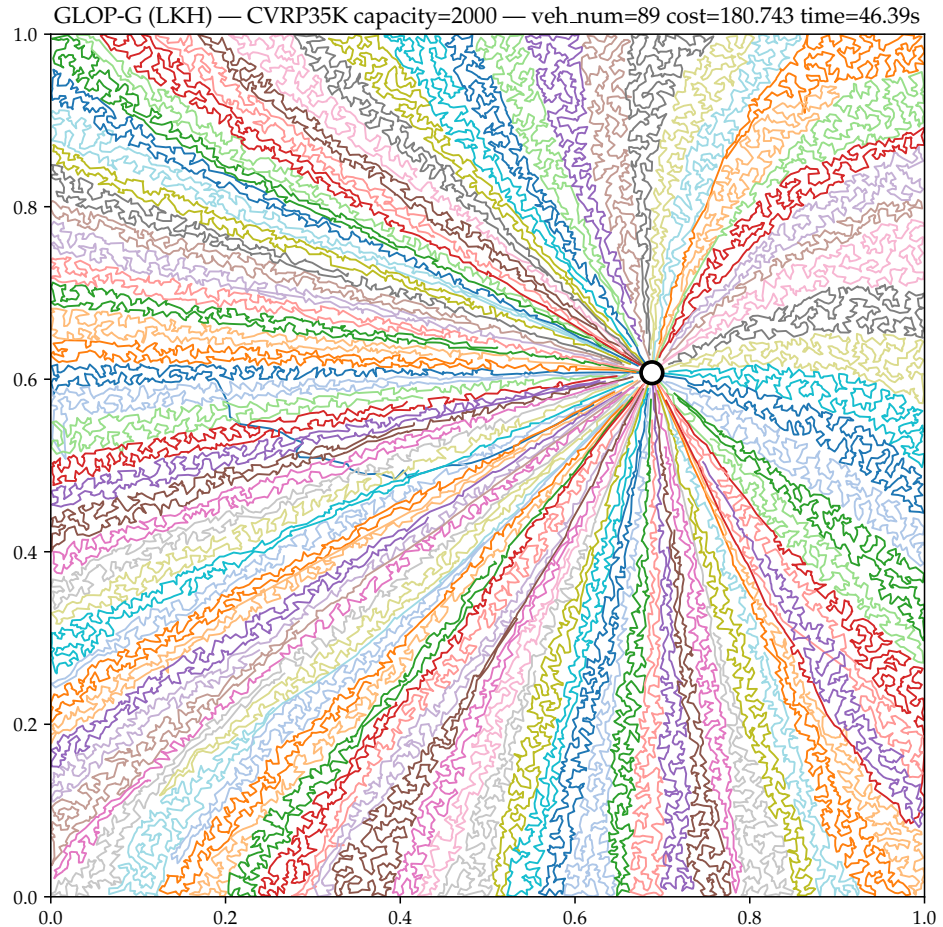


Figure 24: A visualization of the solution generated by GLOP on CVRP35K.

Table 14: Benchmarking results of ACO method in TSP with 200, 500, 1000 nodes. The reported values are obtained by averaging over 128 test instances. The time is the average computation time for solving a single instance.

Method	TSP200			TSP500			TSP1000		
	Cost	Gap(%)	Time(s)	Cost	Gap(%)	Time(s)	Cost	Gap(%)	Time(s)
<i>Concorde</i> [35]	10.72	0.00	0.9	16.55	0.00	10.7	23.12	0.00	108.3
<i>ACO</i>	10.88	1.52	1.0	17.23	4.11	4.0	24.42	5.65	19.8
<i>DeepACO</i>	10.80	0.79	1.0	16.87	1.95	4.3	23.82	3.03	20.7
<i>GFACS</i>	10.75	0.32	1.0	16.80	1.56	4.3	23.78	2.87	20.7

Table 15: Benchmarking results of ACO methods with different τ values in TSP with 500 nodes. The reported values are the average cost of 128 test instances.

Method	$\tau = 0.05$	$\tau = 0.1$	$\tau = 0.25$	$\tau = 0.5$	$\tau = 0.75$	$\tau = 1.0$	$\tau = 1.5$	$\tau = 2.0$
<i>ACO</i>	17.05	16.95	17.03	17.11	17.19	17.23	17.26	17.26
<i>DeepACO</i>	17.00	16.97	16.92	16.84	16.85	16.87	16.88	16.89
<i>GFACS</i>	16.92	16.90	16.86	16.80	16.80	16.80	16.81	16.82

E.2 Learning Heuristics for Ant Colony Optimization

E.2.1 Experiment Settings

We adhered to the hyperparameters specified in the original papers for DeepACO [150] and GFACS [70] for GFlowNets training. We conducted two distinct benchmarks for ACO methods. The first benchmark evaluated the ability to solve the Traveling Salesman Problem (TSP) at different scales: 200, 500, and 1000. We use the test instances provided by DeepACO²². The second benchmark assessed inference capability at various temperature values of τ in TSP with 500 nodes. The temperature τ is a hyperparameter for the heatmap distribution of the heuristic matrix in ACO, where a low τ emphasizes exploitation and a high τ emphasizes exploration. For both experiments, the optimality gaps are calculated with respect to the average cost of solutions obtained using Concorde [35].

E.2.2 Results

TSP Benchmark Table 14 shows the results for the first benchmark. In this benchmark, we observed that GFACS outperforms other baselines, and DeepACO surpasses ACO. These results are consistent with their respective claims [150, 70], providing evidence that our benchmark is sufficiently valid. Notably, our algorithm also performed slightly faster than the original implementation, likely due to the batchified environment of RL4CO.

Performance Comparison for Different Heatmap Temperatures (τ) Table 15 shows the results for the second benchmark. This benchmark compared inference performance across different heatmap temperatures (τ). We observed notable performance variation with changes in τ . This highlights the importance of inference and sampling strategies even after deep network training is completed. Additionally, GFACS produced more consistent results with different τ values. This provides empirical evidence of the robustness of GFACS, which is due to its ability to model a sampler capable of generating diverse and high-reward solutions. The modularization of RL4CO allows for a focused study on inference capabilities, enabling future researchers to contribute to this aspect using the RL4CO pipeline.

E.3 Learning to Schedule

Compared to routing problems, scheduling problems have not been extensively studied by the NCO community. On the one hand side, NCO methods for scheduling are harder to benchmark due to the absence of well-performing heuristics like the LKH algorithm for the TSP. On the other hand,

²²<https://github.com/henry-yeh/DeepACO>

scheduling problems involve more complex graph representations like disjunctive graphs [153], bipartite graphs [77], or heterogeneous graphs [125], making it harder to encode the problem. With RL4CO, we aim to mitigate these entry barriers for NCO researchers by providing established solution methods along with the environments. Further, by being modular by design, RL4CO allows for quick evaluation of different learning algorithms and network architectures, which can already lead to substantial improvements of the solution quality, as demonstrated in the example of the FJSSP in [Table 2](#). Lastly, by providing benchmark instances like Taillard [129] and easy ways of initializing the environments with external benchmark files, we facilitate the comparison of models with existing methods. The following chapter describes established DRL models for scheduling problems as well as their performance on synthetic and benchmark datasets.

E.3.1 JSSP

Models To solve the JSSP using DRL methods, we implement the L2D model described in [Appendix C.2.7](#) in RL4CO. To train the encoder-decoder policy, we use the same Proximal Policy Optimization (PPO) algorithm as Zhang et al. [153]. In contrast to most other work in the NCO domain, L2D uses a (dense) stepwise reward function rather than a sparse episodic reward, which is observed only after a complete solution is obtained. This reward determines the change in the lower bound of the makespan given the partial schedule. Due to the dense nature of the reward, the PPO algorithm for the scheduling problems evaluates actions on a stepwise basis, whereas environments with an episodic reward are evaluated based on a full rollout. We compare these methods and discuss the different implementations in [Appendix E.3.4](#).

Further, we demonstrate RL4CO’s ability to effortlessly implement a state-of-the-art solver for JSSP instances by exchanging the GCN encoder used by Zhang et al. [153] with the MatNet encoder [77] described in [Appendix C.2.11](#). Furthermore, the greedy decoding scheme of Zhang et al. [153] is replaced by $N = 100$ random samples, of which the best is selected.

Reproduction and Improvement of Original Results We demonstrate RL4CO’s capability of learning dispatching rules for the JSSP by training and validating the L2D model of Zhang et al. [153] and our version of L2D with the MatNet encoder on synthetic data. We report the performance achieved with RL4CO together with the baselines the authors of the original papers used, as well as the solutions obtained via the CP-Sat solver Google OR-Tools. The baselines are a set of selected PDRs that have a high practical relevance, namely Most Work Remaining (MWKR) and Most Operations Remaining (MOR).

Table 16: Comparison of RL4CO with L2D [153] and other baselines on the JSSP. For OR-Tools, the fraction of instances solved optimally is reported in parentheses.

Size	Metric	OR-Tools	PDRs		L2D [153]	RL4CO	
			MWKR	MOR		GCN	MatNet ($\times 128$)
6×6	Obj.	487.75 (100%)	656.96	630.19	574.09	569.53	515.11
	Gap	-	34.6%	29.2%	17.7%	16.8%	5.6%
10×10	Obj.	808.32 (100%)	1151.41	1101.08	988.58	972.35	865.78
	Gap	-	42.6%	36.5%	22.3%	20.3%	7.1%
15×15	Obj.	1187.06 (99%)	1812.13	1693.33	1504.79	1492.94	1318.25
	Gap	-	52.6%	42.6%	26.7%	25.7%	11.0%
20×20	Obj.	1555.79 (4%)	2469.19	2263.68	2007.76	1992.36	1847.33
	Gap	-	58.6%	45.5%	29.0%	28.1%	18.7%

The results are listed in [Table 16](#). RL4CO’s implementation of L2D manages to outperform the original implementation on all instance types, even when using the same model architecture, learning algorithm, and hyperparameters. The reason is that RL4CO uses an improved implementation of the environment. In the implementation of Zhang et al. [153] the state of the environment does not contain a time dimension. Instead, the environment schedules the selected operation at the earliest feasible start time, given the current schedule. Here, we use the environment proposed by Tassel et al. [132], where the environment transitions through distinct time steps $t = 0, 1, \dots, T$. In this case,

the start time of a selected operation is set to the time step at which it was selected, leading to a more natural form of credit assignment.

Using the MatNet encoder instead of the GCN and employing a decoding scheme based on multiple random rollouts further reduces the makespan by a large margin. One instances of size 6×6 , the gap to the optimal solutions was reduced by 11 percentage points to 5.6%, which corresponds to a third of the gap realized with the GCN encoder.

Taillard Benchmark and out-of-distribution performance With RL4CO, we also provide the possibility to test models against established benchmarks. For the JSSP, a well-recognized benchmark is that of Taillard [129], which is also used by Zhang et al. [153] to validate their model. In Table 17, we report the results of RL4CO on these instances along with the results obtained by Zhang et al. [153] as well as the MOR and MWKR heuristics. We trained our MatNet models on JSSP instances up to size 20×20 . For larger Taillard instances, we report the out-of-distribution performance to demonstrate the model’s generalization ability. Similar to the synthetic test instances, our RL4CO implementation paired with the MatNet encoder manages to outperform the original L2D by large margins on all instances of the Taillard benchmark dataset, even when evaluating it on out-of-distribution instances.

Table 17: Results on the Taillard [129] benchmark instances. BKS refers to the best known solutions and % opt. specifies the rate of instances with optimal solutions. Values marked with a \dagger indicate out-of-distribution performance of the model trained on 20×20 .

Size	Metric	BKS	PDRs		L2D [153]	RL4CO MatNet ($\times 128$)
			MWKR	MOR		
15×15	Obj.	1230.06 (100%)	1927.5	1782.3	1547.50	1404.30
	Gap	-	56.7%	45.0%	26.0%	14.2%
20×15	Obj.	1363.22 (90%)	2190.7	2015.8	1774.7	1570.70
	Gap	-	60.7%	47.7%	30.0%	15.2%
20×20	Obj.	1617.60 (30%)	2518.6	2309.9	2128.1	1842.90
	Gap	-	55.7%	42.8%	31.6%	13.9%
30×15	Obj.	1787.68 (70%)	2728.0	2601.3	2378.8	2121.19 \dagger
	Gap	-	52.6%	45.6%	33.0%	18.6%
30×20	Obj.	1948.32 (0%)	3193.3	2888.1	2603.9	2357.90 \dagger
	Gap	-	63.9%	48.2%	33.6%	21.0%

E.3.2 FJSSP

Model To solve the FJSSP using DRL methods, we implement the HGNN model described in Appendix C.2.10 in RL4CO and train it with the same PPO algorithm as L2D. Besides HGNN we also implement a second model which exchanges the encoder of HGNN with the MatNet encoder.

Reproduction and Improvement of Original Results We compare the results obtained via RL4CO with those reported by Song et al. [125] and the baseline used by them. Also, Song et al. [125] use MWKR and MOR to benchmark their model as well as the OR-Tools solver. The results, which are obtained on a test set comprising of 100 randomly generated instances, are listed below in Table 18.

Similar to the JSSP, the HGNN implemented in RL4CO achieves better results than the original implementation, although both implementations use the same definition of the environment. However, in RL4CO, we use instance normalization [135] on the input variables as well as between consecutive HGNN layers, which we found to drastically stabilize the training process.

Again, we were able to enhance the quality of the solution further by simply exchanging the encoder with MatNet. Especially on the larger instances, the increased model complexity translates into much better model performance, with the solutions even surpassing OR-Tools on 20×10 instances.

Table 18: Comparison of RL4CO and HGNN [125] on the FJSSP. For OR-Tools, the fraction of instances solved optimally is reported in parentheses. Both RL4CO and [125] make use of random-rollouts for decoding.

Size	Metric	OR-Tools	PDRs		HGNN [125] ($\times 128$)	RL4CO ($\times 128$)	
			MWKR	MOR		HGNN	MatNet
10×5	Obj.	96.59 (15%)	115.29	116.69	105.61	102.49	99.02
	Gap	-	19.4%	20.9%	9.4%	6.1%	2.5%
20×5	Obj.	188.45 (0%)	216.98	217.17	207.50	199.47	192.05
	Gap	-	15.2%	15.3%	10.1%	5.8%	1.9%
15×10	Obj.	145.42 (5%)	169.18	173.40	160.36	155.34	151.93
	Gap	-	16.3%	19.3%	10.3%	6.8%	4.5%
20×10	Obj.	197.24 (0%)	220.85	221.86	214.87	207.52	192.00
	Gap	-	11.9%	12.53%	9.0%	5.2%	-2.7%

Out-of-distribution In this section, we evaluate the out-of-distribution performance of the DRL models trained with RL4CO on FJSSP 20×10 instances, by evaluating them on smaller (20×5 & 15×10) and larger (30×10 & 40×10) instances. The results in Table 19 indicate that both HGNN and MatNet manage to generalize well to problems of different sizes. Despite being trained on smaller instances, the HGNN manages to close the performance gap when evaluated on larger instances, with gaps being as small as 3.7% for FJSSP 40×10 instances. And on FJSSP 20×5 instances, the average makespan increases by only 1.56 (0.8%) when using the model trained on FJSSP 20×10 instead of 20×5 instances. Again, the MatNet model shows superior performance compared to the other baselines and surpasses even the results obtained by OR-Tools on the larger instances. The within-distribution performance of MatNet, therefore, also translates to out-of-distribution instances, indicating that the complexity of the model results in a better generalization ability.

Table 19: Generalization performance of a policy trained on a 20×10 FJSSP instances on smaller and larger instances. We use 100 test instances per instance size. Gaps are reported with respect to the results of OR-Tools

Size	Metric	OR-Tools	PDRs		HGNN [125] ($\times 128$)	RL4CO ($\times 128$)	
			MWKR	MOR		HGNN	MatNet
20×5	Obj.	188.45 (0%)	216.98	217.17	207.50	201.03	193.61
	Gap	-	15.2%	15.3%	10.1%	6.7%	2.7%
15×10	Obj.	145.42 (5%)	169.18	173.40	160.36	162.41	150.59
	Gap	-	16.3%	19.3%	10.3%	11.7%	3.5%
30×10	Obj.	294.10 (0%)	319.89	320.18	312.20	309.10	286.16
	Gap	-	8.8%	8.9%	6.1%	5.1%	-2.7%
40×10	Obj.	397.36 (0%)	425.70	425.19	415.14	412.05	381.19
	Gap	-	7.1%	7.0%	4.4%	3.7%	-4.1%

E.3.3 FFSP

MatNet To solve the FFSP using DRL, RL4CO implements the policy network described by Kwon et al. [77]. It uses separate policy networks for each stage of the FFSP. Each of the stage networks employs the MatNet encoder described in Appendix C.2.11, which generates embeddings for jobs and machines using the processing times of the job-machine pairs of the respective stage. The decoder of the attention model [74] then utilizes the machine embeddings of the respective stage as query and the job embeddings as keys and values to compute the probability distribution over jobs.

Results We use the same three instance types described by Kwon et al. [77] to evaluate our implementations of the FFSP environment and the policy network. The instances only differ in the number of jobs, which are set to 20, 50, and 100. We assume that there are $S = 3$ stages, and each stage has $M = 4$ machines. In the k th stage, the processing time of the job j on the machine m is

given by p_{jmk} . Therefore, an instance of the problem is defined by three matrices (P_1 , P_2 , and P_3), specifying the processing time for each job-machine combination in that stage. We report the results obtained by RL4CO and compare them to those obtained by Kwon et al. [77] in [Table 20](#). Other benchmarks used are the exact solver CPLEX (for which results can only be obtained for FFSP20 instances), the Shortest Job First (SJF) dispatching rule, as well as the evolutionary algorithms Particle Swarm Optimization (PSO), and Genetic Algorithm (GA). One can see that, using RL4CO, we are able to reproduce the results from the original paper.

[Table 20](#): Comparison of RL4CO with the results reported in [77]. Gaps are reported with respect to the best known results.

Instance	Matric	CPLEX (600s)	SJF	GA	PSO	[77]	RL4CO
FFSP20	Obj.	36.6	31.3	30.6	29.1	27.3	27.2
	Gap	34.5%	15.0%	12.5%	6.9%	0.3%	0.0%
FFSP50	Obj.	-	57.0	56.4	55.1	51.5	51.6
	Gap	-	10.7%	9.5%	7.0%	0.0%	0.2%
FFSP100	Obj.	-	99.3	98.7	97.3	91.5	91.3
	Gap	-	8.8%	8.1%	6.6%	0.2%	0.0%

E.3.4 Dense and Episodic Rewards

We additionally compare dense and episodic rewards for the TSP and FJSSP environments, with similar training settings as in other experiments, except for the different reward functions.

Here, we compare the performance of the HGNN [125] in solving the FJSSP and AM [74] in solving the TSP when trained using a stepwise vs. an episodic reward. The results in [Table 21](#) show that evaluating the FJSSP in a stepwise manner and stepwise re-encoding the current state significantly outperforms a policy based on a single, episodic reward. This is reasonable since the state of the FJSSP has many dynamic elements, and a policy that relies on a single encoder step may not fully grasp the problem dynamics. On the other hand, stepwise rewards for the TSP (AM model trained with POMO with the settings as Kwon et al. [76]) do not work well, and interestingly, performance approaches roughly that of the nearest insertion algorithms. Different CO problems react to the same learning setup, which again underpins the importance of a unified framework where different algorithms are implemented and are easily exchangeable.

[Table 21](#): Comparison of dense (i.e. stepwise) and episodic rewards for the TSP and the FJSSP

Reward	TSP			FJSSP		
	20	50	100	10 × 5	20 × 5	15 × 10
Dense	4.51	7.05	9.80	102.49	199.47	155.34
Episodic	3.83	5.81	7.82	110.65	204.88	182.90

E.4 Electronic Design Automation: Learning to Place Decaps

Setup In this section, we benchmark models on the mDPP from [Appendix B.3.2](#). We benchmark 3 variants of online DevFormer (DF), namely DF(PG,Critic): REINFORCE (where PG stands for Policy Gradients, an “alias” of the REINFORCE algorithm) with Critic baseline, DF(PG,Rollout): REINFORCE with Rollout baseline as well as PPO. All experiments are run with the same hyperparameters as the other experiments except for the batch size set to 64, the maximum number of samples set to 10,000, and a total of only 10 epochs due to the nature of the benchmark sample efficiency.

E.4.1 Main Results

[Table 22](#) shows the main numerical results for the task when RS, GA, and DF models are trained for placing 20 decaps. While RS and GA need to take online shots to solve the problems (we restricted the number to 100), DF models can successfully predict in a zero-shot manner and outperform the

classical approaches. Interestingly, the vanilla critic-based method performed the worst, while our implementation of PPO almost matched the rollout policy gradients (PG) baseline; since extensive hyperparameter tuning was not performed, we expect PPO could outperform the rollout baseline given it requires fewer samples. Fig. 25 shows example renderings of the solved environment.

Table 22: Performance of different methods on the mDPP benchmark

Method	# Shots	Score ↑	
		maxsum	maxmin
<i>Online Test Time Search</i>			
Random Search	100	11.55	10.63
Genetic Algorithm	100	11.93	11.07
<i>RL Pretraining & Zero Shot Inference</i>			
DF-(PG,Critic)	0	10.89 ± 0.63	9.51 ± 0.68
DF-(PPO)	0	12.16 ± 0.03	11.17 ± 0.11
DF-(PG,Rollout)	0	12.21 ± 0.01	11.26 ± 0.03

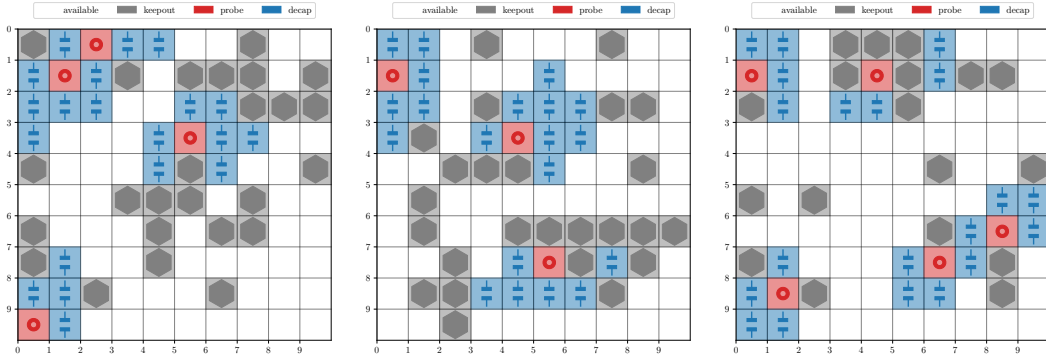


Figure 25: Renders of the environment with *maxmin* objective solved by DF-(PG,Rollout). The model successfully learned one main heuristic for DPP problems, which is that the optimal placement of decaps (blue) is generally close to probing ports (red).

E.4.2 Generalization to Different Number of Components

In hardware design, the number of components is one major contribution to cost; ideally, one would want to use the least number of components possible with the best performance. In the DPP, increasing the number of decaps *generally* improves the performance at a greater cost, hence Pareto-efficient models are essential to identify. Fig. 26 shows the performance of DF models trained on 20 decaps against the baselines. DF models PPO and PG-rollout can successfully generalize and are also Pareto-efficient with fewer decaps, important in practice for cost and material saving.

E.5 Learning to Improve

In this section, we first show the efficiency of RL4CO when reproducing the improvement methods on the TSP and PDP with 50 nodes and discuss the potential collaboration of constructive methods with improvement methods for better inference performance.

E.5.1 Main results

As shown in Table 23, refactoring and implementing the three improvement methods—DACT [96] (TSP50), N2S [97] (PDP50), and NeuOpt [98] (PDP50)—using RL4CO consistently results in better efficiency compared to the original implementations. Specifically, training and testing times ($T = 1,000$) are faster, and peak memory usage is lower. This advancement can be attributed to RL4CO’s streamlined design, which uses a single tensor dictionary variable to store all state information, and the incorporation of efficient libraries like PyTorch Lightning and TorchRL. These enhancements demonstrate RL4CO’s superior efficiency and ease of implementation.

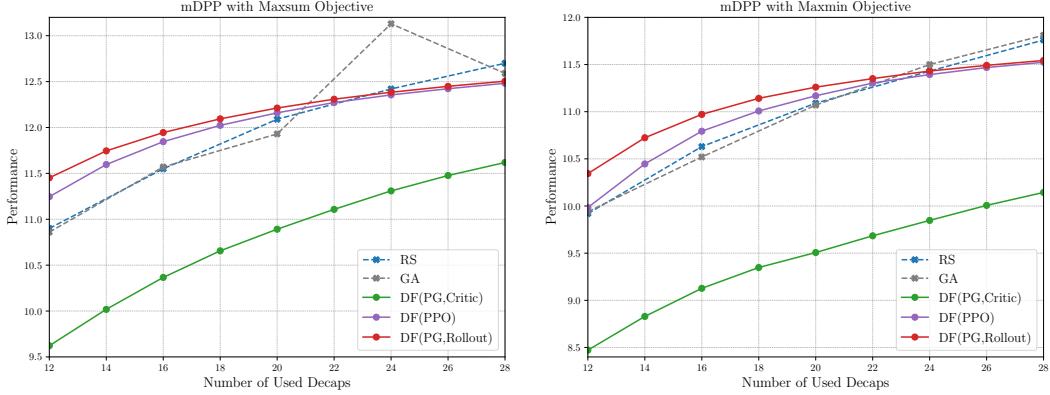


Figure 26: Performance vs number of used decaps for mDPP with *maxsum* objective [Left] and *maxmin* objective [Right].

Table 23: Comparison of time and memory usage for DACT [96] (TSP50), N2S [97] (PDP50), and NeuOpt [98] (PDP50) between the original implementation and the RL4CO implementation.

	T_train (one epoch)	T_test (1k,1k)	Memory
DACT-Origin	16m	38s	8069MB
DACT-RL4CO	10m	26s	7135MB
N2S-Origin	26m	41s	13453MB
N2S-RL4CO	17m	33s	12489MB
NeuOpt-Origin	14m	37s	7273MB
NeuOpt-RL4CO	10m	31s	6313MB

E.5.2 Discussion

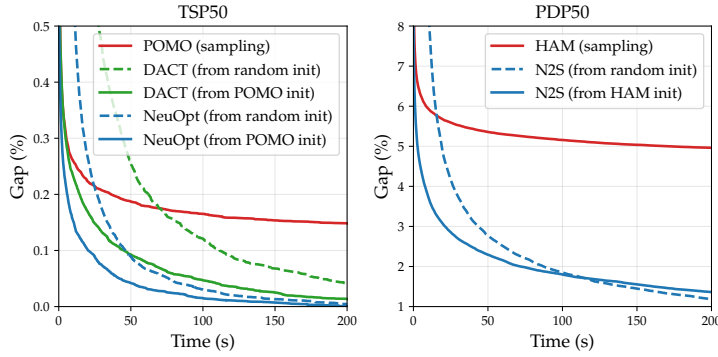


Figure 27: Bootstrapping improvement with constructive methods for TSP50 and PDP50.

As shown in Fig. 27, bootstrapping improvement with constructive methods can greatly improve the performance, especially in terms of the Primal Integral (PI, Appendix D.1.2). While in TSP bootstrapping is consistently better than simply improving with default solutions (i.e. lower final gap to BKS as well as PI), we note that in PDP with N2S, improving starting from a random initialization can yield better performance in terms of gap. However, the PI reveals that while N2S from random init achieves a value of 5.580, N2S from HAM construction initialization achieves a much better 2.234, indicating a much better early convergence speed and Pareto front.

We additionally offer some clues on how to improve such performance. Firstly, we simply initialized from a greedy solution, while more complex inference strategies may offer a significant boost. Furthermore, the trained model as per the setting in Appendix D.3.3 could be further trained and obtain better performance. Importantly, we believe that *end-to-end construction & improvement*, in which

both a constructive and improvement method are trained together, could ultimately outperform a separate training and achieve the best of both worlds.

E.6 Graph Problems: Facility Location Problem (FLP) and Maximum Coverage Problem (MCP)

Here, we present the experimental results and the corresponding discussions on the two CO problems on graphs: the Facility Location Problem (FLP; see [Appendix B.4.1](#)) and the Maximum Coverage Problem (MCP; see [Appendix B.4.2](#)).

E.6.1 Experimental settings

Baseline methods We consider two simple baselines: uniform random (UR) and deterministic greedy (DG), where UR chooses k locations uniformly at random and DG chooses k locations one by one in a greedy manner. We also apply two MIP solvers, Gurobi [44] and SCIP [14], to obtain the optimal solutions.

Benchmark methods We benchmark with the attention model (AM) with different embedding models (i.e., encoders) and different RL baselines. For FLP, the considered embedding models are: the multilayer perception (MLP), the graph convolutional network (GCN) [72], and the graph attention network [137, 24]. For MCP, since the problem instances are formulated on bipartite graphs, the considered embedding models are: the multilayer perception (MLP), the GraphSAGE model [45] (in short ‘‘SAGE’’), and the generalized GCN model [81] (in short ‘‘GEN’’). The considered RL baselines are: Rollout, Mean, Exponential, and Critic. All the models are trained in 100 epochs. The learning rate is $1e - 5$ for FLP and $1e - 4$ for MCP. In each epoch, 100,000 training data are used with batch size 1,000. For the decoding strategies, we consider sampling (with 64 independent samples) and greedy. For sampling (and UR), we report both the ‘‘best’’ performance among the 64 independent samples and the ‘‘mean’’ (i.e., average) performance over the 64 independent samples.

Test-time active search We apply three variants of active search at test time: the original active search (AS) proposed by Bello et al. [8], efficient active search (EAS) proposed by Hottung et al. [50] with two variants: EAS-Emb that finetunes embeddings and EAS-Lay that finetunes new layers. We run all the active search variants for 100 iterations.

E.6.2 Benchmark Results

Main benchmark [Table 24](#) shows the main numerical results when the methods are trained and tested to choose $k = 10$ locations on instances with $n = 100$ locations. [Table 25](#) shows the main numerical results when the methods are trained and tested to choose $k = 10$ sets on instances with $n = 100$ sets and $m = 200$ items in total. Each item has a random weight between 1 and 10, and the number of items in each set is randomly sampled between 5 and 15. The reported results are averaged over 1,000 randomly generated test instances. We also report the average gap between the performance for each setting and the optimum by solvers as described in [Appendix D.1.1](#).

Here we use absolute values since we *minimize* the total distance for FLP while *maximizing* the total weights for MCP. When using absolute values, it is consistent that smaller gaps correspond to better performance. The performance of RL methods with sampling is consistently better than the two baselines, uniform random (UR) and deterministic greedy (DG), showing their effectiveness on those two problems.

Effect of the encoder Overall, the performance of different encoders is similar. For FLP, we can observe GCN’s marginal superiority (except when we use Critic as the RL baseline). For MCP, the best encoders for different RL baselines are different, but MLP’s performance is the overall best.

Effect of the RL baseline For FLP, for the four considered RL baselines (Rollout, Mean, Exponential, Critic), Rollout is consistently better than the other three. For MCP, the differences in the performance of different RL baselines are not significant.

Effect of active search Active search significantly improves performance in almost all cases. For FLP, interestingly, Rollout achieves the best overall performance without active search, but Rollout

Table 24: Performance of different methods on the facility location problem (FLP) benchmark. For the performance, the smaller the better.

Encoder	RL Baseline	Sample (Best)	Sample (Mean)	Greedy	AS	Active Search		
						EAS-Emb	EAS-Lay	
MLP	Exponential	Rollout	10.4895	11.0056	10.9980	10.3004	10.2997	
		(Gap)	(2.19%)	(7.23%)	(7.16%)	(0.35%)	(0.34%)	
		Mean	10.5635	11.1614	10.9350	10.2995	10.3008	
		(Gap)	(2.91%)	(8.75%)	(6.54%)	(0.34%)	(0.35%)	
	Critic	Rollout	10.5726	11.1848	10.9589	10.3054	10.3051	
		(Gap)	(3.00%)	(8.98%)	(6.78%)	(0.40%)	(0.39%)	
		Mean	10.5617	11.1401	10.9439	10.2987	10.2994	
		(Gap)	(2.90%)	(8.55%)	(6.63%)	(0.33%)	(0.34%)	
GCN	Exponential	Rollout	10.4232	10.6404	10.6094	10.2955	10.2958	
		(Gap)	(1.54%)	(3.66%)	(3.36%)	(0.30%)	(0.30%)	
		Mean	10.4321	10.8095	10.6076	10.2807	10.2830	
		(Gap)	(1.63%)	(5.31%)	(3.34%)	(0.15%)	(0.18%)	
	Critic	Rollout	10.4729	10.9573	10.7257	10.2837	10.2859	
		(Gap)	(2.02%)	(6.75%)	(4.49%)	(0.18%)	(0.20%)	
		Mean	10.7086	11.4549	11.0139	10.2859	10.2891	
		(Gap)	(3.82%)	(0.54%)	(6.01%)	(0.20%)	(0.23%)	
GAT	Exponential	Rollout	10.4685	10.9202	10.8916	10.2956	10.2957	
		(Gap)	(1.99%)	(6.40%)	(6.12%)	(0.30%)	(0.30%)	
		Mean	10.6641	11.3499	11.0133	10.2865	10.2898	
		(Gap)	(3.90%)	(0.59%)	(7.31%)	(0.21%)	(0.24%)	
	Critic	Rollout	10.6487	11.3504	10.9869	10.2864	10.2880	
		(Gap)	(3.75%)	(0.60%)	(7.05%)	(0.21%)	(0.22%)	
		Mean	10.6566	11.3440	10.8813	10.2859	10.2888	
		(Gap)	(4.33%)	(1.62%)	(7.31%)	(0.20%)	(0.23%)	
						12.4788		
						(21.62%)		
						15.6327		
						(52.40%)		
						10.9831		
						(7.02%)		
						10.2650		
						(0.00%)		

underforms in many cases with test-time active search. Notably, the performance of the original active search (AS) is less stable than the two variants of efficient active search (EAS), especially for MCP. In our understanding, AS was originally designed for routing problems and uses multi-start sampling with distinct initial action (i.e., the first location/set to choose). Such a strategy is useful for routing problems due to symmetry but is less useful for problems without symmetry, such as FLP and MCP.

Test-time sampling techniques We also consider other test-time sampling techniques: top- p sampling [48] and different sampling temperatures. Top- p sampling discards actions with low probabilities, and top- p sampling with lower p values discards more low-probability actions. For sampling temperatures, higher temperatures give more uniform sampling. The considered p values are: 0.5, 0.6, 0.7, 0.8, 0.9, 0.95, 0.99, 1.0. The sampling temperatures considered are 0.01, 0.03, 0.1, 0.3, 0.5, 0.7, 0.8, 0.9, 1.0, 1.1, 1.2, 1.5, and 2.0. Fig. 28 show the heatmaps for each combination of encoder and RL baseline, for FLP and MCP. In each subplot, the x -axis represents the value of p in top- p sampling, and the y -axis represents the sampling temperature. For each combination, the best performance is marked with a red star. For FLP, the best performance is usually achieved with a proper (i.e., neither too high nor too low) level of randomness. As the p value of top- p sampling increases, the best sampling temperature decreases. Recall that both increasing the p value and increasing the sampling temperature would increase the randomness in sampling. Overall, compared to other RL baselines, Rollout needs a higher level of randomness to perform best. For MCP, the best performance is usually achieved without top- p sampling and with a high sampling temperature, i.e., without high randomness in the sampling space.

Table 25: Performance of different methods on the maximum coverage problem (MCP) benchmark. For the performance, the larger the better.

Encoder	RL Baseline	Sample (Best)	Sample (Mean)	Greedy	AS	Active Search	
						EAS-Emb	EAS-Lay
MLP	Rollout	682.4741	662.4359	665.1740	689.6200	689.6070	689.6070
	(Gap)	(0.96%)	(3.31%)	(3.05%)	(0.09%)	(0.09%)	(0.09%)
	Mean	682.4011	664.7105	668.7470	682.0610	689.5900	689.5900
	(Gap)	(1.06%)	(3.96%)	(3.56%)	(1.18%)	(0.09%)	(0.09%)
	Exponential	683.0300	665.1467	666.6640	671.3130	689.5870	689.5870
	(Gap)	(1.09%)	(3.99%)	(3.64%)	(9.68%)	(0.09%)	(0.09%)
	Critic	683.1511	666.9047	668.6411	687.8240	689.3510	689.3510
	(Gap)	(1.43%)	(5.40%)	(4.92%)	(0.35%)	(0.13%)	(0.13%)
SAGE	Rollout	681.8690	664.1233	665.9901	689.4810	689.5020	689.4930
	(Gap)	(1.14%)	(3.71%)	(3.44%)	(0.11%)	(0.11%)	(0.11%)
	Mean	682.1360	669.2791	670.4091	666.0360	689.5990	689.5890
	(Gap)	(1.06%)	(3.63%)	(3.05%)	(10.44%)	(0.09%)	(0.09%)
	Exponential	680.3970	653.0383	656.3170	675.2220	689.5990	689.5980
	(Gap)	(1.06%)	(3.95%)	(3.46%)	(2.18%)	(0.09%)	(0.09%)
	Critic	676.9190	645.9108	649.6940	647.9050	688.4500	688.4650
	(Gap)	(1.94%)	(6.43%)	(5.89%)	(6.12%)	(0.26%)	(0.26%)
GEN	Rollout	680.2640	648.2318	656.3710	689.4430	689.4660	689.4660
	(Gap)	(1.10%)	(2.96%)	(2.80%)	(0.12%)	(0.11%)	(0.11%)
	Mean	682.1960	662.1896	664.6721	681.3950	689.5670	689.5670
	(Gap)	(0.97%)	(3.56%)	(3.34%)	(1.28%)	(0.10%)	(0.10%)
	Exponential	682.4290	662.5012	665.8010	689.4060	689.5650	689.5650
	(Gap)	(1.07%)	(3.70%)	(3.18%)	(0.12%)	(0.10%)	(0.10%)
	Critic	682.3510	664.1604	667.7340	689.6170	689.3940	689.3940
	(Gap)	(1.45%)	(6.08%)	(4.91%)	(0.09%)	(0.12%)	(0.12%)
						527.9360	
						(-23.50%)	
						432.7287	
						(-37.30%)	
						680.2050	
						(-1.46%)	
						690.2350	
						(0.00%)	

E.6.3 Out-of-distribution

Results on out-of-distribution instances Table 26 shows the main numerical results when the methods are trained to choose $k = 10$ locations on instances with $n = 100$ locations, but tested to choose $k' = 20$ locations on instances with $n' = 200$ locations. Table 27 shows the main numerical results when the methods are trained to choose $k = 10$ sets on instances with $n = 100$ sets and $m = 200$ items in total and tested to choose $k' = 20$ sets on instances with $n' = 200$ sets and $m' = 400$ items in total. Each item has a random weight between 1 and 10, and the number of items in each set is randomly sampled between 5 and 15. The reported results are averaged over 1,000 randomly generated test instances. We also report the average gap for each setting. Overall, the performance of RL methods generalizes well to out-of-distribution instances, being significantly higher than both Uniform Random and Deterministic Greedy with enough sampling.

Effect of the encoder For FLP, unlike the main benchmark, the superiority of GCN no longer exists for out-of-distribution instances. For MCP, the best encoders for different RL baselines are still different, and the performance of MLP is the best.

Effect of the RL baseline For FLP, again, Rollout is overall better than the other three. For MCP, the best RL baselines for different encoders are different, and Mean and Critic are overall good choices.

Effect of active search Again, active search clearly improves performance in almost all cases. For FLP, unlike the main benchmark, for out-of-distribution instances, Rollout overall performs best

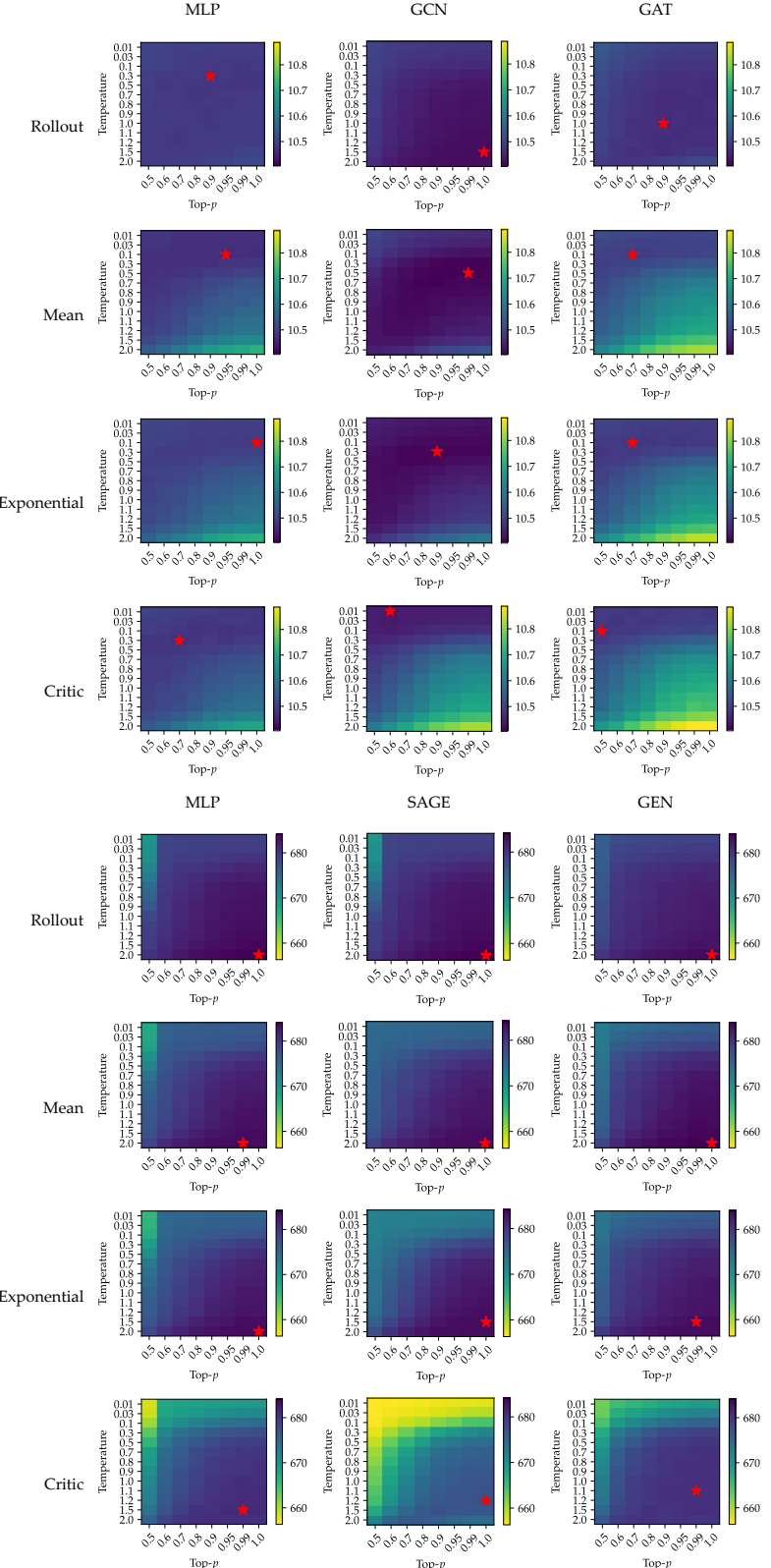


Figure 28: Performance of sampling with different p values for top- p sampling and different sampling temperatures. Top: FLP; Bottom: MCP. For each combination of encoder and RL baseline, the best performance is marked with a star.

Table 26: Performance of different methods on the facility location problem (FLP) out-of-distribution instances. For the performance, the smaller the better.

Encoder	RL Baseline	Sample (Best)	Sample (Mean)	Greedy	AS	Active Search		
						EAS-Emb	EAS-Lay	
MLP	Exponential	Rollout	14.7612	15.2979	15.2709	14.4160	14.4181	
		(Gap)	(3.85%)	(7.63%)	(7.44%)	(1.42%)	(1.43%)	
		Mean	15.0045	15.7343	15.3075	14.5315	14.5331	
		(Gap)	(5.56%)	(10.70%)	(7.70%)	(2.23%)	(2.24%)	
	Critic	15.0022	15.7144	15.3131	14.5274	14.5266	14.5266	
		(Gap)	(5.54%)	(10.56%)	(7.74%)	(2.20%)	(2.19%)	
		14.9670	15.6631	15.2781	14.5147	14.5132	14.5132	
		(Gap)	(5.30%)	(10.20%)	(7.49%)	(2.11%)	(2.10%)	
GCN	Exponential	Rollout	14.9564	15.4230	15.3610	14.6254	14.6248	
		(Gap)	(5.22%)	(8.51%)	(8.07%)	(2.89%)	(2.89%)	
		Mean	15.1380	15.8310	15.3713	14.6554	14.6572	
		(Gap)	(6.50%)	(11.38%)	(8.14%)	(3.10%)	(3.12%)	
	Critic	15.2197	15.9598	15.4441	14.6961	14.6963	14.6973	
		(Gap)	(7.08%)	(12.29%)	(8.66%)	(3.39%)	(3.40%)	
		15.1754	15.9835	15.2815	14.6579	14.6634	14.6642	
		(Gap)	(6.53%)	(12.00%)	(8.23%)	(3.12%)	(3.16%)	
GAT	Exponential	Rollout	14.7503	15.2808	15.2593	14.4142	14.4150	
		(Gap)	(3.77%)	(7.51%)	(7.36%)	(1.40%)	(1.40%)	
		Mean	15.1147	15.9092	15.2895	14.5944	14.5946	
		(Gap)	(6.34%)	(11.93%)	(7.57%)	(2.67%)	(2.67%)	
	Critic	15.1639	15.9886	15.2945	14.5991	14.6004	14.6011	
		(Gap)	(6.68%)	(12.49%)	(7.60%)	(2.70%)	(2.72%)	
		15.1428	15.9191	15.3835	14.6053	14.6111	14.6111	
		(Gap)	(6.76%)	(12.46%)	(7.51%)	(2.75%)	(2.79%)	
						18.3215		
						(28.92%)		
						21.7044		
						(52.74%)		
						15.3090		
						(7.71%)		
						14.2148		
						(0.00%)		

with and without active search. Still, the performance of the original active search (AS) is less stable than the two variants of efficient active search (EAS). With active search (especially EAS), the performance of RL methods is consistently better than that of Deterministic Greedy and is close to the optimum.

Test-time sampling techniques For out-of-distribution instances, we also consider top- p sampling and different sampling temperatures as the main benchmark. The considered p values are: 0.5, 0.6, 0.7, 0.8, 0.9, 0.95, 0.99, 1.0. The sampling temperatures considered are 0.01, 0.03, 0.1, 0.3, 0.5, 0.7, 0.8, 0.9, 1.0, 1.1, 1.2, 1.5, and 2.0. Fig. 29 show the heatmaps for each combination of encoder and RL baseline, for FLP and MCP. In each subplot, the x -axis represents the value of p in top- p sampling, and the y -axis represents the sampling temperature. For each combination, the best performance is marked with a red star. For both FLP and MCP, the best performance is usually achieved with a proper (i.e., neither too high nor too low) level of randomness. As the p value of top- p sampling increases, the best sampling temperature decreases. Recall that both increasing the p value and increasing the sampling temperature would increase the randomness in sampling.

E.7 Efficient Software Routines

E.7.1 Mixed-Precision Training

RL4CO supports multiple device types as well as floating point precisions by leveraging PyTorch Lightning [39].

Table 27: Performance of different methods on the maximum coverage problem (MCP) out-of-distribution instances. For the performance, the larger the better.

Encoder	RL Baseline	Sample (Best)	Sample (Mean)	Greedy	AS	Active Search		
						EAS-Emb	EAS-Lay	
MLP	Rollout	1356.8970	1299.8690	1307.5250	1385.3340	1385.3280	1385.3280	
		(Gap) (-1.83%)	(-5.48%)	(-5.03%)	(-0.32%)	(-0.33%)	(-0.33%)	
		Mean	1360.7710	1306.4015	1312.6290	1319.8180	1383.3580	
	Exponential	(Gap) (-2.34%)	(-6.45%)	(-5.89%)	(-5.04%)	(-0.47%)	(-0.47%)	
		1360.7830	1306.3337	1312.7070	1088.0180	1383.9670	1383.9670	
		(Gap) (-2.49%)	(-6.64%)	(-6.23%)	(-21.71%)	(-0.42%)	(-0.42%)	
SAGE	Critic	1363.9190	1313.2830	1319.5280	1353.9080	1377.3780	1377.3780	
		(Gap) (-3.29%)	(-7.83%)	(-7.33%)	(-2.59%)	(-0.90%)	(-0.90%)	
		Rollout	1353.9790	1297.5763	1303.7120	1382.2220	1382.1140	
	Exponential	(Gap) (-2.55%)	(-6.61%)	(-6.16%)	(-0.55%)	(-0.56%)	(-0.56%)	
		Mean	1366.0050	1320.5641	1325.5570	1121.7650	1384.3780	
		(Gap) (-2.06%)	(-5.98%)	(-5.53%)	(-19.30%)	(-0.39%)	(-0.40%)	
GEN	Exponential	1344.1420	1281.0377	1288.0360	1288.2830	1383.6030	1383.5500	
		(Gap) (-2.30%)	(-6.38%)	(-5.73%)	(-7.31%)	(-0.45%)	(-0.45%)	
		Critic	1331.1100	1266.6130	1276.0670	1092.0550	1367.4660	
	Rollout	(Gap) (-4.23%)	(-8.87%)	(-8.19%)	(-21.42%)	(-1.61%)	(-1.61%)	
		1334.2700	1269.0966	1284.4550	1385.6540	1385.5750	1385.5750	
		(Gap) (-1.68%)	(-4.96%)	(-4.60%)	(-0.30%)	(-0.31%)	(-0.31%)	
	Mean	1354.8450	1297.2153	1302.8560	1305.4070	1384.3080	1384.2980	
		(Gap) (-2.06%)	(-5.98%)	(-5.52%)	(-6.08%)	(-0.40%)	(-0.40%)	
		Exponential	1357.4750	1300.7056	1309.8040	1376.1300	1384.3780	
	Deterministic Greedy	(Gap) (-2.11%)	(-6.18%)	(-5.45%)	(-0.99%)	(-0.39%)	(-0.39%)	
		Critic	1360.0420	1303.4360	1313.6640	1366.2960	1374.8630	
		(Gap) (-4.00%)	(-8.68%)	(-7.58%)	(-1.69%)	(-1.08%)	(-1.08%)	
						1003.3390		
						(-27.80%)		
						866.3536		
						(-37.66%)		
						1367.2240		
						(-1.63%)		
						GUROBI/SCIP (Optimum)		
						1389.8450		
						(0.00%)		

Table 28: Running time and memory usage of the AM model trained using FP32 and FP16 mixed precision (FP16-mix), evaluated over 5 epochs with a training size of 10,000 in the CVPR20, CVPR50, and CVPR100.

Problem	Precision	Running time [s]	Memory usage [GiB]
CVRP20	FP32	6.33 ± 0.26	1.41 ± 0.04
	FP16-mix	5.89 ± 0.07	0.84 ± 0.01
CVRP50	FP32	13.58 ± 0.12	4.79 ± 0.40
	FP16-mix	11.68 ± 0.30	2.30 ± 0.25
CVRP100	FP32	35.09 ± 0.71	13.47 ± 0.63
	FP16-mix	25.11 ± 0.66	8.14 ± 0.82

As Table 28 shows mixed-precision training can successfully reduce computational costs both in terms of runtime and especially with memory usage.

E.7.2 FlashAttention

Given that the Attention operator is used on several occasions, especially in autoregressive models, there is a need to support fast and efficient software routines that can compute this ubiquitous operation. In RL4CO, we natively support FlashAttention [34, 33] from both PyTorch 2.0+ and the original FlashAttention repository ²³, to which we also made some minor contributions when we found bugs.

²³ Available at <https://github.com/Dao-AI-Lab/flash-attention>.

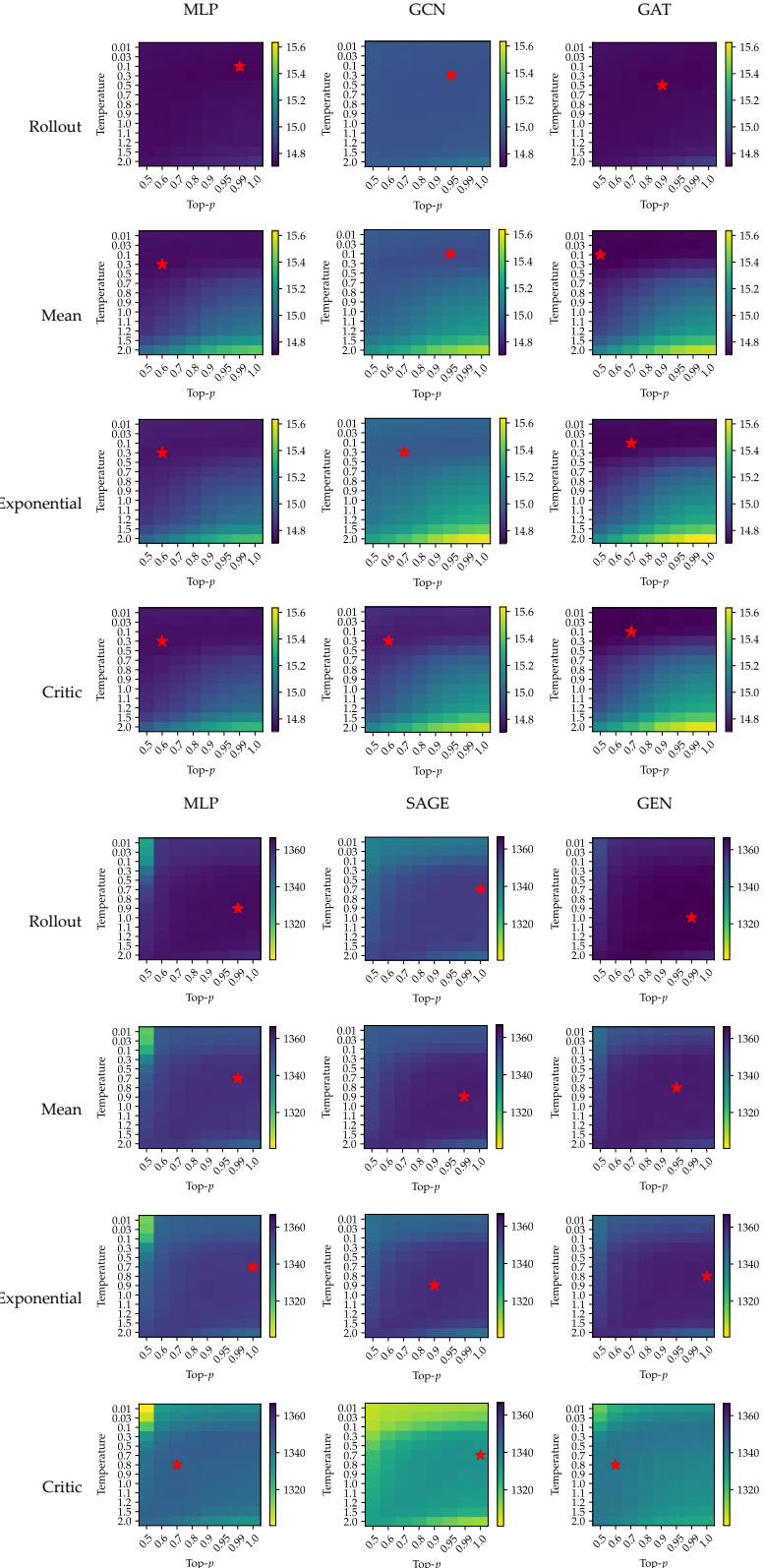


Figure 29: Performance of sampling on out-of-distribution instances with different p values for top- p sampling and different sampling temperatures. Top: FLP; Bottom: MCP. For each combination of encoder and RL baseline, the best performance is marked with a star.

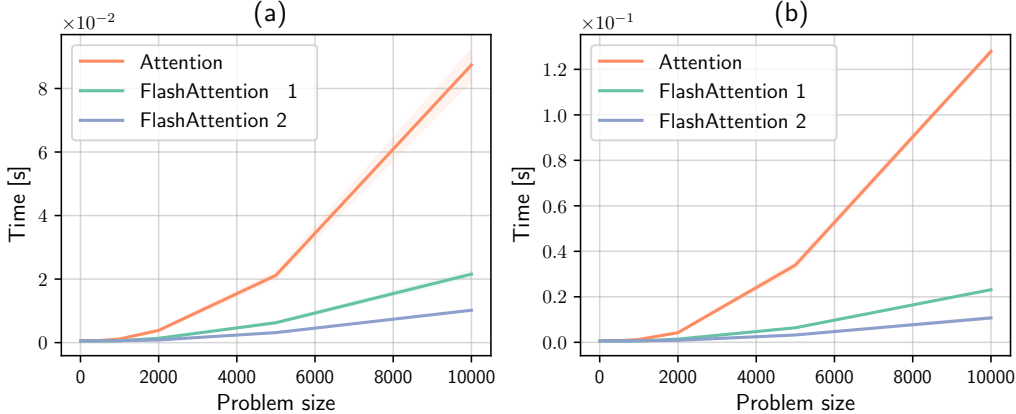


Figure 30: Running time of the graph attention encoder from the Attention Model, equipped with a standard attention layer, FlashAttention1, and FlashAttention2, across different problem sizes for both (a) the TSP and (b) the CVRP environments.

As shown in Fig. 30, different implementations can make a difference, especially with large problem sizes. It should be noted that while more scalable, FlashAttention at the moment is restricted to no or causal masks only. Therefore, usage in the masked attention decoding scheme is not possible at the moment, although it could be even more impactful due to the auto-regressive nature of our encoder-decoder scheme. Recent works as Pagliardini et al. [107] may be useful in extending FlashAttention to other masking patterns. We note that masking should, in principle, be even faster than un-masked attention, given that operations can be skipped in a per-block manner.

E.7.3 Efficient Memory Handling in Environments

When dealing with RL problems, there is usually a tradeoff between memory and speed. This happens because environments are parallelized using multiple processes or threads, the policy network is replicated to each environment, or observations incoming from each environment need to be gathered, sent to the policy network, and then the output action scattered back to the representative environment. In the first case, network duplication causes large memory consumption; in the second case, communication between processes slows down. In RL4CO, we solve the problem by using batched environments, i.e., every environment is responsible not for a single instance of a problem but a batch of instances at the same time. By doing so, the policy can live in the same process of the environment, in the same device, and receive and send batched data without any communication overhead or additional memory consumption. To further improve performances, we rewrite a core component of the TorchRL environment, namely the `step` method of the TorchRL base environment. The original `step` method performs some checks that, while useful for generic environments, can be omitted for RL4CO ones. It also duplicates the information in the output `TensorDict` by returning both the previous and the new state. In RL4CO, the previous state is always redundant, hence our `step` method does not keep it, reducing the memory consumption. We can see in Table 29 that using RL4CO step method has a great benefit in terms of speed, especially for high-dimensional environments. The results are collected for the TSP and CVRP environment during one epoch of training for a dataset of size 100000. The table shows the difference in training time and peak allocated memory for the training when the environment uses the TorchRL step method and the RL4CO step method. The peak allocated memory is computed using the `torch.cuda.max_memory_allocated` method from PyTorch, and experiments are run on a Tesla V100 DGX 32GB.

Table 29: Comparison of training time in seconds for one epoch with RL4CO and TorchRL step method.

Environment	Nodes	Step method	
		RL4CO	TorchRL
TSP	50	46.3	49.6
	100	102.9	108.6
	200	284.9	302.2
CVRP	50	72.9	73.4
	100	147.3	154.3
	200	371.7	406.4

Table 30: Performance on 1,000 test instances. * represents 0.000%, with which the gaps are computed.

Method	N = 50			N = 100			Method	N = 50			N = 100			
	Obj.	Gap	Time	Obj.	Gap	Time		Obj.	Gap	Time	Obj.	Gap	Time	
CVRP	HGS-PyVRP	10.287	*	4.6m	15.543	*	9.2m	HGS-PyVRP	16.032	*	4.6m	25.433	*	9.2m
	OR-Tools	10.523	2.294%	4.6m	16.361	5.263%	9.2m	OR-Tools	16.124	0.574%	4.6m	25.923	1.927%	9.2m
	MTPOMO	10.408	1.176%	2s	15.809	1.711%	10s	MTPOMO	16.396	2.270%	2s	26.391	3.767%	11s
	MVMoE	10.397	1.069%	3s	15.782	1.538%	13s	MVMoE	16.394	2.258%	3s	26.357	3.633%	14s
OVRP	MVMoE-L	10.404	1.137%	3s	15.790	1.589%	12s	MVMoE-L	16.393	2.252%	3s	26.359	3.641%	13s
	HGS-PyVRP	6.494	*	4.6m	9.730	*	9.2m	HGS-PyVRP	10.328	*	4.6m	15.637	*	9.2m
	OR-Tools	6.555	0.939%	4.6m	10.081	3.607%	9.2m	OR-Tools	10.570	2.343%	4.6m	16.466	5.302%	9.2m
	MTPOMO	6.712	3.357%	2s	10.241	5.252%	10s	MTPOMO	10.454	1.220%	2s	15.921	1.816%	12s
VRPB	MVMoE	6.696	3.111%	3s	10.213	4.964%	13s	MVMoE	10.442	1.104%	3s	15.886	1.592%	13s
	MVMoE-L	6.704	3.234%	2s	10.215	4.985%	12s	MVMoE-L	10.450	1.181%	2s	15.898	1.669%	10s
	HGS-PyVRP	9.688	*	4.6m	14.386	*	9.2m	HGS-PyVRP	10.485	*	4.6m	16.900	*	9.2m
	OR-Tools	9.829	1.455%	4.6m	15.010	4.338%	9.2m	OR-Tools	10.497	0.114%	4.6m	17.023	0.728%	9.2m
OVRPB	MTPOMO	9.975	2.962%	2s	15.014	4.365%	10s	MTPOMO	10.664	1.707%	2s	17.426	3.112%	11s
	MVMoE	9.954	2.746%	3s	14.962	4.004%	13s	MVMoE	10.665	1.717%	3s	17.421	3.083%	15s
	MVMoE-L	9.963	2.839%	2s	14.976	4.101%	11s	MVMoE-L	10.665	1.717%	2s	17.411	3.024%	14s
	HGS-PyVRP	6.897	*	4.6m	10.304	*	9.2m	HGS-PyVRP	6.904	*	4.6m	10.310	*	9.2m
OVRPBLTW	OR-Tools	6.940	0.623%	4.6m	10.611	2.979%	9.2m	OR-Tools	6.949	0.652%	4.6m	10.613	2.939%	9.2m
	MTPOMO	7.392	7.177%	2s	11.787	14.392%	10s	MTPOMO	7.400	7.184%	2s	11.786	14.316%	10s
	MVMoE	7.566	9.700%	3s	11.873	15.227%	13s	MVMoE	7.577	9.748%	3s	11.875	15.179%	13s
	MVMoE-L	7.388	7.119%	2s	11.806	14.577%	12s	MVMoE-L	7.391	7.054%	2s	11.814	14.588%	12s
OVRPBLTW	HGS-PyVRP	11.597	*	4.6m	19.005	*	9.2m	HGS-PyVRP	11.590	*	4.6m	19.167	*	9.2m
	OR-Tools	11.612	0.129%	4.6m	19.198	1.016%	9.2m	OR-Tools	11.610	0.173%	4.6m	19.314	0.767%	9.2m
	MTPOMO	11.986	3.354%	2s	20.048	5.488%	11s	MTPOMO	11.980	3.365%	2s	20.209	5.436%	11s
	MVMoE	11.949	3.305%	3s	20.092	5.720%	15s	MVMoE	11.957	3.167%	3s	20.254	5.671%	15s
OVRPL	MVMoE-L	11.961	3.139%	3s	20.033	5.409%	14s	MVMoE-L	11.951	3.115%	2s	20.173	5.249%	14s
	HGS-PyVRP	6.510	*	4.6m	9.709	*	9.2m	HGS-PyVRP	10.455	*	4.6m	16.962	*	9.2m
	OR-Tools	6.571	0.937%	4.6m	10.047	3.481%	9.2m	OR-Tools	10.465	0.096%	4.6m	17.100	0.814%	9.2m
	MTPOMO	6.732	3.410%	2s	10.216	5.222%	10s	MTPOMO	10.625	1.626%	2s	17.486	3.089%	11s
VRPBL	MVMoE	6.713	3.118%	3s	10.187	4.923%	13s	MVMoE	10.631	1.683%	3s	17.483	3.072%	15s
	MVMoE-L	6.725	3.303%	2s	10.185	4.903%	12s	MVMoE-L	10.635	1.722%	3s	17.474	3.019%	14s
	HGS-PyVRP	9.688	*	4.6m	14.373	*	9.2m	HGS-PyVRP	18.361	*	4.6m	29.026	*	9.2m
	OR-Tools	9.820	1.363%	4.6m	15.084	4.947%	9.2m	OR-Tools	18.422	0.332%	4.6m	29.830	2.770%	9.2m
VRPBL	MTPOMO	9.994	3.159%	2s	15.033	4.592%	10s	MTPOMO	19.028	3.633%	2s	31.062	7.014%	11s
	MVMoE	9.971	2.921%	3s	14.979	4.286%	13s	MVMoE	18.967	3.300%	3s	31.114	7.194%	15s
	MVMoE-L	9.977	2.983%	2s	14.990	4.293%	11s	MVMoE-L	18.998	3.469%	3s	31.032	6.911%	13s
	HGS-PyVRP	18.167	*	4.6m	29.000	*	9.2m	HGS-PyVRP	15.951	*	4.6m	25.678	*	9.2m
VRPBLTW	OR-Tools	18.374	1.139%	4.6m	29.964	3.324%	9.2m	OR-Tools	16.036	0.533%	4.6m	26.156	1.862%	9.2m
	MTPOMO	18.995	4.558%	2s	31.184	7.531%	11s	MTPOMO	16.310	2.251%	2s	26.650	3.785%	11s
	MVMoE	18.934	4.222%	3s	31.223	7.666%	15s	MVMoE	16.315	2.282%	3s	26.635	3.727%	14s
	MVMoE-L	18.970	4.420%	2s	31.138	7.372%	14s	MVMoE-L	16.311	2.257%	3s	26.637	3.735%	13s

E.8 Towards Foundation Models

Motivation Although learning to solve VRPs has gained significant attention, previous methods are only structured and trained independently on a specific problem, making them less generic and practical. Inspired by the recent success of foundation models in the language and vision domains, some works started to build foundation models for VRPs [89, 157, 13], aiming to solve a wide spectrum of problem variants using a single model. The main idea is to train a (large) model on diverse VRPs, which can be represented by a unified template. Typically, VRPs share several common attributes. For example, CVRP and VRPTW share the capacity attribute while only differing in the time window attribute. Therefore, a simple template could be a union set of attributes that exist in all VRP variants. By training on diverse VRP variants leveraging this unified representation, the foundation VRP model has the potential to efficiently and effectively solve any variant, making it a favorable choice versus traditional solvers (e.g., OR-Tools [111]) in the future.

E.8.1 Experimental Setting

For traditional solvers, we use HGS-PyVRP [144], an open-source VRP solver based on the state-of-the-art HGS-CVRP [138], and Google’s OR-Tools [111], an open-source solver based on constraint programming for complex optimization problems, to solve all VRP variants considered in this study.

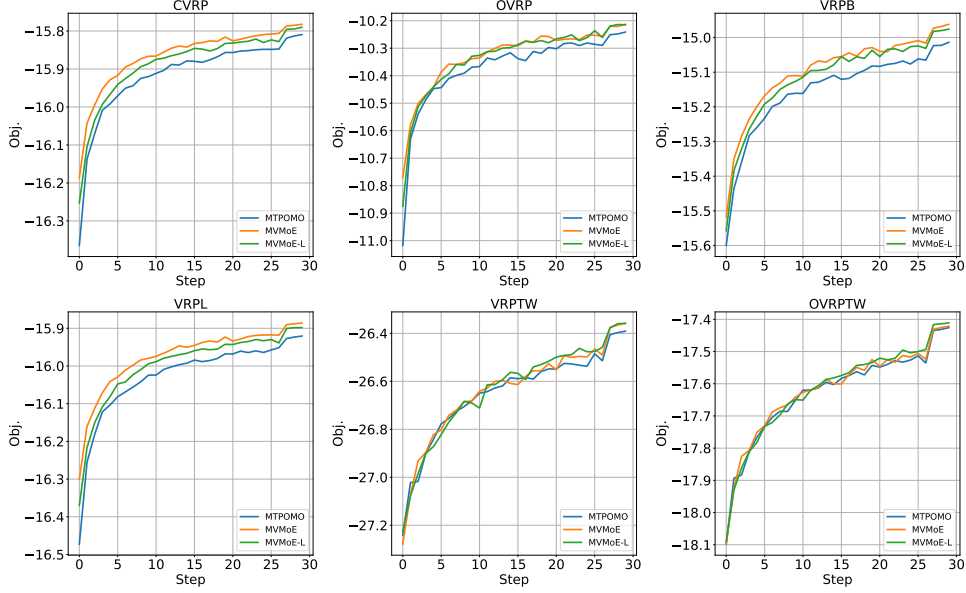


Figure 31: The validation curves of foundation models on $N = 100$.

Both baseline methods solve each instance on a single CPU core with a time limit of 10 and 20 seconds for instances with 50 and 100 nodes, respectively. We parallelize traditional solvers across 16 CPU cores as in [74]. For neural solvers, we mostly follow the training setups from previous works [89, 157, 13]. In specific, the model is trained over 300 epochs, with each epoch containing 100,000 instances generated on the fly. The Adam optimizer is used with a learning rate of $3e - 4$, a weight decay of $1e - 6$, and a batch size of 256. The learning rate decays by 10 at 270 and 295 epochs. Note that different from Liu et al. [89], Zhou et al. [157], we allow various problem variants to be trained in each batch training following Berto et al. [13]. We consider 16 VRP variants as shown in Table 7, including the constraints of capacity, time window, backhaul, open route, and duration limit. The training variants include CVRP, OVRP, VRPL, VRPB, VRPTW, and OVRPTW. During inference, we use greedy rollout with x8 instance augmentation following Kwon et al. [76]. We report the average results (i.e., objective values and gaps) over the test dataset that contains 1,000 instances, and the total time to solve the entire test dataset. The gaps are computed with respect to the results of HGS-PyVRP. All neural solvers are implemented using RL4CO.

E.8.2 Empirical Results

We show the comprehensive evaluation results and validation curves in Table 30 and Fig. 31, respectively. The conclusions are consistent with previous studies [89, 157, 13] that 1) the foundation VRP solvers exhibit remarkable zero-shot generalization performance, even only trained on several VRPs with simple constraints; 2) conditional computation (e.g., mixture-of-experts [57, 121]) can greatly enhance the model capacity without a proportional increase in computation. In Table 31, we further show the performance on CVRPLIB [86], which is a real-world benchmark dataset including instances with diverse distributions. We empirically observe that training on multiple VRPs can significantly improve the out-of-distribution generalization performance of neural VRP solvers, demonstrating the great promise of developing foundation models in VRPs.

E.8.3 Discussion

Foundation models, a class of large-scale deep learning models pre-trained on extensive datasets of diverse tasks, have recently revolutionized the fields of language and vision domains. They can generate text, translate languages, summarize content, and more, all without task-specific training. This versatility makes them incredibly useful across various applications, from chatbots to academic research. Aiming for a more powerful and general solver, recent studies explore the possibility of pretraining a large model on a huge amount of optimization tasks. The long-term goal is to develop a foundation model for VRPs (or more broadly COPs), which can efficiently solve any problem

Table 31: Results on CVRPLib datasets with diverse distributions and sizes. All models are only trained on the uniformly distributed data with the size $N = 100$.

Benchmark	Size N	Ins. Num.	POMO-CVRP		MTPOMO		MVMoE		MVMoE-L	
			Obj.	Gap	Obj.	Gap	Obj.	Gap	Obj.	Gap
Set A	31-79	27	1088.5	4.9%	1084.2	4.3%	1081.0	3.8%	1085.4	4.4%
Set B	30-77	23	1013.9	5.5%	1010.3	5.0%	1003.5	4.0%	1001.2	4.0%
Set F	44-134	3	796.0	12.7%	812.7	16.3%	819.0	13.8%	799.0	14.1%
Set M	100-199	5	1157.4	6.3%	1179.4	8.6%	1181.8	8.8%	1151.4	6.0%
Set P	15-100	23	643.9	14.7%	621.8	8.4%	616.1	5.9%	619.8	6.9%
Set X	100-1000	100	77199.6	21.1%	71153.8	11.7%	72798.7	15.0%	72446.1	13.9%

variant, comparably or better to the conventional solvers with respect to the solution quality and inference speed. Despite the recent advancements of foundation VRP models [89, 157, 13], there are many challenges that need to be addressed by the NCO community, including but not limited to: 1) *scaling*: current autoregressive-based models are challenging to scale to the parameter levels of large language models (e.g., billions of parameters) due to the expensive training cost. RL-based training is data inefficient and converges slowly, whereas SL-based training requires a significant amount of optimal solutions, which are non-trivial to obtain for NP-hard problems. They also fail to be efficiently trained on large-scale instances; 2) *performance*: the empirical results are still far short of traditional solvers (e.g., OR-Tools). They may also suffer from generalization and robustness issues; 3) *generality*: the current problem formulation or template cannot solve novel problem variants in a zero-shot manner; 4) *interpretability*: the decision-making of foundation models is hard to explain.

Moreover, there is another line of research leveraging the existing large language models (LLMs) to generate solutions [149, 91, 55] or algorithms [117, 90, 151], yielding impressive results when integrated with problem-specific heuristics or general meta-heuristics. Some studies employ LLMs to investigate the interpretability of solvers [66], automate problem formulation or simplify the use of domain-specific tools [146, 2, 142] through text prompts. However, their performance is highly dependent on the utilized LLMs, and their outputs may be extremely sensitive to the designed prompts.

We view both as promising directions towards foundation models in combinatorial optimization. We call the attention from both the machine learning (ML) and operations research (OR) communities to advance the development of impactful foundational models and learning methods that are scalable, robust, generalizable, and interpretable across various optimization tasks in future work.

E.9 Generalization of Training on Multiple Distributions and Multiple Tasks

Recent neural methods mostly train and test neural networks on the same task with instances of the same distribution and size, and hence suffer from inferior generalization performance. Some attempts have been made to alleviate the generalization issue, focusing on either distribution [16, 59, 147] or size [122]. More aligned to the diverse distribution and size settings in the benchmark dataset TSPLib and CVRPLib, Manchanda et al. [100] and Zhou et al. [156] consider generalization across both distribution and size in VRPs.

However, these generalization methods adopt extra model architectures and training paradigms, resulting in additional computational burdens. As a more efficient alternative, we observe that diversified training datasets significantly improve generalization performance. Specifically, as indicated in the prior works, training on mixed distributions [16] and mixed VRP variants [89, 157, 13] boosts the generalization capability. RL4CO, detailed in Appendix B.1.6, supports multiple VRP variants and the generation of diverse coordinate distributions, enabling straightforward experimental setups. The implementation specifics are outlined in Appendix D.3.4. Evaluation results on the CVRPLib [86], summarized in Table 4 and fully detailed in Table 32, demonstrate that training across multiple distributions (i.e., MDPOMO) achieves better generalization on datasets of similar size to the training set, whereas training across multiple VRP tasks (i.e., MTPOMO) exhibits superior generalization across larger and more diverse distributions. This indicates that different VRP variants share foundational knowledge, and learning from this diversity enhances generalization beyond conventional training on a single distribution, size, and task. These key findings highlight the necessity of developing foundational models across diverse combinatorial optimization domains.

Table 32: Full Results on CVRPLIB instances with models trained on $N = 50$. Greedy multi-start decoding is used.

Instance	BKS	POMO		MTPOMO		MDPOMO		Instance	BKS	POMO		MTPOMO		MDPOMO	
		Obj.	Gap	Obj.	Gap	Obj.	Gap			Obj.	Gap	Obj.	Gap	Obj.	Gap
A-n32-k5	784	821	4.72%	831	5.99%	817	4.21%	X-n125-k30	55539	58759	5.80%	58560	5.44%	59924	7.90%
A-n33-k5	661	683	3.33%	689	4.24%	685	3.63%	X-n129-k18	28940	30611	5.77%	30437	5.17%	30516	5.45%
A-n33-k6	742	759	2.29%	745	0.40%	750	1.08%	X-n134-k13	10916	11805	8.14%	12043	10.32%	11771	7.83%
A-n34-k5	778	791	1.67%	791	1.67%	791	1.67%	X-n139-k10	13590	14562	7.15%	14993	10.32%	15328	12.79%
A-n36-k5	799	831	4.01%	803	0.50%	812	1.63%	X-n143-k7	15700	17293	10.15%	17337	10.43%	17062	8.68%
A-n37-k5	669	712	6.43%	699	4.48%	673	0.60%	X-n148-k46	43448	47711	9.81%	46442	6.89%	49444	13.80%
A-n37-k6	949	995	4.85%	998	5.16%	999	5.27%	X-n153-k22	21220	24506	15.49%	23928	12.76%	24562	15.75%
A-n38-k5	730	753	3.15%	749	2.60%	774	6.03%	X-n157-k13	16876	18702	10.82%	18201	7.85%	18560	9.98%
A-n39-k5	822	835	1.58%	842	2.43%	842	2.43%	X-n162-k11	14138	15678	10.89%	15615	10.45%	16257	14.99%
A-n39-k6	831	838	0.84%	844	1.56%	842	1.32%	X-n167-k10	20557	22331	8.63%	23083	12.29%	22839	11.10%
A-n44-k6	937	962	2.67%	959	2.35%	958	2.24%	X-n172-k51	45607	50471	10.67%	48799	7.00%	50689	11.14%
A-n45-k6	944	984	4.24%	981	3.92%	965	2.22%	X-n176-k26	47812	54316	13.60%	53773	12.47%	53197	11.26%
A-n45-k7	1146	1166	1.75%	1163	1.48%	1162	1.40%	X-n181-k23	25569	27331	6.89%	27571	7.83%	27572	7.83%
A-n46-k7	914	924	1.09%	945	3.39%	938	2.63%	X-n186-k15	24145	26981	11.75%	27157	12.47%	27011	11.87%
A-n48-k7	1073	1108	3.26%	1121	4.47%	1102	2.70%	X-n190-k8	16980	19414	14.33%	19955	17.52%	18355	8.10%
A-n53-k7	1010	1040	2.97%	1080	6.93%	1047	3.66%	X-n195-k51	44225	50357	13.87%	47675	7.80%	49878	12.78%
A-n54-k7	1167	1192	2.14%	1191	2.06%	1181	1.20%	X-n200-k36	58578	66149	12.92%	62862	7.31%	62466	6.64%
A-n55-k9	1073	1095	2.05%	1124	4.75%	1123	4.66%	X-n204-k19	19565	22013	12.51%	22297	13.96%	23018	17.65%
A-n60-k9	1354	1388	2.51%	1398	3.25%	1389	2.58%	X-n209-k16	30656	33810	10.29%	33745	10.08%	34060	11.10%
A-n61-k9	1034	1059	2.42%	1090	5.42%	1051	1.64%	X-n214-k11	10856	13108	20.74%	13005	19.80%	12586	15.94%
A-n62-k8	1288	1343	4.27%	1329	3.18%	1364	5.90%	X-n219-k73	117593	133173	13.25%	125415	6.65%	126942	7.95%
A-n63-k9	1616	1660	2.72%	1660	2.35%	1654	2.35%	X-n223-k34	40437	44173	9.24%	44066	8.97%	44609	10.32%
A-n63-k10	1314	1349	2.66%	1342	2.13%	1347	2.51%	X-n228-k23	25742	30685	19.20%	29896	16.14%	29593	14.96%
A-n64-k9	1401	1432	2.21%	1438	2.64%	1441	2.86%	X-n233-k16	19230	22082	14.83%	22602	17.54%	23553	22.48%
A-n65-k9	1174	1231	4.86%	1234	5.11%	1239	5.54%	X-n237-k14	27042	31000	14.64%	31880	17.89%	31617	16.92%
A-n69-k9	1159	1224	5.61%	1207	4.14%	1205	3.97%	X-n242-k48	82751	89900	8.64%	87933	6.26%	90125	8.91%
A-n80-k10	1763	1839	4.31%	1825	3.52%	1840	4.37%	X-n247-k50	37274	41688	11.84%	42340	13.59%	43318	16.22%
B-n31-k5	672	688	2.38%	705	4.91%	694	3.27%	X-n251-k28	38684	43430	12.27%	42379	9.55%	42721	10.44%
B-n34-k5	788	798	1.27%	802	1.78%	803	1.90%	X-n256-k16	18839	23449	24.47%	21559	14.44%	25704	36.44%
B-n35-k5	955	979	2.51%	975	2.09%	976	2.20%	X-n261-k13	26558	30384	14.41%	31345	18.02%	30630	15.33%
B-n38-k6	805	830	3.11%	817	1.49%	834	3.60%	X-n266-k58	75478	83838	11.08%	83806	11.03%	91188	20.81%
B-n39-k5	549	561	2.19%	561	2.19%	557	1.46%	X-n270-k35	35291	40274	14.12%	39378	11.58%	41661	18.05%
B-n41-k6	829	849	2.41%	850	2.53%	848	2.29%	X-n275-k28	21245	25909	21.95%	25718	21.05%	26474	24.61%
B-n43-k6	742	762	2.70%	756	1.89%	770	3.77%	X-n280-k17	35305	37659	12.40%	39309	17.33%	38119	13.78%
B-n44-k7	909	942	3.63%	940	3.41%	934	2.75%	X-n284-k15	20226	25024	23.72%	24791	22.57%	23504	16.21%
B-n45-k5	751	772	2.80%	775	3.20%	771	2.66%	X-n289-k60	95151	106703	11.48%	104253	9.57%	107238	12.70%
B-n45-k6	678	736	8.55%	745	9.88%	736	8.55%	X-n294-k50	47161	54318	15.18%	53458	13.35%	54899	16.41%
B-n50-k7	741	767	3.51%	765	3.24%	753	1.62%	X-n298-k31	34231	40064	17.04%	39609	15.71%	41296	20.64%
B-n50-k8	1312	1347	2.67%	1330	1.37%	1328	1.22%	X-n303-k21	21736	26078	19.98%	25228	16.07%	25380	16.76%
B-n52-k7	747	762	2.01%	762	2.01%	763	2.14%	X-n308-k13	25859	30557	18.17%	31927	23.47%	31625	22.30%
B-n56-k7	707	740	4.67%	744	5.23%	734	3.82%	X-n313-k71	94043	106936	13.71%	101767	8.21%	116306	23.67%
B-n57-k7	1153	1153	0.00%	1175	1.91%	1162	0.78%	X-n317-k53	78355	96382	23.01%	84483	7.82%	106138	35.46%
B-n57-k9	1598	1645	3.32%	1645	2.94%	1644	2.88%	X-n322-k28	29834	35987	20.62%	35503	19.00%	37562	25.90%
B-n63-k10	1496	1537	2.74%	1589	6.22%	1572	5.08%	X-n327-k20	27532	33039	20.00%	33478	21.60%	34083	23.79%
B-n64-k9	861	937	8.83%	931	8.13%	923	7.20%	X-n331-k15	31102	36123	16.14%	37292	19.90%	37114	19.33%
B-n66-k9	1316	1355	2.81%	1374	4.41%	1350	2.58%	X-n336-k84	139111	153850	10.60%	150341	8.07%	158211	13.73%
B-n67-k10	1032	1070	3.68%	1115	8.04%	1065	3.20%	X-n344-k43	42050	48339	14.96%	48035	14.23%	49217	17.04%
B-n68-k9	1272	1337	5.11%	1339	5.27%	1343	5.58%	X-n351-k40	25896	30923	19.41%	30498	17.77%	30965	19.57%
B-n78-k10	1221	1306	6.96%	1311	7.37%	1307	7.04%	X-n359-k29	51505	58300	13.19%	59810	16.12%	59431	15.39%
E-n22-k4	375	421	12.27%	427	13.87%	433	15.47%	X-n367-k17	22814	30083	31.86%	28335	24.20%	27747	21.62%
E-n23-k3	569	621	9.14%	574	0.88%	578	1.58%	X-n376-k94	147713	162451	9.98%	160107	8.39%	173422	17.40%
E-n33-k4	835	844	1.08%	845	1.20%	858	2.75%	X-n384-k52	65928	76341	15.79%	76040	15.34%	77891	18.15%
E-n51-k5	521	534	2.50%	555	6.53%	546	4.80%	X-n393-k38	38260	45226	18.21%	44953	17.49%	47317	23.67%
E-n77-k7	682	708	3.81%	721	5.72%	721	5.72%	X-n401-k29	66154	73618	11.28%	76247	15.26%	73121	10.53%
E-n76-k8	735	775	5.44%	770	4.76%	777	5.71%	X-n411-k19	19712	26432	34.09%	25671	30.23%	25525	29.49%
E-n76-k10	830	876	5.54%	863	3.98%	868	4.58%	X-n420-k130	107798	123789	14.83%	119818	11.15%	128982	19.65%
E-n76-k14	1021	1051	2.94%	1070	4.80%	1058	3.62%	X-n429-k61	65449	75236	14.95%	76115	16.30%	78711	20.26%
E-n101-k8	815	876	7.48%	879	7.85%	887	8.83%	X-n439-k37	36391	44326	21.80%	43772	20.28%	47436	30.35%
E-n101-k14	1067	1137	6.56%	1150	7.78%	1138	6.65%	X-n449-k29	55233	63887	15.67%	67416	22.06%	66168	19.80%
F-n45-k4	724	753	4.01%	747	3.18%	729	0.69%	X-n459-k26	24139	32530	34.76%	31774	31.63%	31437	30.23%
F-n77-k4	237	272	14.77%	270	13.92%	268	13.08%	X-n469-k138	221824	26794	20.79%	248139	11.86%	260902	17.62%
F-n135-k7	1162	1415	21.77%	1385	19.19%	1478	27.19%	X-n480-k70	89449	100833	12.73%	103101	15.26%	103785	16.03%
M-n101-k10	820	974	18.78%	908	10.73%	905	10.37%	X-n491-k59	66483	78531	18.12%	78999	18.83%	80703	21.39%
M-n121-k7	1034	1242	20.12%	1181	14.22%	1204	16.44%	X-n502-k39	69226	79183	14.38%	77585	12.07%	78419	13.28%
M-n151-k12	1015	1143	12.61%	1116	9.95%	1164	14.68%	X-n513-k21	24201	34479	42.47%	32744	35.30%	39592	63.60%
M-n200-k16	1274	1468	15.23%	1464	14.91%	1521	19.39%	X-n524-k153	154593	179926	16.39%	174390	12.81%	193416	25.11%
M-n200-k17	1275	1468	15.14%	1473	15.53%	1521	19.29%	X-n536-k96	94846	112396	18.50%	111393	17.45%	111191	17.23%
P-n19-k8	450														